UC San Diego

UC San Diego Electronic Theses and Dissertations

Title

Insight into translational regulation through quantitative measurements of translation elongation in S. cerevisiae

Permalink

https://escholarship.org/uc/item/5x3692t5

Author

Hou, Wanfu

Publication Date

2023

Peer reviewed|Thesis/dissertation

eScholarship.org Powered by the California Digital Library
University of California

UNIVERSITY OF CALIFORNIA SAN DIEGO

Insight into translational regulation through quantitative measurements of translation elongation in S. cerevisiae

A Dissertation submitted in partial satisfaction of the requirements
for the degree Doctor of Philosophy

in

Chemistry

by

Wanfu Hou

Committee in charge:

Professor Brian M. Zid, Chair
Professor Eric Bennett
Professor Thomas Hermann
Professor Simpson Joseph
Professor Susan Taylor

2023

Copyright

Wanfu Hou, 2023

All rights reserved.

The Dissertation of Wanfu Hou is approved, and it is acceptable in quality and form for publication on microfilm and electronically.

University of California San Diego

2023

DEDICATION

To my lovely family
(My dear father, mother, and sister)
Thanks for your support throughout my graduate study

TABLE OF CONTENTS

LIST OF FIGURES

LIST OF TABLES

LIST OF ABBREVIATIONS

AA	Amino Acids
ATC	Anhydrotetracycline
cDNA	Complementary DNA
CDS	Coding Sequence
ChIP	Chromatin immunoprecipitation
DMSO	Dimethyl sulfoxide
DNA	Deoxyribonucleic Acid
dNTPs	Deoxyribonucleoside triphosphates
eIF5A	Eukaryotic translation initiation factor 5A
HSP	Heat shock protein
kb	kilobase
MIM	Mitochondrial inner membrane
miRFP	Monomeric Infrared Fluorescent Protein
mRNA	Messenger RNA
mRNP	Messenger Ribonucleoprotein
mitoCPR	Mitochondrial compromised import response
Mitoprotein	Mitochondrial protein
MOM	Mitochondrial outer membrane
MTS	Mitochondrial targeting signal

NAC	Nascent chain-associated heteromeric complex
NGD	No-Go Decay
nLuc	Nanoluciferase
OD	Optical density
ORF	Open Reading Frame
PBs	Processing Body
PCR	Polymerase Chain Reaction
Pro	Proline
qPCR	Quantitative Polymerase Chain Reaction
RLU	Relative Light Unit
RNA	Ribonucleic Acid
RQC	Ribosome Quality Control
RT	Reverse Transcription
SG	Stress Granule
TET	Tetracycline
tRNA	Transfer RNA
UTR	Untranslated Region
WT	Wild Type
YFP	Yellow Fluorescent Protein
YPD	Yeast extract-peptone-dextrose

ACKNOWLEDGEMENTS

I am sincerely thankful to my PhD advisor, Professor Brian M. Zid, for his extensive mentorship and passion for science, which inspired me during my PhD research. He has been incredibly supportive, providing opportunities for scientific projects, conferences, and so on. Additionally, Brian has shown unwavering trust, flexibility, and optimism, creating a friendly and supportive lab environment. I am grateful for the opportunities to learn and grow as both a person and scientist under their guidance. Brian's support and mentorship have been invaluable throughout my PhD research, and I am truly appreciative for everything he has done.

I would like to thank my committee members (Professor Susan Taylor, Professor Simpson Joseph, Professor Thomas Hermann, and Professor Eric Bennett) for their helpful suggestions and advice for my PhD research and dissertation. I am deeply thankful for the assistance and supervision they have provided me over the years, especially the feedback I received during my qualifying exam.

I would like to thank my colleagues (Vince Harjono, Tatsuhisa Tsuboi, Sophie Chan, Anna R. Guzikowski, Alexander T. Harvey, Joon Choi, Ximena Garcia Arceo, Yuko Sugiyama, MS and undergraduate students in Zid's lab) for their collaboration in science and their helpful suggestions and assistance with my projects. To Vince and Tatsu, thank you very much for mentoring me patiently during my early stage in Zid's lab.

I would like to thank my undergraduate school (Xiamen University) and lab (Chaoyong Yang's lab) for the training in scientific research and support for my MS and PhD applications.

I would like to thank my family for their love and trust. I am also grateful for their unwavering support in my decision to study abroad and for providing valuable suggestions regarding my future career plans.

Chapter 2, in full, is prepared for publication: Harjono, V, Hou, W, Harvey, AT, Subramaniam, AR, and Zid, BM. Quantification of elongation stalls and impact on gene expression in yeast. The dissertation author is the first author of this publication.

Chapter 3 consists of both published and unpublished material. Section 3.2.1 and part of Section 3.2.2 are unpublished material. Figure 3.2.2 in Section 3.2.2 is quoted from published PhD dissertation of Marina Barba Aliaga: Barba Aliaga, M. Functions of the translation factor eIF5A in cellular metabolism and transcriptional control [Doctoral thesis]

Chapter 4 is part of a published paper: Yang S Chen, Wanfu Hou, Sharon Tracy, Alex T Harvey, Vince Harjono, Fan Xu, James J Moresco John R Yates III, Brian M Zid. Rvb1/Rvb2 proteins couple transcription and translation during glucose starvation. The dissertation author is the second author of this publication.

VITA

EDUCATION

2017 Bachelor of Science in Chemical Biology, Xiamen University

2020 Master of Science in Chemistry, University of California San Diego

2023 Doctor of Philosophy in Chemistry, University of California San Diego

PUBLICATIONS

Hou, Wanfu, Harjono, Vince, Harvey, Alex T., Subramaniam, Arvind Rasi, and Zid, Brian M., "Quantification of elongation stalls and impact on gene expression in yeast." bioRxiv. 2023. in revision for RNA.

Yang S Chen, **Wanfu Hou**, Sharon Tracy, Alex T Harvey, Vince Harjono, Fan Xu, James J Moresco John R Yates III, Brian M Zid. "Rvb1/Rvb2 proteins couple transcription and translation during glucose starvation." Elife. 2022 Sep 15;11:e76965.

Yanling Song, Yuan An, Weizhi Liu, **Wanfu Hou**, Xingrui Li, Bingqian Lin, Zhi Zhu, Shengxiang Ge, Huang-hao Yang and Chaoyong Yang. "Centrifugal Micropipette-Tip with Pressure Signal Readout for Portable Quantitative Detection of Myoglobin." Chem Commun (Camb). 2017 Aug 22;53(86):11774-11777.

ABSTRACT OF THE DISSERTATION

Insight into translational regulation through quantitative measurements of translation elongation in S. cerevisiae

by

Wanfu Hou

Doctor of Philosophy in Chemistry

University of California San Diego, 2023

Professor Brian M. Zid, Chair

While we have learned that mRNA sequence strongly influences translation and co-translational pathways, the exact mechanisms by which this sequence and the RNA structures encoded impact these steps of gene expression are less understood. Therefore, more investigations

are needed to reveal how translation elongation and efficiency is influenced by RNA sequence and how the affected translation regulates and determines a variety of co-translational pathways. In this dissertation, I explore the effects of translational kinetics on a series of co-translational pathways using the budding yeast *Saccharomyces cerevisiae* as a model organism. In Chapter 2, I developed an in-vivo elongation reporter in *Saccharomyces cerevisiae* to quantitatively monitor translation elongation duration and protein expression. Using this elongation reporter, I investigated the effects of elongation stalls induced by different types of genetic factors on gene expression and demonstrated that distinct ribosomal stalls may trigger distinct co-translational pathways. In Chapter 3, I studied co-translational mRNA localization to mitochondrion, and proposed that translational kinetics, such as ribosomal stall caused by polyprolines, play an important role in mediating co-translational import. In addition, I further studied the effects of elongation stalls on mitochondrial import stress and triggering of relevant quality control pathways. In Chapter 4, I investigated the mechanism of cytosolic mRNP granule formation under glucose deprivation condition. In this study, I use CRISPRi to knockdown expression of RVB2 and confirm its essential role in deciding the fate of mRNA localization and translatability after glucose depletion. Finally in Chapter 5, I address the enhancements made to the developed method, outline potential future directions for the research presented in this dissertation, and conclude with my final remarks.

Chapter 1 Introduction

1.1 Translation and Translation Elongation Kinetics

Since 1958 when Francis Crick first proposed the central dogma that describes the flow of genetic information from DNA to messenger RNA (mRNA) to proteins, large amounts of investigations have been done to underly mechanism and regulation of mRNA and protein expression (Francis Crick, 1958). Translation refers to the process by which the genetic information encoded in mRNA molecules is used to synthesize proteins. This is a fundamental biological process existing in all kingdoms of life because proper regulation of protein production is essential for cell survival and functioning (Stein & Frydman, 2019). Reversely, errors in translation can lead to serious health problems, such as genetic disorders and diseases caused by misfolded or malfunctioning proteins (Eshraghi et al., 2021; Ishimura et al., 2014).

In eukaryotic cells, translation is carried out in the cytoplasm with the help of large complexes of ribosomes, tRNAs, and other translation factors. In general, eukaryotic translation is composed of three stages, including initiation, where the ribosome binds to the mRNA and initiator tRNA, elongation, where amino acids are added to the growing polypeptide chain, and termination, where a release factor triggers the release of the completed polypeptide and dissociation of the ribosome. In addition, a fourth step, called ribosome recycling, rescues the dissociated ribosome subunits and acts as a preparatory step for the next round of translation (Schuller & Green, 2018). With decades of studies, translational initiation is confirmed to be the rate-limiting step in protein synthesis

because it determines the rate of ribosome loading onto the mRNA and the number of ribosomes that can be loaded simultaneously onto a single mRNA molecule (Jackson et al., 2010). However, further investigations into the translation elongation process have revealed its significant effects on regulating the overall efficiency of protein synthesis and maintaining translation fidelity. For example, a slower elongation speed can facilitate proper protein folding or translocation by affecting the recruitment of molecular chaperones or signal recognition particles (SRP) (Komar, 2019; Y. Liu, 2020; Zhao et al., 2021), while may increase the likelihood of ribosomal pause, ultimately leading to ribosome collisions and triggering specialized surveillance pathways to maintain cellular homeostasis (Collart & Weiss, 2020; Goldman et al., 2021). Conversely, a faster elongation rate can improve protein expression levels by influencing ribosome density and mRNA stability (Hanson et al., 2018; Narula et al., 2019), while may also cause issues in translation fidelity by increasing the possibility of protein misfolding (Kim et al., 2015; Sherman & Qian, 2013). Taken together, proper translation elongation kinetics are essential for maintaining proteostasis by balancing translational efficiency and co-translational regulations (Stein & Frydman, 2019).

At the same time, there are plenty of factors affecting the rate and fidelity of protein synthesis by regulating the interactions between the ribosome, mRNA, tRNAs, and other cellular components. For example, mRNA sequence, such as codon usage, are well-investigated elements that influence translation efficiency of the mRNA by altering mRNA stability, tRNA availability and so on (Bae & Coller, 2022; Y. Liu et al., 2021). Some protein factors are involved in the process

of translational elongation, including elongation factors eEF1 and eEF2, which facilitate the movement of the ribosome along the mRNA (Xu et al., 2022). Additionally, change of environmental factors, like nutrients, can alter the modification and conformation of the ribosome or other translation factors, leading to changes in protein synthesis (Gameiro & Struhl, 2018; Proud, 2019).

In this chapter, I will introduce the mechanisms of certain factors derived from mRNA sequences, such as codon usage and amino acid sequences, which regulate translation elongation. I will also discuss a few co-translational pathways, such as NGD and RQC, that are regulated by translation elongation. Furthermore, methods and techniques for quantitatively studying translation elongation kinetics are commonly employed to understand how mRNA sequence affects translation elongation and its impact on co-translational pathways.

1.2 Codon Optimality and Amino Acids Sequence Affect Translation Elongation Kinetics

Translation elongation is a complex and highly regulated process that can be influenced by a variety of factors which could be broadly categorized as molecular factors (such as amino acid sequence, codon usage, tRNA availability) (Choi et al., 2018; Neelagandan et al., 2020), regulatory factors (such as RNA binding proteins, and MicroRNA) (Fabian et al., 2010; Xu et al., 2022) and environmental factor (such as temperature, PH and ion concentration) (Starosta et al., 2014; Xu et al., 2022). Understanding the effects of these factors on translation elongation is crucial for

elucidating the underlying mechanisms of protein synthesis and for developing strategies to modulate this process. Furthermore, in these three categories, molecular factors have been widely investigated for decades since they directly affect the translation process by influencing the efficiency and speed of protein synthesis.

In some cases, certain amino acid sequences may be less optimal for translation elongation by interfering peptide bond formation and leading to ribosomal stalling. For example, proline is a typical poor amino acid both as donor and accepter when it participates in peptide formation (Pavlov et al., 2009). The cryo-EM structure of ribosome processing in translational elongation with mRNA demonstrates that translating ribosomes can stall when encountering polyproline (PPP) sites. (Huter et al., 2017). Local resolution of peptidyl transferase center (PTC) of ribosome suggests that the favored polyproline conformation is incompatible with the peptide exit tunnel of the ribosome. This incompatibility ultimately destabilizes peptidyl-tRNA loading and prevents the accommodation of new aminoacyl-tRNA (Huter et al., 2017); When hindered by poor amino acids, ribosomal stall can occur more frequently, leading to a reduction in protein synthesis, unless being rescued by the recruitment of specific factors. Eukaryotic initiation factor 5A (eIF5A) is thought to be a key factor in alleviating ribosomal stall induced by proline-rich motifs (Gutierrez et al., 2013), similar to elongation factor P (EF-P) for bacteria (Ude et al., 2013). In addition to sequential proline sequence, recent studies also reveal that the newly generated positively charged amino acids, such as polylysine, in the nascent peptide can also impede translational elongation due to their electrostatic interaction with the ribosomal exit tunnel (Charneski & Hurst, 2013). In this

scenario, premature translation termination, which was activated and mediated by Release Factor eRF3, triggers to promote release of C-terminally truncated translation products from ribosomes stalled on polylysine segments (Chiabudini et al., 2014).

Along with the amino acids sequence, another molecular factor, the codon usage, also plays crucial roles in mediating translation elongation kinetics. Codons are the three-nucleotide sequences in mRNA molecules that code for a specific amino acid during protein synthesis. Due to the degeneracy of the genetic code, meaning that multiple codons can code for the same amino acid, the term "synonymous codons" is used to describe codons encoding the same amino acid. Furthermore, it has been confirmed that synonymous codons are not equally distributed in the genome, and the frequency of codons in the mRNA transcriptome, referred to as codon usage or bias, is proposed to significantly influence the translation efficiency and downstream co-translational effects (Y. Liu et al., 2021). Codon usage affects translation elongation through multifaceted ways, including copy number of respective isoacceptor tRNA and affinity of codon-anticodon coupling (dos Reis et al., 2003). On one hand, The tRNA availability is proposed to be the major determinant of codon usage, meaning that rare codons (also named as nonoptimal codon) are less frequently used in specific organisms and believed to inhibit translation efficiency because an nonoptimal codon site may spend more time recruiting a tRNA molecule with low copy number, while more frequently used optimal codons may speed up the process (Hershberg & Petrov, 2008; Ikemura, 1985). On the other hand, translation of some codons, such as arginine CGA, has been found to be inhibited primarily through its weaker wobble base pairing with $tRNA^{Arg}$(ICG)

(Letzring et al., 2010). Beyond this straightforward mediation in translational elongation, the effects of codon usage on co-translational behaviors are more complicated. For example, recent studies suggest that the codon usage impacts local translational dynamics, which coordinates with the co-translational folding of nascent proteins to facilitates proper protein folding (Pechmann & Frydman, 2013; Yu et al., 2015). Reversely, synonymous codon substitutions or mutations may impair cell fitness by significantly perturbing co-translational protein folding (Komar et al., 1999; Walsh et al., 2020). More investigations also underly the regulation of codon usage on mRNA stability, protein trafficking and so on (Komar et al., 1999; Plotkin & Kudla, 2011).

1.3 Translation Elongation Mediates Protein and RNA Surveillance Pathways

During translation, multiple ribosomes are concurrently translating across a single mRNA molecule and a ribosome usually do not uniformly read through mRNA. Transient ribosomal pauses or stalls, referring to a phenomenon in which the ribosome slows down upon encountering an obstacle in the mRNA transcript, are widespread across transcripts. (Gardin et al., 2014; Hanson & Coller, 2018; Li et al., 2012). Transcriptome-wide studies using techniques such as ribosome profiling suggest that nearly 10% of translating ribosomes become trapped in a di-some state when encountering stalled sites, such as sequences enriched with polyproline, or nonoptimal codons discussed in previous sections. In such scenarios, the leading ribosome can decelerate or stall and ultimately collide with a trailing ribosome, resulting in a unique di-some conformation state (Arpat et al., 2020; P. Han et al., 2020; Zhao et al., 2021). Ribosomal pauses can be functional in ensuring

the proper function of cellular proteins (Rodnina & Wintermeyer, 2016). For example, a ribosomal pause may offer time for the nascent protein chain to recruit molecular chaperones or attain a proper conformation before continuing with translation. This can be important for proteins that require complex or multi-domain structures to prevent the misfolding or aggregation of the protein chain (Komar, 2019; Y. Liu, 2020). Sometimes, the mature N-terminus of s nascent peptide acts as a targeting signal, which recruits signal recognition particles (SRP) and helps co-translational targeting or translocation to a specific organelle or location within the cell, such as the endoplasmic reticulum (ER) or mitochondrion (Nyathi et al., 2013). In other cases, detrimental ribosomal stalling may happen as a consequence of genetic mutations or chemical damage, which disrupts natural protein synthesis and cellular function through production of truncated or misfolded proteins (Eshraghi et al., 2021; Ishimura et al., 2014; P. B. Martin et al., 2020). To avoid aggregation of aberrant proteins and non-functional mRNA, surveillance pathways take place to maintain cellular homeostasis.

When ribosomes encounter a problematic mRNA region, such as a rigid mRNA structure or a nonoptimal codon sequence, they can stall or even collide during translation. This event may trigger the ribosome-associated quality control (RQC) pathway and No-go decay (NGD) pathway, which work to rescue stalled or collided ribosomes and degrade aberrant mRNA and nascent proteins, thereby maintaining homeostasis intracellularly. The first step of the surveillance pathways is to sense and rescue stalled ribosome. It has been suggested that RQC and NGD pathways could be concurrently triggered when the conformation of collided ribosomes are sensed

by the E3 ubiquitin ligase Hel2 in yeast *Saccharomyces cerevisiae* (or ZNF598 in mammals) (Matsuo et al., 2017; Sundaramoorthy et al., 2017). It has also been proposed that the recruitment of Hel2 (ZNF598) can arrest stalled ribosome and mediate polyubiquitination of uS10 protein of 40S ribosomal subunit, which ultimately activates both RQC and NGD pathways (Ikeuchi, Tesina, et al., 2019; Simms et al., 2017; Tomomatsu et al., 2023). The next step of RQC and NGD pathways is to dissociate the collided ribosome.

In RQC pathway, RQC-trigger (RQT) complex which consists of RNA helicase Slh1 (Rqt2), the ubiquitin-binding protein Cue3 and Rqt4 protein, is shown to be responsible for dissociating polyubiquitinated stalled ribosomes into 60S-associated nascent protein and 40S subunit (Hashimoto et al., 2020; Juszkiewicz et al., 2020; Matsuo et al., 2020). The resolution of 60S-associated nascent protein is proposed to be initiated by binding of Rqc2 (NEMF) which facilitates recruitment of E3 ligase Ltn1 (Listerin) to ubiquitinate nascent peptide in concerted action with Rqc1 (TCF25) (Brandman et al., 2012; Shao et al., 2015). In addition, Rqc2 also mediates synthesizing of C-terminal alanine and threonine tails (CAT tailing) which has been suggested to act as a fail-safe mechanism for effective ubiquitination by Ltn1 (Kostova et al., 2017; Shen et al., 2015). Interestingly, a recent cryo-EM structure revealed that eIF5A, a universal translation-promoting factor, also acts as a eukaryotic RQC factor, being required for efficient peptidyl transfer during the synthesis of CAT tailing (Tesina et al., 2023). The ubiquitinated peptides are then extracted by AAA ATPase Cdc48 (VCP/p97) and its cofactors after releasing of the conjugated peptidyl-tRNA by Vms1 (ANKZF1) (Brandman et al., 2012; Defenouillère et al., 2013, 2016;

Verma et al., 2013, 2018). Finally, the dissociated and ubiquitinated peptide can be degraded by the proteasome (Klaips et al., 2017).

As for NGD pathway, dissociation of stalled ribosome is initiated by recruitment of a ternary complex which is composed of Dom34 (Pelota), Hbs1, Rli (ABCE1) and GTP (Harigaya & Parker, 2010; Pisareva et al., 2011; Shoemaker et al., 2010). Structural insights into RNA quality control pathway revealed that Dom34:Hbs1 complex senses and bind to an empty ribosome A-site to activate ribosome split (Hilal et al., 2016; Tsuboi et al., 2012; van den Elzen et al., 2010). It has been recently reported that Syh1 responds to collided ribosome in NGD to connect severe translational blocks with mRNA decay (Veltri et al., 2022). While the loss of Syh1 results in the activation of Hel2-dependent endonucleolytic NGD by Cue2 (NONU-1) which cleaves mRNAs at stalled ribosome site into 5'NGD intermediate and 3'NGD intermediate during NGD pathway (D'Orazio et al., 2019; Glover et al., 2020). After dissociation of stalled ribosome, the degradation of 5'NGD intermediate is mediated through the SKI complex and exosome, while 3'NGD intermediate is degraded by the exonuclease Xrn1 (Doma & Parker, 2006; Ikeuchi, Izawa, et al., 2019).

While insights into protein and RNA rescuing pathways have been widely investigated for decades, whether and how do RQC and NGD happen in a single stalled site of mRNA transcript is still poorly understood. A recent study investigated collided ribosomes which undergoes Hel2-driven quality control pathway, proposed that NGD can be but isn't necessary to be coupled with RQC (Ikeuchi, Tesina, et al., 2019). Even though Hel2-mediated polyubiquitination is required

both for RQC-coupled NGD (named as NGD^{RQC+}) and RQC-uncoupled NGD (named as NGD^{RQC-}), NGD^{RQC+} is distinct from NGD^{RQC-} due to differences in ubiquitinated and endonucleolytic cleavage sites (Ikeuchi, Izawa, et al., 2019). In NGD^{RQC+} pathway, endonucleolytic cleavage occurs at sites within stalled disome unit and this mRNA cleavage is dependent on Hel2-mediated polyubiquitination of uS10 of leading ribosome, while in NGD^{RQC-} pathway, cleavages occur upstream of the stalled disome which requires polyubiquitination of ribosomal protein eS7 (Ikeuchi, Izawa, et al., 2019). Further investigation confirmed that the two modes of NGD are mediated by Cue2-induced mRNA cleavage (Tomomatsu et al., 2023). In addition, it is also implicated that the NGD^{RQC+} pathway generates a 5'NGD intermediate with trailing ribosome which is split by Dom34:Hbs1 complex and a 3'NGD intermediate with leading ribosome which may undergo RQC pathway (Eisenack & Trentini, 2023; Ikeuchi, Izawa, et al., 2019).

1.4 Codon Optimality Couples Translation and mRNA Stability through COMD

The effects of codon optimality on translation elongation have been introduced systematically in previous sections. Briefly, codon optimality which refers to the non-uniform decoding rate of 61 codons by the ribosome, can lead to non-uniform translation elongation rates (Hanson & Coller, 2018). When ribosomes encounter optimal codons, which are recognized efficiently by the corresponding tRNAs, they can rapidly incorporate amino acids into the growing polypeptide

chain. This results in a faster movement of the ribosome along the mRNA during translation. Reversely, nonoptimal codons can lead to slower translation elongation speed by impeding ribosome movement because of the inefficient recruitment or shortage of tRNA. Therefore, codon optimality is proposed to play an important role mediating the kinetics of translation elongation and protein production (Choi et al., 2018; Neelagandan et al., 2020).

Along with translation elongation, it has also been established that codon optimality is a major determinant of mRNA stability. Using genome-wide RNA decay analysis, the correlation between mRNA half-life and codon optimality of coding genes can be revealed (Hanson et al., 2018; Presnyak et al., 2015). In addition, it is also suggested that the DEAD-box protein Dhh1 (DDX6 in human), which is a decapping regulator, senses codon optimality to couple mRNA degradation and translation elongation (Radhakrishnan et al., 2016; Sweet et al., 2012). Another pathway that has been investigated and confirmed to mediate mRNA degradation is initiated by shortening of the poly(A) tail of mRNA transcript via Ccr4-Not deadenylase complex, of which components such as Not5 are implicated to bind to certain decapping activators and promote mRNA decapping (Alhusaini & Coller, 2016; Passmore & Coller, 2022). Taken together, a codon-optimality-mediated mRNA degradation (COMD) pathway was implicated.

The initiation of COMD pathway is thought to be the monitoring of Ccr4-Not complex across translating ribosomes. Structural analysis by cryo-EM revealed that the recruitment of Ccr4-Not complex to ribosome is induced by engagement of Not5 subunit to the E-site only when the translating ribosome lacks an A-site tRNA (Buschauer et al., 2020). This unique ribosome

conformation implies the correlation between codon optimality and recruitment of Ccr4-Not complex, because a nonoptimal codon-induced ribosomal pause can lead to the lack of new A-site tRNA binding even after dissociation of tRNA from E-site of ribosome, where the Not5 subunit can bind to (Buschauer et al., 2020). Thus, it is the A-site tRNA decoding rate that directly drive mRNA decay during translation (Hanson et al., 2018). Additionally, A-site occupation also distinguishs the E-site recruitment of Not5 and eIF5A, since eIF5A has preference to vacant E-site when peptidyl transfer of A-site tRNA is stalled by polyproline sequence (Buschauer et al., 2020; Schmidt et al., 2016). Upon recruitment of the Ccr4-Not complex, an exonuclease (such as Ccr4 and Caf1) within the complex shortens the poly(A) tail of the mRNA transcript and dissociate its poly(A)-binding proteins (Pab1, or PABPC in mammalian), which had been bound to the poly(A) tails to protect mRNA from degradation and activate specific translation initiation factors (Caponigro & Parker, 1995; Sachs & Davis, 1989; Webster et al., 2018). By this way, the engagement of Ccr4-Not complex triggers deadenylation of poly(A) tails and association of decapping machinery, such as Dhh1, to 5'cap of mRNA, which is followed by degradation of mRNA from 5'end through 5'-3' exoribonuclease 1(Xrn1) or from 3' end through cytoplasmic exosome complex (Bae & Coller, 2022; Passmore & Coller, 2022).

1.5 Mitochondrial Import System and Impot Stress Response

Mitochondria are crucial organelles in eukaryotic cells, containing hundreds of proteins that play essential roles in metabolic processes such as oxidative phosphorylation, TCA cycle β-

oxidation and so on. Mitochondria exhibit a dual-membrane configuration comprising the mitochondrial outer membrane (MOM) and mitochondrial inner membrane (MIM). These membranes enclose two distinct aqueous compartments within the mitochondria: the intermembrane space (IMS) and the mitochondrial matrix (MM). The inner membrane is organized into cristae, which house the respiratory chain complexes, while the region underlying the outer membrane facilitates the exchange of metabolites, proteins, and lipids between mitochondria and the rest of the cell. Because of their crucial role in cell metabolism, any damage to mitochondria and the subsequent dysfunction they experience become significant factors contributing to various human diseases, such as neurological disorders and ageing-related disorders (Balaban et al., 2005; Griffiths & Levy, 2017).

The mitochondrial genome displays significant diversity among various eukaryotic organisms. In most eukaryotic species, including yeast and humans, mitochondria possess a compact genome responsible for expressing only a limited number of proteins when compared to the overall cellular DNA. Within *S. cerevisiae*, the mitochondrial DNA (mtDNA) is responsible for encoding eight proteins, of which seven function as subunits within the electron transport chain and oxidative phosphorylation (Foury et al., 1998). These proteins are exceptionally hydrophobic membrane proteins, which cannot be produced as precursors in the cytosol. Instead, they are co-translationally integrated into the inner membrane by mitochondrial ribosomes and remain tightly bound to the inner membrane during this process (Pfeffer et al., 2015). All other mitochondrial proteins (mitoproteins) are encoded by the nuclear genome, synthesized by cytosolic ribosomes, then

targeted to receptors on the mitochondrial surface, and finally transported across or inserted into the outer and inner mitochondrial membrane. As nuclear-encoded mitoproteins have distinct destinations to the mitochondria, mitoprotein recognition, targeting, and import are significant processes to finally acquire correct mitochondrial functions.

In general, mitoproteins are imported in an unfolded state, with chaperones and folding factors aiding this process by keeping them import-competent and facilitating their binding to receptor proteins on the MOM (Cichocki et al., 2018; Jores et al., 2018). These proteins are synthesized with targeting signals that guide them to specific compartments within the mitochondria, and a significant portion of them possess a mitochondria-targeting sequence (MTS) at their N-terminal. Furthermore, recent studies also propose the existence of internal MTS-like sequences that also help mitoproteins import and translocate to different compartments (Backes et al., 2018; Boos et al., 2018). In addition to distinct destinations within mitochondrion after import, the precursors of mitoproteins, which remain unfolded and import-competent, are targeted to translocase of the outer membrane (TOM) of mitochondrion through multiple pathways, including post-translational targeting, co-translational targeting and ER-mediated mitochondrial targeting (Hansen & Herrmann, 2019).

For decades, it has been well-known that most mitoproteins are synthesized on cytosolic ribosomes and are post-translationally imported into the organelle (Gold et al., 2017). A series of investigations propose that it is the cytosolic chaperones, such as HSP40, HSP70 and HSP90 families, that are recruited to precursors to prevent spontaneous folding and maintain in import-

competent conformation facilitating its recognition by TOM complex to translocate, while mutants in those chaperones may trigger import defects or aggregation of precursors (Deshaies et al., 1988; Opaliński et al., 2018; Young et al., 2003). In addition to post-translational manner, a portion of mitoproteins, especially some MIM proteins, have been reported to be imported co-translationally (Gadir et al., 2011; Zabezhinsky et al., 2016). It was proposed that the nascent chain-associated heteromeric complex (NAC), functioning as a chaperone, can simultaneously bind to ribosomes and nascent polypeptides within the ribosomal exit tunnel, which was suggested to facilitate the tethering of translating ribosomes to the MOM by associating with the MOM protein Om14 (Gamerdinger et al., 2019; Lesnik et al., 2014). Meanwhile, an RNA-binding protein called Puf3, interacts with a specific motif in the 3'UTR of some mRNAs encoding mitoproteins to facilitate this reaction (García-Rodríguez et al., 2007; Saint-Georges et al., 2008). Interestingly, the natural existence of a polyproline sequence within Tim50 has been observed to pause translation elongation and promote co-translational import, which indicates that translation itself plays a role in mediating co-translational targeting (Tsuboi et al., 2020). Further investigations reveal the effects of endoplasmic reticulum (ER) surface on mitoproteins import. The ER is found to actively facilitate intracellular targeting of precursor proteins from ribosomes to mitochondria, with J protein Djp1 from ER to recognize and deliver precursors (Hansen et al., 2018). In summary, diverse targeting mechanisms of mitoproteins have been identified after decades of studies, however, the details of the import pathway, especially ER-mediated pathway, remain poorly understood and require further investigations for clarification.

As an essential organelle for energy production and macromolecular synthesis, stressful stimuli, mutations in translocase components, or excessive precursor loads can clog the translocases, leading to impaired mitochondrial import which results in proteotoxic effects both inside and outside the mitochondria, as unfolded precursors accumulate on the translocases and in the cytosol (Barba-Aliaga & Alepuz, 2022; Bogorodskiy et al., 2021; Lu & Guo, 2020). To counteract these effects, cells have evolved several stress responses, such as mitochondrial precursor overaccumulation stress (mPOS) (X. Wang & Chen, 2015), unfolded protein response activated by mistargeting of proteins (UPRam) (Wrobel et al., 2015), mitochondrial unfolded protein response (mtUPR) (Münch & Harper, 2016), and mitochondrial compromised protein import response (mitoCPR) (Weidberg & Amon, 2018). Triggering of these stress responses helps restore and maintain cellular homeostasis by increasing the activity of chaperones or proteasome to remove accumulated precursors.

1.6 Stress Response and mRNP

Cells often encounter fluctuating and potentially harmful environmental conditions rather than stable and optimal conditions. These environments expose cells to diverse types of stressors, such as nutrient deprivation, heat shock, toxins, pathogens, and osmotic imbalances (Alagar Boopathy et al., 2022; Majmundar et al., 2010; Richter et al., 2010; Russell et al., 2014). To ensure their survival in the face of adverse changes, cells must quickly modify their gene expression to maintain internal stability. This adaptive reprogramming triggered by disruptive or unfavorable external

fluctuations is commonly known as the stress response. The cellular stress response usually involves a slowdown or halt in growth, accompanied by a suppression of overall protein synthesis. However, specific genes vital for cell survival and repair undergo significant induction during this process. For example, elevated cellular temperature (or heat shock) can cause the denaturation of proteins and disrupt metabolic activity, leading to an upsurge in reactive oxygen species that can harm various biological macromolecules, including proteins (Somero, 2020). To manage the increased burden of unfolded and misfolded proteins, cells can trigger the heat shock response (HSR) which refers to activation of heat shock proteins (HSPs) as molecular chaperone to promote protein folding (Alagar Boopathy et al., 2022; Rosenzweig et al., 2019). Concurrently, as the overall translation is suppressed, numerous regulatory proteins and mRNAs undergo a phenomenon known as phase separation. This process leads to the creation of concentrated cytoplasmic structures, commonly referred to as granules or foci. When the cell is under stress, this phase separation mechanism selectively segregates proteins and mRNAs in a manner that holds functional significance for the cell's survival. As a result, these structures have become a topic of growing interest. Although many advancements have been made in recent years to identify the proteins and mRNAs residing within these granules, as well as the physical characteristics governing their formation, our understanding of the phenotypic and functional consequences arising from their generation during stress remains limited. Consequently, the extent to which they contribute to the cellular stress response remains largely unknown.

Stress granules (SGs) and processing bodies (PBs) are two types of membrane-less messenger

ribonucleoprotein (mRNP) granules that undergo liquid-liquid phase separation under stress condition. These granules are primarily composed of RNA-binding proteins (RBPs), non-translating mRNAs, and are nucleated through interactions involving RNA-RNA, RNA-protein, and protein-protein interactions (Begovich & Wilhelm, 2020; Guzikowski et al., 2019). SGs and PBs have been proposed to be distinct yet closely related mRNP granules. For example, in both mammals and yeast, PBs and SGs are found to only share 10% - 25% of their protein components, while proteomic studies revealed high enrichment of RBPs and proteins containing intrinsically disordered regions within the shared components (Guzikowski et al., 2019). It is has been revealed that formation of SGs and PBs is consistently driven by impaired translation initiation through various methods, including stress responses (N. L. Kedersha et al., 1999; Zid & O'Shea, 2014), addition of some small molecules to block translation initiation (Dang et al., 2006; Mazroui et al., 2006), genetic knockdown of specific translation initiation factor proteins (Mokas et al., 2009) and overexpression of RBPs that represses translation (Gilks et al., 2004; Wilczynska et al., 2005). Interestingly, there is an investigation suggests PBs can promote stress granule assembly (Buchan et al., 2008), while another study argued that PBs and SGs assembly occur by independent and differentially regulated pathways (Shah et al., 2013). This contradictory result supports the notion that mRNP granules are distinct yet closely related, while also indicating the complexity involved in their characteristics and formation.

SGs are thought to form by means of nontranslating mRNAs acting as frameworks for RBPs, which interact with each other through a variety of protein-protein interactions (Panas et al., 2016;

Protter & Parker, 2016). At the same time, PBs also show very similar transcriptome to SGs under stress condition (Matheny et al., 2019). Thus, based on a current model of mRNA localization within these granules, it is speculated that the formation of RNA-RNA interactions can be hindered due to the steric obstruction caused by ribosomes during elongation (Khong et al., 2017; Van Treeck et al., 2018). Once translation initiation is impaired by stress condition, ribosomes already engaged with transcripts will persist in elongation and eventually disengage, leaving the transcripts vulnerable to RNA-RNA interactions. In addition, t-Transcripts that are free of ribosomes will subsequently combine with other RBPs, initiating the formation of these mRNP granules. This model could explain why transcriptome studies show enrichment of longer poorly translated transcripts and mRNAs with lower ribosome density (Khong et al., 2017; Matheny et al., 2019). Studies on polysome engagement also further confirm this speculation, for example, the addition of cycloheximide, which inhibits ribosomal translocation and traps mRNAs in polysomes, can suppress the formation of both PBs and SGs, and it can even disassemble preexisting granules (Teixeira et al., 2005). Conversely, the introduction of puromycin, a drug that separates ribosomes from mRNAs, actually induces the formation of SGs (N. Kedersha et al., 2000).

Another universal feature of stress response is transcriptional upregulation of genes that encode proteins important for survival, such as heat shock genes, while overall translation is repressed (Arribere et al., 2011; Ashe et al., 2000). An interesting question is: How are the transcription and translation of different classes of genes related to mRNA localization and mRNP formation under stress conditions? In our previous discovery, we observed that when yeast

undergoes glucose starvation, the promoter sequences assume a vital role in determining the destiny of mRNAs within the cytoplasm (Zid & O'Shea, 2014). Using ribosomal profiling and microscopy, mRNAs that are actively transcribed before glucose deprivation (class III, e.g., PGK1, PAB1) demonstrate limited translation efficiency and exhibit a tendency to localize to P-bodies. In contrast, mRNAs induced by stress display two distinct patterns of response: mRNAs from most heat shock genes (class I, e.g., HSP30, HSP26) undergo transcriptional induction, active translation, and remain dispersed throughout the cytoplasm. However, class II mRNAs, also induced transcriptionally under stress, become sequestered within both P-bodies and stress granules, showing reduced translation activity. Notably, class II mRNAs are particularly enriched in functions related to alternative glucose metabolism, such as GSY1 and GLC3. Concurrently, based on the model of RNA incorporation into mRNP granules and recent studies, it is suspected that translatability serves as the primary driving force for mRNA localization during stressful conditions (Matheny et al., 2019). Interestingly, the promoter sequences-mediated transcription and translatability-driven mRNA localization occur in distinct cellular compartments, which implies transcripts are imprinted in a co-transcriptional manner to ultimately determines their fate within the cytoplasm. Therefore, we propose the existence of factors that interact with promoters and undergo co-transcriptional loading onto mRNA before it is exported from the nucleus.

1.7 Tools or Methods to Quantify Translational Elongation Speed

In previous sections, we have discussed the important effects of codon optimality on mediating

translation kinetics, such as the speed of translation elongation and protein production. In addition, upon fine-tuned movement of ribosomes across mRNA transcripts, amounts of co-translational pathways can happen, which further regulates translation efficiency and protein fidelity. For example, accumulation of non-optimality codons, such as CGA, could suddenly stall ribosomes and even lead to ribosome collision, which triggers surveillance pathways, such as RQC and NGD, to avoid aggregation of truncated polypeptide and harmful mRNA transcripts. Furthermore, it is proposed that weak ribosomal pauses play important effects determining mRNA half-life by inducing COMD pathway, which further influences elongation rates and protein expression levels. Taken together, we hypothesize that translation elongation stalls, or in other words, the elongation duration of stalled ribosomes, are directly sensed by various co-translational factors. This sensing then triggers distinct co-translational pathways that regulate translation kinetics and proteomics. Thus, quantitatively monitoring elongation duration is a wonderful way to acquire valuable insights into the function of specific genomic sequences and how cells determine co-translational pathways.

1.7.1 Metabolic Labeling

Investigations on tools to quantify translational elongation can be traced back to 1960s using metabolic labeling techniques. By labeling newly synthesized proteins with isotopically labeled amino acids and monitoring the incorporation over time, the speed of translation elongation can be estimated. In 1968, Lacroute and Stent used pulse-labeling followed by electrophoresis to measure peptide chain growth rate of β-galactosidase in exponentially growing *E.coli* (F.

LACROUTE & G. S. STENT, 1968). In the next few decades, this technique was widely utilized to monitor translational elongation in *E.coli*, while only average elongation rate of a molecular weight section (Gatsing, 1972; Schleif et al., 1973) or relative differential rates of peptides (Lemaux et al., 1978; O'Farrell, 1975) were obtained. Until 1984, Perdersen acquired translational elongation rate of individual protein based on pulse-chase method and two-dimensional gel system which was developed in 1975 (O'Farrell, 1975; Pedersen, 1984). With elongation rate of single genes quantified, Perdersen quantitatively verified that the translation rate changes varied by codon optimality. In recent years, mass spectrometry, as an advanced analytic method for proteins, is widely used for investigating the proteome. For example, pSILAC (pulsed stable isotope labeling by amino acids in cell culture) was developed in 2009 to directly quantify protein translation on a proteome-wide scale in both Hela and Yeast cell (Schwanhäusser et al., 2009). Using metabolic labeling techniques, translation elongation speed can be quantitatively measured in a variety of cell types and conditions, while incorporation of labeled amino acids into proteins may introduce metabolic changes that affect translation dynamics. Moreover, these metabolic labeling techniques don't allow to capture real-time translation dynamics, which limits further understanding of translation.

1.7.2 Ribosome Profiling

Ribosome profiling, also known as Ribo-seq, is a powerful technique that allows genome-wide analysis of in-vivo translation and involves sequencing of mRNA fragments protected by ribosomes. By comparing the distribution and density of ribosome footprints along the mRNA,

researchers can estimate translation elongation rates. During a ribosome profiling procedure, the ribosome-protected mRNA fragments are recovered and quantitatively measured by next-generation sequencing for precise measurements (Ingolia et al., 2009). This technique is further improved to monitor the kinetics of in-vivo translation by taking a variety of snapshots of ribosome dynamics across time, by which an average ribosome progression speed of 5.6 aa/s can be measured (Ingolia et al., 2011). Due to the universal biophysical properties of ribosome across species, ribosome profiling is highly adaptative across species, such as bacteria, Mouse and Human (Ingolia et al., 2011; Li et al., 2014; Lian et al., 2016). Another significant benefit of ribosome profiling is the abundant and detailed information it can yield, such as identification of ribosomal pause sites and regulatory elements. Compared with the global and steady-state level of mRNA and protein measured by metabolic labeling techniques, ribosome profiling reveals the sequencing readout of all ribosome positions at genome-wide scale and instantaneous ribosome dynamics of a series of snapshots during translation, while real dynamic change in translation elongation speed is still difficult to quantify using Ribo-seq. In addition, bioinformatics analysis and additional normalization steps are also time-consuming.

1.7.3 Fluorescence Microscopy

Based on ribosome profiling and other advanced technologies, investigations on translation regulation have made great progress in recent years, while most studies on translational elongation presume a pool of homogenous translating mRNA. New insights into the regulation of translation reveals the heterogeneity of mRNA transcripts (Yan et al., 2016). mRNA molecules transcribed by

the same gene may behave differently by alternative transcriptional start sites (Rojas-Duran & Gilbert, 2012), post-transcriptional modifications (Franks et al., 2017), or regulations through RNP complexes (Tauber et al., 2020) and so on. Additionally, mRNA molecules won't act the same way across time and space. It has been suggested that individual mRNA may translate non-continuously (Tatavarty et al., 2012)and its activity is highly adjusted by localization state (Hüttelmaier et al., 2005). Considering the heterogeneity, developing methods to acquire long-term monitoring of translation of single mRNA molecule in-vivo is desirable.

A fluorescent tagging system has long been used for monitoring real-time translation, including quantifying the average protein synthesis rate and imaging the first round of translation. (Chao et al., 2012; Halstead et al., 2015; K. Han et al., 2014). This method involves tagging specific components of the translation machinery, such as the ribosome or the elongation factors, with fluorescent molecules. By tracking the movement of individual ribosomes or associated factors, their speed can be quantitatively determined. Because of the low signal-to-noise fluorescence and long maturation time of existing fluorescence proteins, it is a huge trouble to achieve long-term imaging of translation with single mRNA resolution. Since 2014, new fluorescent tagging systems, such as SunTag (Tanenbaum et al., 2014), TRICK reporter (Halstead et al., 2015) and MoonTag (Boersma et al., 2019), were developed to visualize translation of individual mRNA molecules over time (Morisaki et al., 2016; B. Wu et al., 2016; Yan et al., 2016). In those studies, translational elongation rates (3~10 aa/s) of different genes in single mammalian cells were quantified in-vivo. Through single molecular imaging, real-time measurements of translation elongation speed in live

cells are acquired. Additionally, more detailed information about translation is available, including dynamic changes in translation speed and spatial information about translation within the cellular context. However, there are still some drawbacks, such as the altered natural cellular environment by fluorescent tagging and challenge to track ribosomes over long periods or at high throughput.

1.7.4 Cell-free In-vitro Translation System

Cell-free translation systems involve extracting the necessary components from cells, such as ribosomes, initiation factors, elongation factors, and amino acids, and combining them in a test tube or reaction mixture. This allows researchers to monitor translation processes outside the confines of living cells, providing greater control, and easier measurement of translation elongation speed. In 1997, Zhong Wang and Matthew S. Sachs developed a cell-free in-vitro translation system using luciferase as reporter (Z. Wang & Sachs, 1997). Compared with fluorescence, luciferase is more advantageous to quantitative measurement because it has higher signal-to-noise, larger dynamic rage, and shorter half-life (Fleiss & Sarkisyan, 2019; X. Wang et al., n.d.). This cell-free in vitro translation system is then widely applied in studying widespread areas of translational regulation, such as upstream open reading frame (uORF) (Hood et al., 2009; Z. Wang & Sachs, 1997; C. Wu et al., 2007), ribosomal stall (Z. Wang et al., 1999) and codon selection (Wei et al., 2013). In 2015, Chien-Hung Yu et al directly visualized mRNA translational speed influenced by codon usage using this cell-free in-vitro translation system (Yu et al., 2015). Benefit from the quick co-translational folding of luciferase, Chien-Hung Yu et al suggested that the difference in TFA values (time of first appearance, which indicates the first time point when

significant luciferase signal is observed) could reflects the difference in translation elongation speed of two mRNA transcripts. By this way, translation elongation of a coding gene or effects of certain genomic elements, such as stem loops, on translation elongation can be quantitatively measured. In summary, cell-free in-vitro translation system contains some special benefits, such as providing a controlled environment for studying translation and allowing manipulation of translation components and conditions. At the same time, in-vitro assay doesn't perfectly reflect translation dynamics in living cells, because of the lack of some factors or regulatory elements and missing of the real cellular context. Reversely, because of the complexity of intracellular conditions and interval readout of luciferase signal, similar in-vivo assay using luciferase reporter is usually less consistent and less applicable.

Upon comparison of a series of techniques for quantifying translation elongation, we realized that the need for a method that enables in-vivo quantitative measurement of translation elongation with high throughput, minimal time consumption, and simple operations. For that purpose, we attempted to conduct luciferase assay to trace elongation within an in-vivo system and employed data analysis known as Schleif Plot to yield significant results (Schleif et al., 1973; Z. Wang & Sachs, 1997).

1.8 Dissertation Overview

Post-transcriptional and co-translational regulations stand as potent and flexible mechanisms, enabling precise fine-tuning of gene expression to align with the specific requirements of cells and their surrounding environment. In this dissertation, I employ a range of biochemical and molecular biology techniques to delve into the mechanistic regulation of translation, including how translation is mechanistically regulated by both mRNA and protein factors and how translational kinetics mediates induction of co-translational pathways. In Chapter 2, I developed an in-vivo elongation reporter in *Saccharomyces cerevisiae*, allowing for the quantitative monitoring of translation elongation duration and protein expression. Based on this elongation reporter, we quantified the elongation delay induced by poly-CGA and demonstrated that the stalling triggers a Hel2-driven surveillance pathway to rescue the elongation stall. Simultaneously, we quantitatively measured another elongation stall triggered by stem-loop structure of the translating mRNA, while further investigations propose inducing of a non-Hel2-mediated pathway. Chapter 3 centers on the study of co-translational mRNA localization of nuclear encoded mitochondrial proteins, particularly investigating co-translational import. It proposes that translational kinetics, such as elongation delays caused by polyproline sequences in Tim50, play a significant role in mediating co-translational import. Furthermore, the research explores the effects of elongation stalls on mitochondrial import stress and the activation of relevant quality control pathways. In Chapter 4, I focused on understanding the mechanism behind the formation of cytosolic mRNP granules under glucose deprivation conditions. The study involved using CRISPRi to down-regulate the

expression of RVB, confirming its crucial role in determining the fate of mRNA localization after glucose depletion. Taken together, these chapters contribute to a better mechanistic understanding of regulations of co-translational and post-transcriptional behaviors intracellularly. In particular, our advancement in the elongation assay will provide invaluable assistance to future researchers in gaining a more quantified understanding of how cellular machinery manages elongation stalling.

Chapter 2 Quantification of Elongation Stalls and Impact on Gene Expression in Yeast

2.1 Abstract

According to what we have discussed in the introduction section, it has been confirmed that ribosomal pauses or stalls can be induced by a variety of factors, especially accumulation of nonoptimal codons. These ribosomal pauses have been found to play a vital role in triggering various co-translational processes, such as protein folding and localization. Nevertheless, prolonged pauses can give rise to ribosome collisions, triggering the activation of pathways that rescue ribosomes and degrade both proteins and mRNA. Although this connection has been acknowledged, the precise threshold distinguishing acceptable pauses from the initiation of rescue pathways remains unquantified. In this study, we have employed a modified version of a technique used to measure elongation time for evaluating the consequences of elongation stalls in *S. cerevisiae*. Our study reveals that transcripts with pronounced, localized stalls experience a Hel2-dependent reduction in protein and mRNA expression, accompanied by an elongation delay that is dose-dependent. Conversely, transcripts with synonymous substitutions to nonoptimal codons show decreased protein and mRNA expression, along with a similar increase in elongation delay, albeit through a mechanism independent of Hel2. These findings indicate that distinct distributions of unfavorable codons within a transcript can trigger varying rescue pathways, despite similar durations of elongation stalls. Further examinations on a particular transcript harboring dispersed

nonoptimal codons reveals a strong ribosomal stall induced by a weak stem loop sequence, which implies the existence of an unknown mechanism wherein RNA secondary structure provokes a stall in ribosome progression. Furthermore, we find that Dhh1 selectively impacts different types of stalls. Collectively, these findings offer fresh quantitative understanding of mechanisms involved in translation surveillance and the specific functions of Hel2 and Dhh1 in mediating ribosomal pause events.

2.2 Introduction

Translation is a vital biological process that converts mRNA into proteins. Proper regulation of protein production is crucial for cell survival, while errors in translation can result in genetic disorders and diseases related to faulty proteins (Eshraghi et al., 2021; Ishimura et al., 2014; Stein & Frydman, 2019). In eukaryotic cells, translation takes place in the cytoplasm and involves the coordinated actions of numerous molecular components, including large complexes of ribosomes, transfer RNAs (tRNAs), and various translation factors, to facilitate the different stages of translation. The process consists of initiation, elongation, termination, and ribosome recycling. While translational initiation is known to be the rate-limiting step, recent studies have highlighted the significance of translation elongation in protein synthesis efficiency (Jackson et al., 2010; Schuller & Green, 2018).

Numerous factors contribute to the rate and fidelity of protein synthesis by modulating interactions among the ribosome, mRNA, tRNAs, and other cellular components. The sequence of

the mRNA molecule, especially codon usage, has been extensively studied as a crucial determinant of translation efficiency. Codon optimality refers to the efficiency of translation for each of the 61 amino acid specifying codons and varies across different species. It takes into account various factors that impact elongation rate, such as tRNA availability and demand, frequency of codon usage in the genome, GC content, and interactions with the ribosome exit tunnel (dos Reis et al., 2003; Gardin et al., 2014; Pechmann & Frydman, 2013; Presnyak et al., 2015). Furthermore, codon optimality has been found to be associated with elongation speed and mRNA decay. Transcripts enriched in "optimal" codons, which promote efficient translation, exhibit faster elongation rates and lower rates of mRNA decay. On the other hand, transcripts enriched in "non-optimal" codons, which hinder translation efficiency, are associated with slower elongation rates and higher rates of mRNA decay (Hershberg & Petrov, 2008; Ikemura, 1985). Hence, codon optimality is suggested to have a significant influence on the dynamics of translation elongation and the production of proteins (Choi et al., 2018; Neelagandan et al., 2020).

When ribosomes encounter certain sequences, such as enriched nonoptimal codons, within the mRNA, they may temporarily halt or slow down their movement along the mRNA strand, resulting in ribosomal pause. Ribosomal pause during translation can have profound effects on protein folding and translocation processes, because it provides time for chaperone proteins to assist in correct protein folding and aids in the recruitment of signal recognition particles for efficient protein translocation (Komar, 2019; Pechmann & Frydman, 2013; Yu et al., 2015). However, upon extended stalling events, translating ribosomes may collide with stalled ribosomes, resulting in a

ribosome collision which can lead to protein misfolding and aggregation, contributing to proteotoxic stress and potential disease development (Komar, 2019; Y. Liu, 2020). When ribosomes encounter challenging regions within mRNA, such as nonoptimal codon sequences, they can stall or even collide during translation. This, in turn, can activate the ribosome-associated quality control (RQC) pathway and the No-go decay (NGD) pathway, which play essential roles in rescuing stalled or collided ribosomes and maintaining cellular homeostasis. it has been proposed that the E3 ubiquitin ligase Hel2 (or ZNF598) detects the conformation of collided ribosomes, which concurrently triggers activation of both the RQC and NGD pathways (Matsuo et al., 2017; Sundaramoorthy et al., 2017). In the RQC pathway, the RQT complex is recruited to dissociate the ribosomal subunits, while Rqc1, Ltn1 and proteosome are involved in degrading the nascent peptide chain (Hashimoto et al., 2020; Kostova et al., 2017; Matsuo et al., 2020; Shen et al., 2015). Conversely, in the NGD pathway, the Dom34/Hbs1/GTP ternary complex is recruited to the vacant ribosomal A-site, leading to ribosome dissociation (Harigaya & Parker, 2010; Pisareva et al., 2011; Shoemaker et al., 2010). Additionally, Cue2, the exosome, Xrn1, and Ski7 are recruited to degrade the mRNA transcript (Doma & Parker, 2006; Ikeuchi, Izawa, et al., 2019).

Along with surveillance pathways triggered by collided ribosomes, it has also been established that accumulation of weak ribosomal pauses also plays crucial effects on determining mRNA stability (Hanson et al., 2018; Presnyak et al., 2015). Emerging evidence suggests that the DEAD-box protein Dhh1 (DDX6), a regulator of decapping, plays a role in sensing codon optimality to coordinate mRNA degradation and translation elongation (Radhakrishnan et al., 2016; Sweet et al.,

2012). Moreover, another pathway implicated in mRNA degradation involves the shortening of the poly(A) tail through the Ccr4-Not deadenylase complex. Specific components of this complex, such as Not5, are associated with binding to certain decapping activators, thereby facilitating mRNA decapping (Alhusaini & Coller, 2016; Passmore & Coller, 2022). Collectively, these findings support the existence of a codon-optimality-mediated mRNA degradation (COMD) pathway, where the involvement of the Ccr4-Not complex initiates the deadenylation process, leading to the removal of poly(A) tails, and facilitates the association of decapping machinery, including Dhh1, with the 5' cap of mRNA (Bae & Coller, 2022; Passmore & Coller, 2022). Subsequently, mRNA degradation occurs either from the 5' end through the action of the 5'-3' exoribonuclease 1 (Xrn1) or from the 3' end through the cytoplasmic exosome complex (Bae & Coller, 2022; Passmore & Coller, 2022).

While numerous studies have investigated the effects of synonymous codon substitutions on protein expression, mRNA decay, and ribosomal pause, the quantification of their specific impact on elongation time has not been widely available. In addition, how paused and stalled ribosomes are recognized by different sensors, such as chaperone, Hel2 and Not5, to trigger distinct co-translational pathways remains unclear. In this study, we established an in-vivo luciferase-based assay capable of quantitatively measuring elongation time. We utilized this assay to evaluate the time delay resulting from acute stalls induced by the insertion of nonoptimal arginine codon CGA repeats. Remarkably, we observed a dose-dependent increase in elongation time. Interestingly, despite the prolonged translation elongation times and decreasing protein expression, we made the

unexpected discovery that the decay of no-go RNA reaches its peak at a specific stall length. This acute stall is found to experience a Hel2-dependent, and as comparison, another transcript harboring dispersed nonoptimal codons is mediated through a hel2-independent manner. Through in-depth investigations on a specific transcript containing scattered nonoptimal codons, we have discovered a pronounced ribosomal stall triggered by a weak stem loop sequence. This observation suggests the presence of an unidentified mechanism by which RNA secondary structure induces a halt in ribosome movement. Additionally, our findings indicate that Dhh1 exhibits selectivity in its impact on different types of stalls. Collectively, these findings provide novel quantitative insights into the mechanisms underlying translation surveillance and shed light on the specific roles of Hel2 and Dhh1 in mediating ribosomal pause events.

2.3 Results

2.3.1 Development of In-vivo Elongation Assay for Quantifying Elongation Duration

To create a quantitative elongation duration reporter assay, we utilized a tetracycline-inducible promoter to control mRNA induction of a bioluminescent nanoluciferase (nLuc) reporter downstream of open reading frames (ORFs) of interest. The nLuc reporter has been previously studied in yeast under the control of a stress-inducible promoter and its bioluminescent output faithfully recapitulates induced mRNA levels after heat shock (Masser et al., 2016). To test this system, we developed a series of constructs in which we varied the length of the upstream ORF by insertion of yeast-optimized yellow fluorescent protein (YFP) or yeast-optimized monomeric infrared red fluorescent protein (miRFP) ORFs upstream of nLuc (Figure 2.3.1A). Tet-nLuc is included to control for the time cost of initiation steps including anhydrotetracycline (ATc) penetration, transcription initiation, mRNA export, and translation initiation. nLuc protein expression was collected for each construct over 60 minutes and normalized to OD600 measured at T=0 min (time of ATC addition). Elongation time was calculated using a Schleif plot (Schleif et al., 1973) and adjusted based on an average mRNA transcription time of 1500 nucleotides per minute (Edwards et al., 1991; Mason & Struhl, 2005). We find a delay in the first appearance of nLuc upon the addition of optYFP and a further delay in the longer miRFP-optYFP-nLuc reporter (Figure 2.3.1B). We then used these measured delays to calculate the translation elongation rate of optYFP and miRFP ORFs as approximately 4 AA/sec and 3 AA/sec (Figure 2.3.1C), respectively, which is consistent with bulk elongation rate measurements of 3-10 AA/sec (Karpinets et al., 2006;

Riba et al., 2019). We do not find a significant difference in elongation rate between the two optimized ORFs. This implies that our reporter can quantify the in vivo translation rates of our reporters.

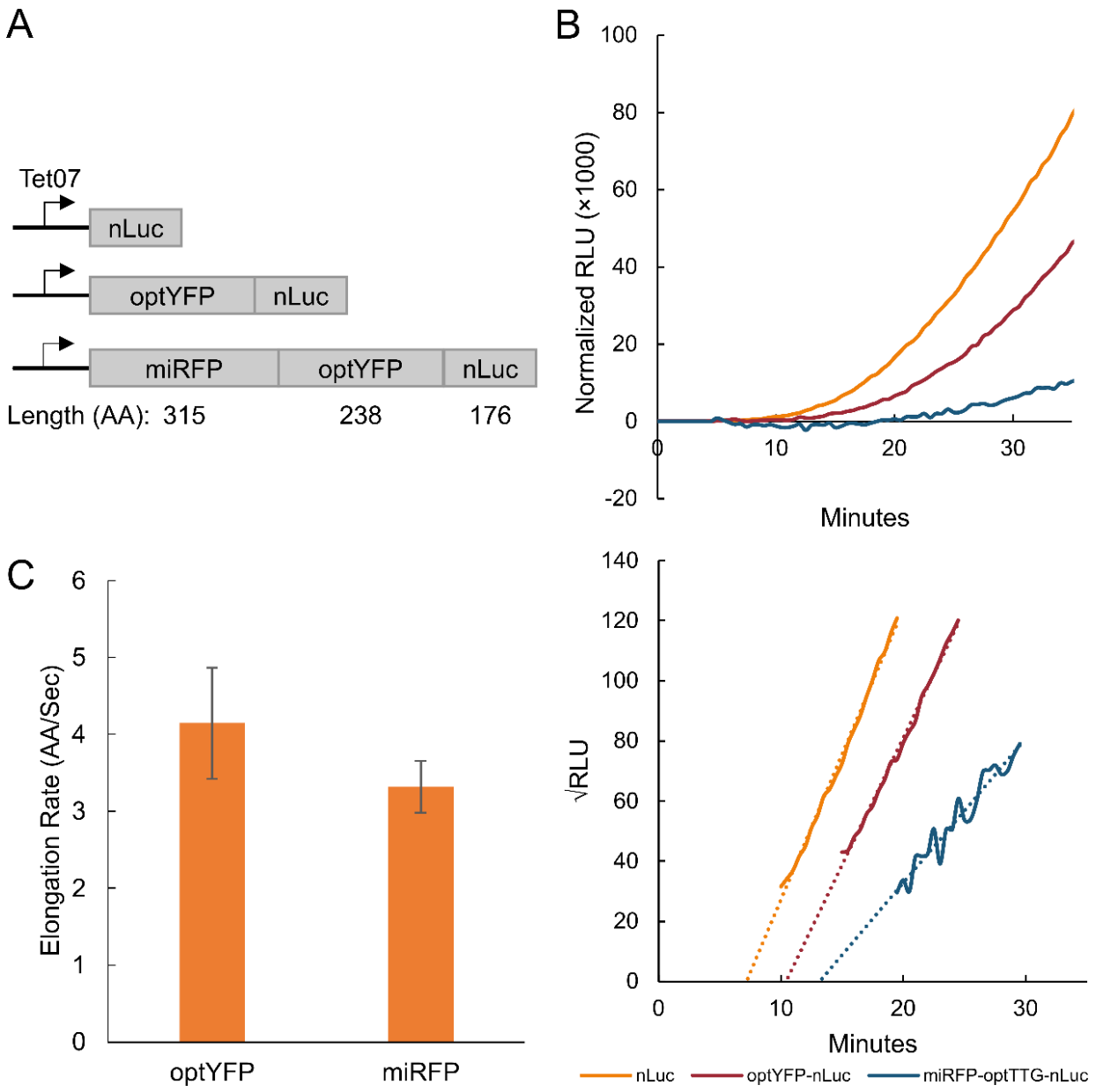

Figure 2.3.1 Assay validation via elongation rate measurements

A: Diagram of yeast-optimized constructs of various lengths. Optimized YFP (optYFP) or both optYFP and optimized miRFP (miRFP) are set upstream of a nanoluciferase (nLuc) reporter. Constructs are expressed from an inducible Tet07 promoter.

B: (Top) Representative assay data of relative light units (RLU) of each construct over time normalized to OD600. (Bottom) Schleif plot and associated trendlines of the top graph.

C: Calculated elongation rate measurements of optYFP (n=9) and miRFP (n=4) ORFs.

Error bars indicate SEM. All statistical significances were calculated for each construct using two-tailed paired Student's t-Test against TetO7-nLuc constructs.

2.3.2 Hel2 Decreases Protein Expression, mRNA Levels, and Delays Elongation in Acute CGA Constructs

To further explore the utility of our reporter, we wanted to verify this system could quantify the duration of elongation pauses of known ribosomal stall sequences. Consecutive nonoptimal CGA arginine codons are known to induce slow translation elongation and terminal stalling through wobble decoding of CGA (Letzring et al., 2010; Tesina et al., 2020; Tsuboi et al., 2012; Veltri et al., 2022). To quantify the effect of these nonoptimal codons on elongation time and gene expression, we developed a series of constructs in which we inserted between 2 and 6 tandem CGA repeats between the yeast-optimized YFP ORF and nLuc reporter ORF shown previously (Figure 2.3.2A). First, we tested the protein expression of our induced constructs and found a dose-dependent exponential decline in protein production as the number of CGA codons increased, similar to a previous study by Letzring and colleagues (Letzring et al., 2010) (Figure 2.3.2B). We, however, did not see a significant impact on protein expression until 3×CGA codons were included. Next, we measured mRNA levels and found that mRNA levels significantly decreased with the addition of 3×CGA codons but mRNA levels remained constant around 40% of our control construct regardless of additional CGA codons (Figure 2.3.2C). We then measured the elongation delay in each of our constructs by comparing to a control reporter lacking any CGA codons (Figure 2.3.2D). We found that elongation delay increased in a dose-dependent manner beginning at 3×CGAs, with 6×CGA causing an ~4.5 minute extension of the translation duration. There was a relatively linear relationship between CGA stall number after 3×CGAs and elongation time which

allowed us to calculate that each CGA adds approximately 76 seconds to the overall elongation time. We found that this elongation delay was specifically due to CGA codons as a 6×AGA codon, which also encodes for arginine, had no effect on elongation time (Figure 2.3.3).

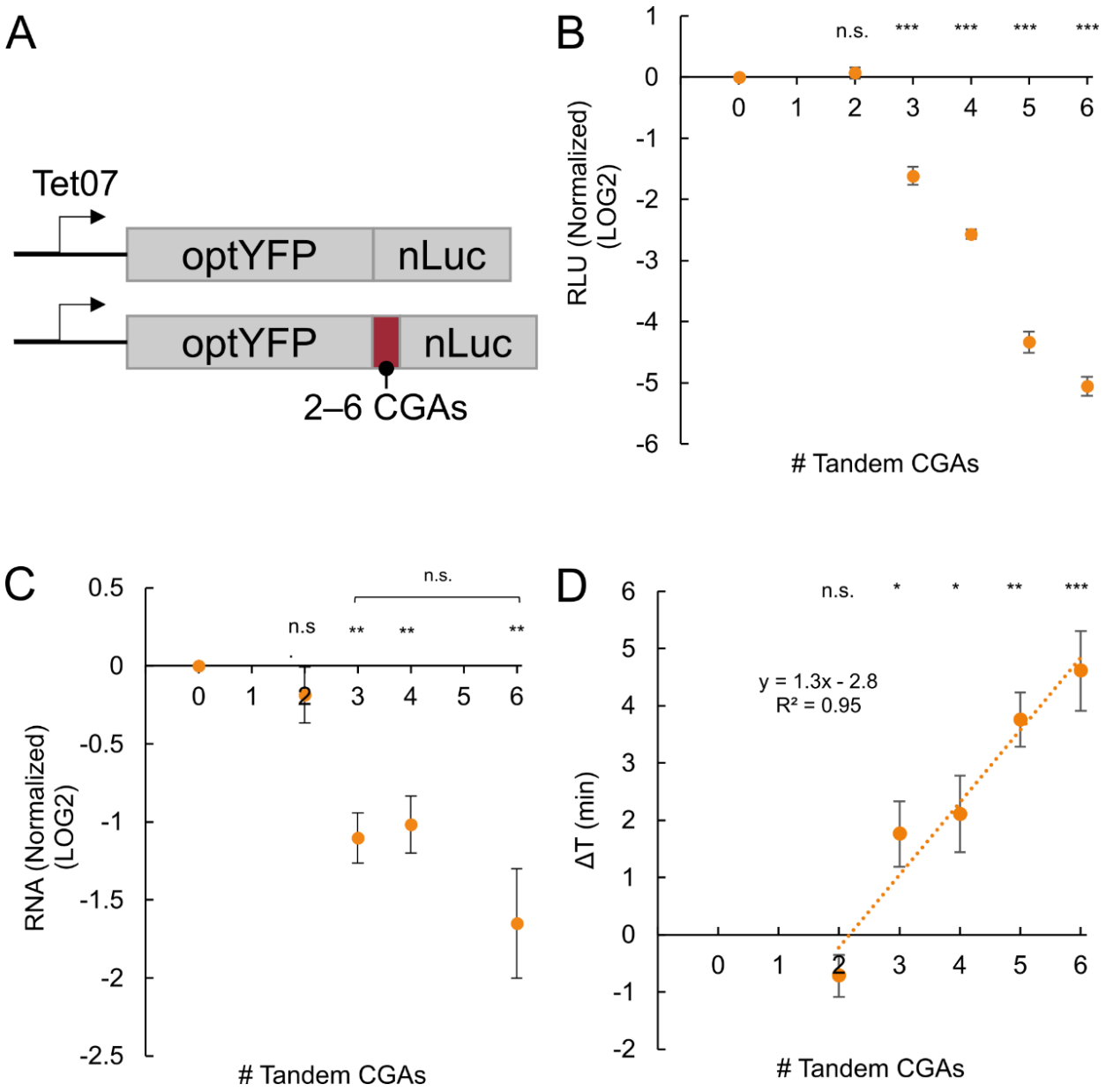

Figure 2.3.2 CGA-derived acute stalls negatively impact gene expression and increase elongation time in a dose-dependent manner

A: Diagram of optimal and CGA-containing constructs. Between 2 and 6 CGAs are inserted between the optYFP and nLuc ORFs.

B: Protein expression of CGA constructs at T=60 min normalized to optimized control (2×CGA n=10, 3×CGA n=8, 4×CGA n=10, 5×CGA n=5, 6×CGA n=10). C: mRNA levels of CGA constructs at T=60 min normalized to optimized control. (n=3 for all).

C: Elongation delay of CGA-containing constructs compared to optimized control. (n=3 for all). All error bars indicate SEM. All statistical significances were calculated for each construct using two-tailed paired Student's t-Test against optYFP control.

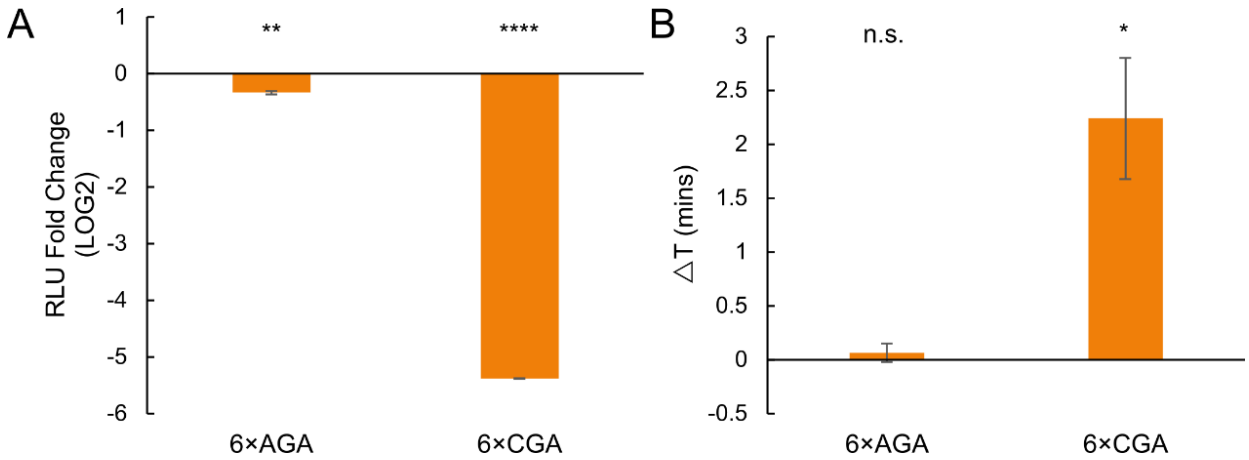

Figure 2.3.3 6×CGA acute stall is induced by sequential nonoptimal CGA codons, instead of its coding Arginine

A: Protein expression fold change of 6×AGA and 6×CGA constructs. (n=3 for both)

B: Elongation change of 6×AGA and 6×CGA constructs vs. (n=3 for both)

All error bars indicate SEM. All statistical significances were calculated for each construct using two-tailed paired Student's t-Test against optYFP.

We then tested the role of Hel2 and Syh1, two factors implicated in impacting gene expression due to prolonged ribosomal stalls. Hel2 is a translation surveillance factor that senses ribosome collisions and activates the ribosome rescue pathways ribosome quality control (RQC) and no-go decay (NGD) pathways which result in protein and mRNA turnover, respectively. Syh1 is a homolog of the mammalian NGD factor GIGYF1/2 that was previously found to have a role in NGD in yeast (Hickey et al., 2020; Veltri et al., 2022). We measured protein expression in our constructs containing 2, 4, and 6×CGAs in a hel2Δ background and 6×CGAs in a syh1Δ background and we compared it to their wild type (WT) counterparts (Figure 2.3.4A and Figure 2.3.5A). We found that deletion of Hel2 partially rescued protein expression in the 4×CGA and 6×CGA, but SYH1 deletion had no effect on the 6×CGA protein expression. We next measured RNA levels in our 2×CGA, 4×CGA, and 6×CGA strains and found that RNA levels were increased in our 4×CGA and 6×CGA-containing hel2Δ strains but there was no change in the 2×CGA strain (Figure 2.3.4B). We found no significant difference in RNA levels for the 6×CGA in our syh1Δ strain (Figure 2.3.5B). Together, these results imply Hel2-mediated RQC and NGD are partially responsible for the observed decrease in protein and RNA levels, respectively, in the wild-type strains. Lastly, we sought to measure the impact of Hel2 on elongation time. A recent review by Meydan and Guydosh proposed two non-mutually exclusive models of Hel2's activity on the stability of ribosome collisions: (1) Hel2 is necessary to rescue stalled ribosomes and Hel2 deletion would result in further buildup of collided ribosomes and (2) Hel2 stabilizes collided ribosomes and Hel2 deletion would result in reduced ribosomal pausing (Meydan & Guydosh, 2021). Model

2 that Hel2 stabilizes collided ribosomes was further supported by experimental data that hel2Δ reduces disome pauses in ribosome profiling data sets (Meydan & Guydosh, 2020). To assess the effect of Hel2 on elongation time and distinguish between these two models, we compared the elongation time of our control, 4×CGA, and 6×CGA strains between WT and hel2Δ backgrounds and found no significant difference in our control strain but a decrease in overall elongation time in our 4×CGA and 6×CGA strains when expressed in a hel2Δ background (Figure 2.3.4C). This suggests that Hel2 functions to slow down elongation in our CGA-containing strains and is consistent with the second proposed model in which Hel2 stabilizes collided ribosomes.

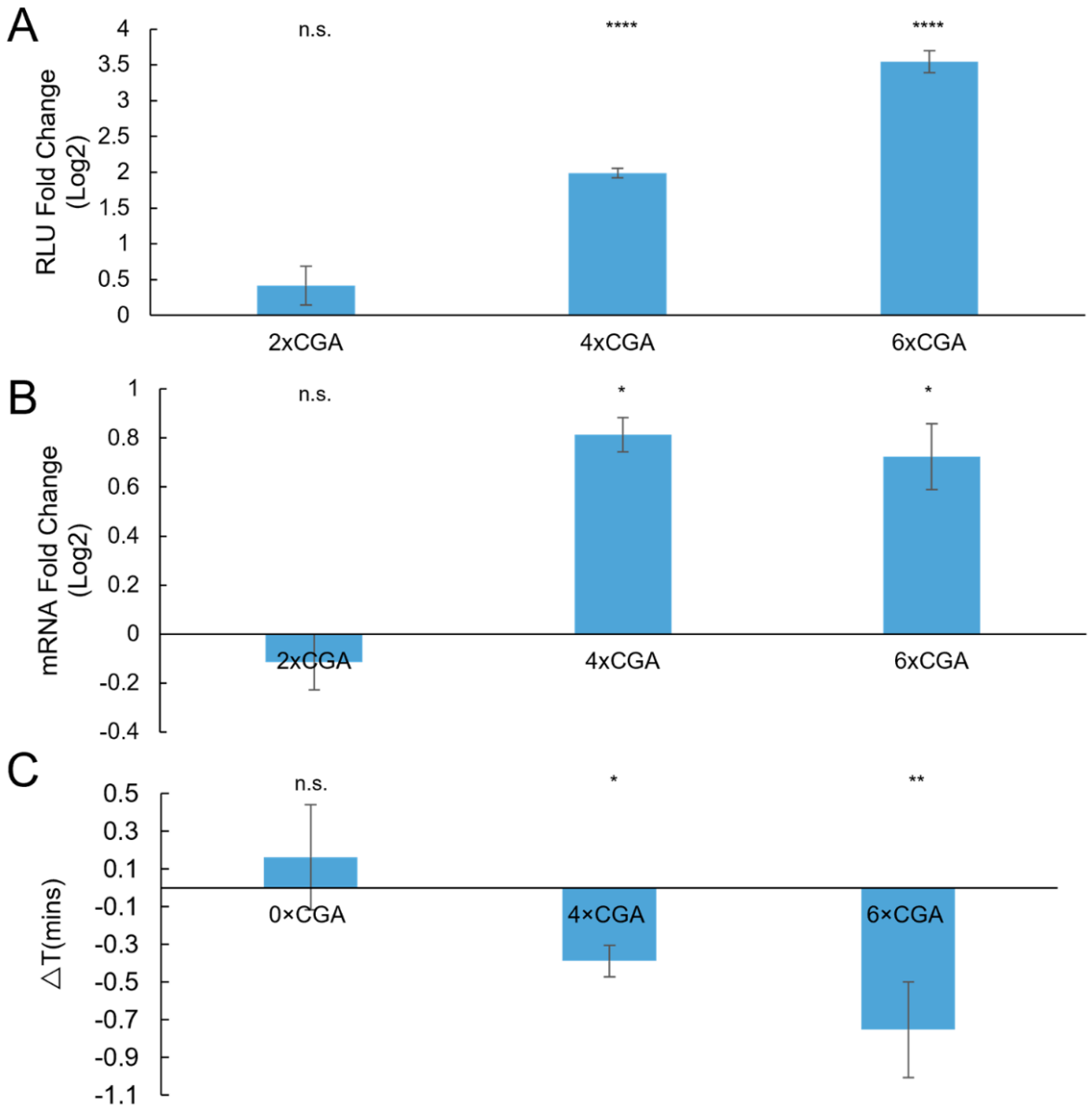

Figure 2.3.4 Hel2 deletion rescues protein expression, mRNA levels, and elongation time
A: Protein expression fold change of CGA constructs in a hel2Δ vs WT background (n=2 for 2×CGA strain, n=7 for 4×CGA and 6×CGA strains).
B: mRNA level fold change of CGA constructs in a hel2Δ vs WT background (n = 3 for all). C: Elongation delay of CGA constructs in a hel2Δ vs WT background (n = 3 for all).
All error bars indicate SEM. All statistical significances were calculated for each construct using two-tailed paired Student's t-Test against WT control.

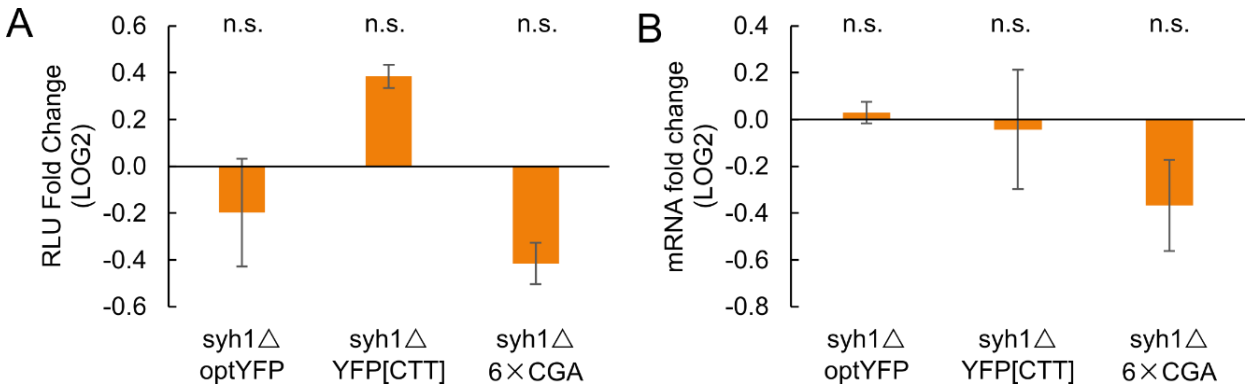

Figure 2.3.5 Syh1 doesn't significantly affects protein expression, mRNA expression and elongation of CTT and CGA-derived ribosomal stalls

A: Protein expression fold change of optYFP, YFP[CTT] and 6×CGA constructs in syh1△ vs WT (n=3 for all)

B: mRNA expression fold change of optYFP, YFP[CTT] and 6×CGA constructs in syh1△ vs WT (n=3 for all)

All error bars indicate SEM. All statistical significances were calculated for each construct using two-tailed paired Student's t-Test against WT constructs.

2.3.3 Synonymous Substitution to Nonoptimal Leu Codons Negatively Impacts Gene Expression

Next, we asked how distributed slowdowns of nonoptimal codons impact gene expression and elongation time. To study the impact of distributed nonoptimal codons, we used our optYFP-nLuc construct and synonymously substituted the first 20 of 21 leucines for a nonoptimal leucine variant (Figure 2.3.6A and Figure 2.3.7). First, we wanted to determine the impact of these synonymous substitutions on overall elongation time. We measured the elongation time in each of our strains and compared it to the optimized strain to determine the elongation time delay associated with each synonymous substitution (Figure 2.3.6A). We found that substitution of the optimal leucine codon TTG for the nonoptimal codons CTC and CTT resulted in a significant delay in elongation time of approximately 0.5 and 2.5 minutes, respectively (Figure 2.3.6B). Due to the statistically significant differences in elongation time, we selected both the CTC and CTT-containing constructs for further study. Next, we measured the impact of codon substitution on protein and RNA levels (Figures 2.3.6C and 2.3.6D). As compared to the optimized control, we determined that substitution to the CTC codon reduced both protein and mRNA levels by approximately 20% and substitution to the CTT codon reduced both protein and mRNA levels by 50%. This was distinct from the RQC inducing CGA stalls that decreased protein production more substantially than they did mRNA levels.

We sought to determine whether the increase in elongation time and decrease in protein expression observed was either contributed equally by each nonoptimal codon or the specific

placement of nonoptimal codons in the YFP ORF. To assess this, we created a set of chimeric reporters in which the first 10 leucine codons in the YFP ORF were either optimal or nonoptimal followed by the next 10 leucine codons of the opposite optimality (YFP[1-10CTT] and YFP[11-20CTT]). We hypothesized that if each codon contributed equally to elongation time, the elongation time delay of our chimeric constructs would be half of the delay between optYFP and YFP[CTT]. Instead, we found that both the elongation delay and protein expression of our chimeric YFP[1-10CTT] closely resembled YFP[CTT] and that our chimeric YFP[11-20CTT] closely resembled YFP[TTG] (Figures 2.3.6E and 2.3.6F). This provides evidence that substitution of leucine codons to a nonoptimal variant in the 5' half of the YFP ORF is sufficient to drive protein expression and elongation time outcomes.

A previous study by Chu and colleagues showed that poor codons in the 5' region of a transcript could negatively affect translation initiation through ribosome buildup preventing initiation from occurring, thereby reducing overall translational output (Chu et al., 2014; Hanson & Coller, 2018). To test if the observed decrease in protein expression was a result of interference with initiation, we inserted a yeast-optimized miRFP (315 amino acids) upstream of our optYFP-nLuc and YFP[CTT]-nLuc constructs. We hypothesized that if initiation was negatively impacted by ribosome buildup, addition of a long yeast-optimized ORF upstream of the nonoptimal YFP[CTT] would rescue protein expression as compared to the optimal construct. Instead, we found that a statistically significant difference remained between the optimal and CTT-containing nonoptimal constructs (Figure 2.3.6E). Furthermore, we assessed the impact on elongation time

and found that elongation time was not rescued to WT levels and the magnitude of delay is similar to the YFP[CTT] construct (Figure 2.3.6F). This suggests that the decrease in protein expression in the reporter is a result of the specific placement of the nonoptimal CTT codons within the 5' half of the YFP ORF, but does not depend on the nonoptimal codons to be near the initiation codon.

To further dissect which leucine codons were important for the repression of protein expression, we made constructs that contained diminishing numbers of CTT codons from the first 10 leucine codons (Figure 2.3.8A). We found that the first 8 and 9 codons showed similar levels of elongation delay but the first 7 leucine codons as CTT did not diminish elongation (Figure 2.3.6F). As the switch took place from the 7th to 8th leucine codons, we tested whether the 8th leucine codon as a nonoptimal CTT codon was sufficient to see the full effects. We found that a single CTT at the 8th leucine codon isn't significantly affect elongation time (Figure 2.3.5F) while we did however find that two leucine codons, 7 and 8, at amino acid position 60 and 64 respectively (Figure 2.3.6A), switched to CTT were sufficient to fully repress protein expression and elongation time (Figure 2.3.6E and F). The switching of leucine 7 and 8 from TTG to CTT were associated with a more strongly folded local stem-loop structure as predicted by mFold (Figure 2.3.8B). To test if local RNA structure was important to the increased elongation time, we made synonymous mutations to G65 from GGT to GGC and T62 from ACT to ACA. We found a significant reduction of elongation delay after G65 mutation, and even higher reduction of elongation delay after T62 and G65, which are accord with mFold prediction (Figure 2.3.9). These data point to the importance of a local stem-loop structure in affecting translation duration.

Figure 2.3.6 Distributed stalls in the YFP ORF decrease protein expression, mRNA levels, and delays elongation time

A: Diagram of synonymously substituted leucine constructs. YFP contains 21 leucine codons which are marked in orange. The first 20 leucine codons are substituted for a nonoptimal leucine variant and the 21st leucine remains the optimal TTG codon No.7 and No.8 Leucine from 5'end of YFP ORF are labeled as L60 and L64.

B: Elongation delay of distributed stall constructs compared to optYFP (n= 6, 6, 5 and 7 from left to right). The first 20 out of 21 total optimal TTG leucine codons in optYFP are synonymously substituted to a nonoptimal codon specified in brackets.

C: Protein expression of distributed stall constructs normalized to optYFP control (n=4 for all).

D: mRNA levels of distributed stall constructs normalized to optYFP control (n=3 for all).

E: E: Protein expression of chimeric constructs normalized to optYFP control (n= 11, 5, 5 and 12 from left to right).

F: (Left) Elongation delay measurements of chimeric constructs normalized to optYFP control (n= 12, 9, 9, 3, 3, 3, 13 and 3 from left to right); (Right) Elongation delay measurements of miRFP-YFP[CTT] normalized to miRFP-optYFP control (n=6).

All error bars indicate SEM. All statistical significances, except miRFP-YFP[CTT], were calculated for each construct using two-tailed paired Student's t-Test against optYFP control unless otherwise specified.

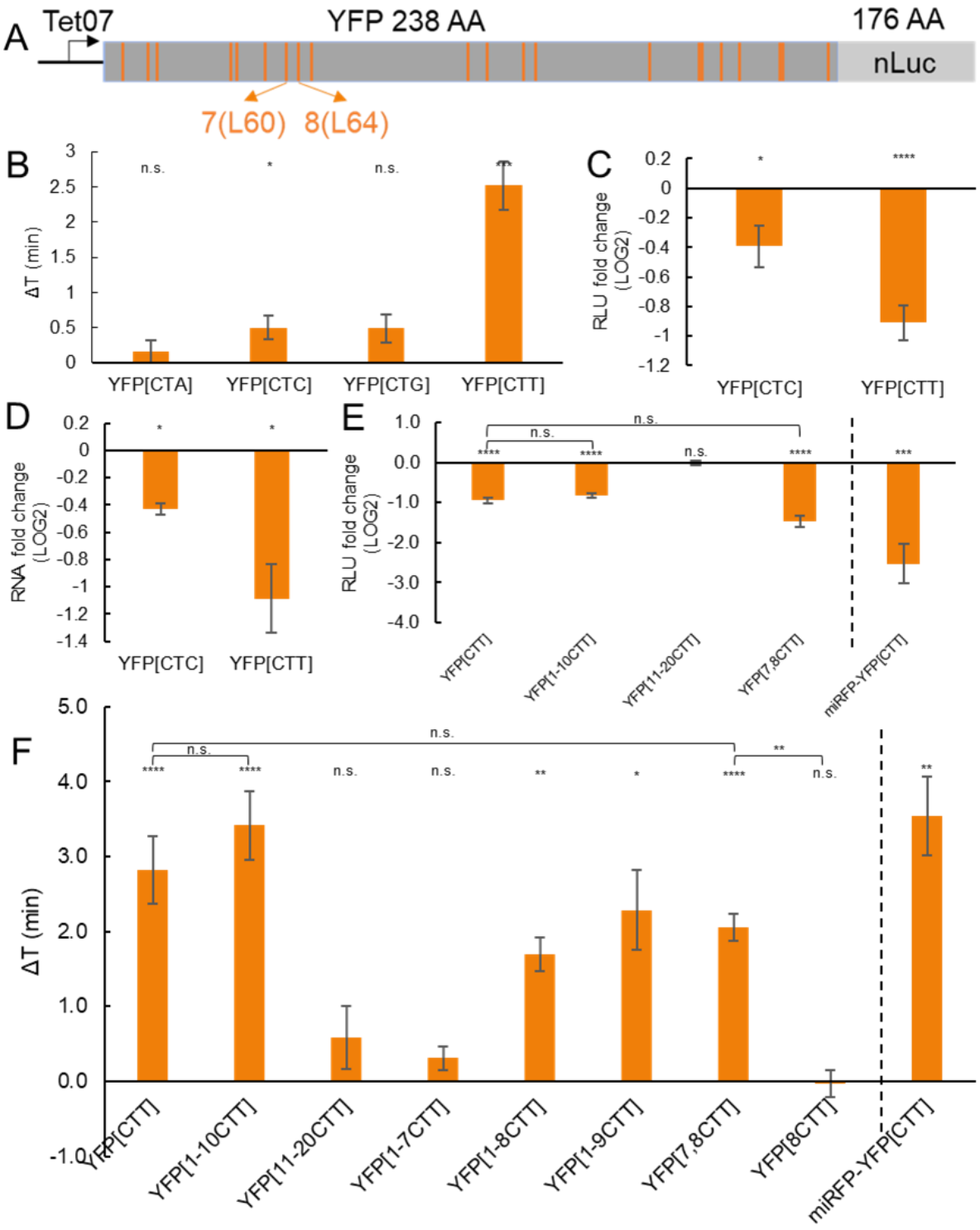
A
Tet07
YFP 238 AA
176 AA
nLuc
7(L60)
8(L64)
B
ΔT (min)
n.s.
*
n.s.
**
YFP[CTA]
YFP[CTC]
YFP[CTG]
YFP[CTT]
C
RLU fold change (LOG2)
*
****
YFP[CTC]
YFP[CTT]
D
RNA fold change (LOG2)
*
*
YFP[CTC]
YFP[CTT]
E
RLU fold change (LOG2)
n.s.
n.s.
****
****
n.s.
****
***
YFP[CTT]
YFP[1-10CTT]
YFP[11-20CTT]
YFP[7,8CTT]
miRFP-YFP[CTT]
F
ΔT (min)
n.s.
n.s.
**
****
****
n.s.
n.s.
**
*
****
n.s.
**
YFP[CTT]
YFP[1-10CTT]
YFP[11-20CTT]
YFP[1-7CTT]
YFP[1-8CTT]
YFP[1-9CTT]
YFP[7,8CTT]
YFP[8CTT]
miRFP-YFP[CTT]

A

Leu Codons	tAI	Construct
TTG (optimal)	0.754	optYFP
CTA	0.185	YFP[CTA]
CTC	0.062	YFP[CTC]
CTG	0.059	YFP[CTG]
CTT	0.027	YFP[CTT]

B: YFP ORF

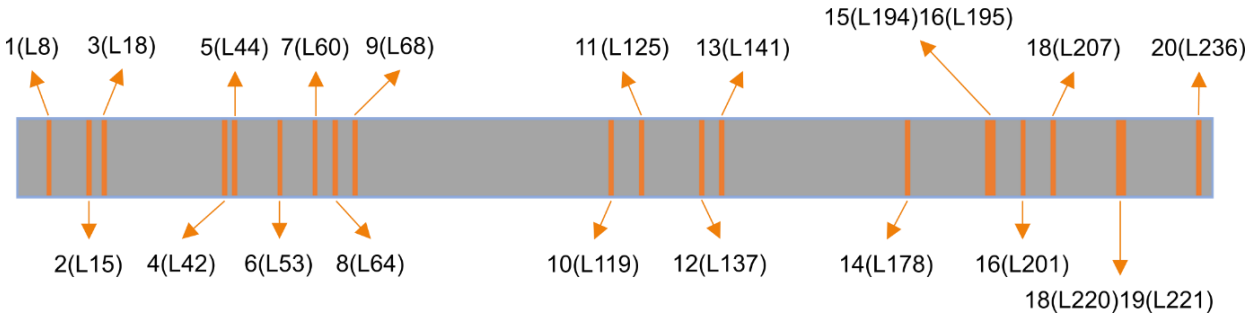

Figure 2.3.7 Location of mutated Leucine codons on YFP and tAI of each synonymous Leucine codons

A:Table of leucine codons used in this study. The optimal TTG codon is present in the optYFP control. Other constructs contain a nonoptimal leucine variant which is denoted in brackets. The tRNA Adaptation Index (tAI) is a metric that represents codon optimality and ranges from 0 (most nonoptimal) to 1 (most optimal).

B: 21 Leucine (L) position on YFP ORF gene. The YFP ORF gene contains 714 bp or 238 aa (stop codon isn't included). Inside the 238 amino acids, there are 21 Leucine amino acids in total and 20 of them are mutated to five different Leu codon (shown in Figure A). The amino acids position and codon number of Leu in YFP are labeled (for example: X(LY) means Xth Leu codon and Yth amino acids from 5' end of YFP)

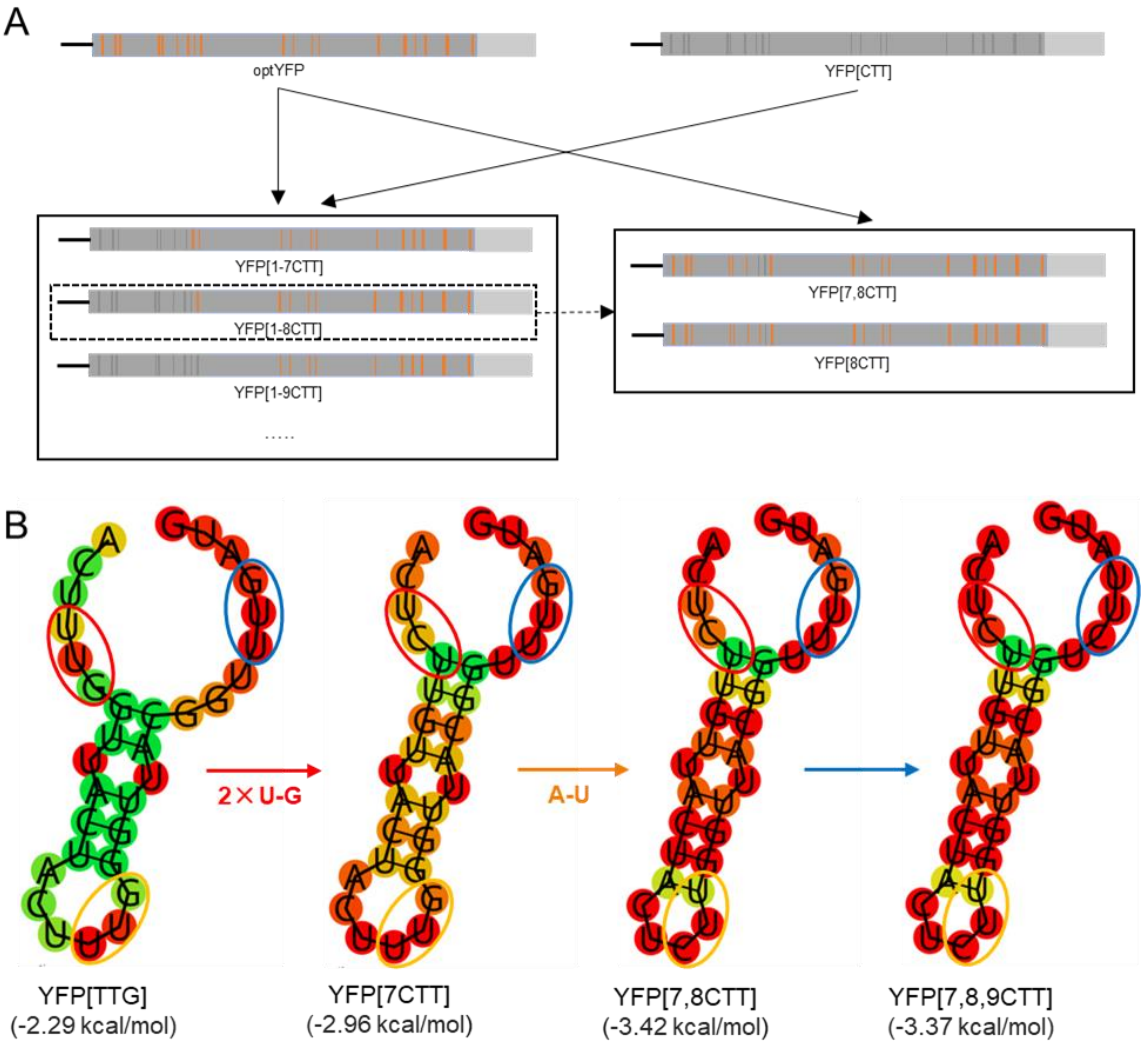

Figure 2.3.8 Cloning strategy of chimeric leucine constructs and mRNA structure induced distributed codon stalls

A: Diagram of Chimeric YFP construction. YFP[1-7CTT], YFP[1-8CTT], YFP[1-9CTT], YFP[1-10CTT], YFP[10-20CTT] are constructed based on optYFP and YFP[CTT]; YFP[7,8CTT] and YFP[8CTT] are constructed based on optYFP and YFP[1-8CTT]

B: mFold prediction, with the sequence of the region from bp178 to bp207 of each construct listed below. Red circle is Leu 7 (L60), Yellow circle Leu 8 (L64), Blue circle Leu 9 (L68) as either TTG(UUG) or CTT(CUU).

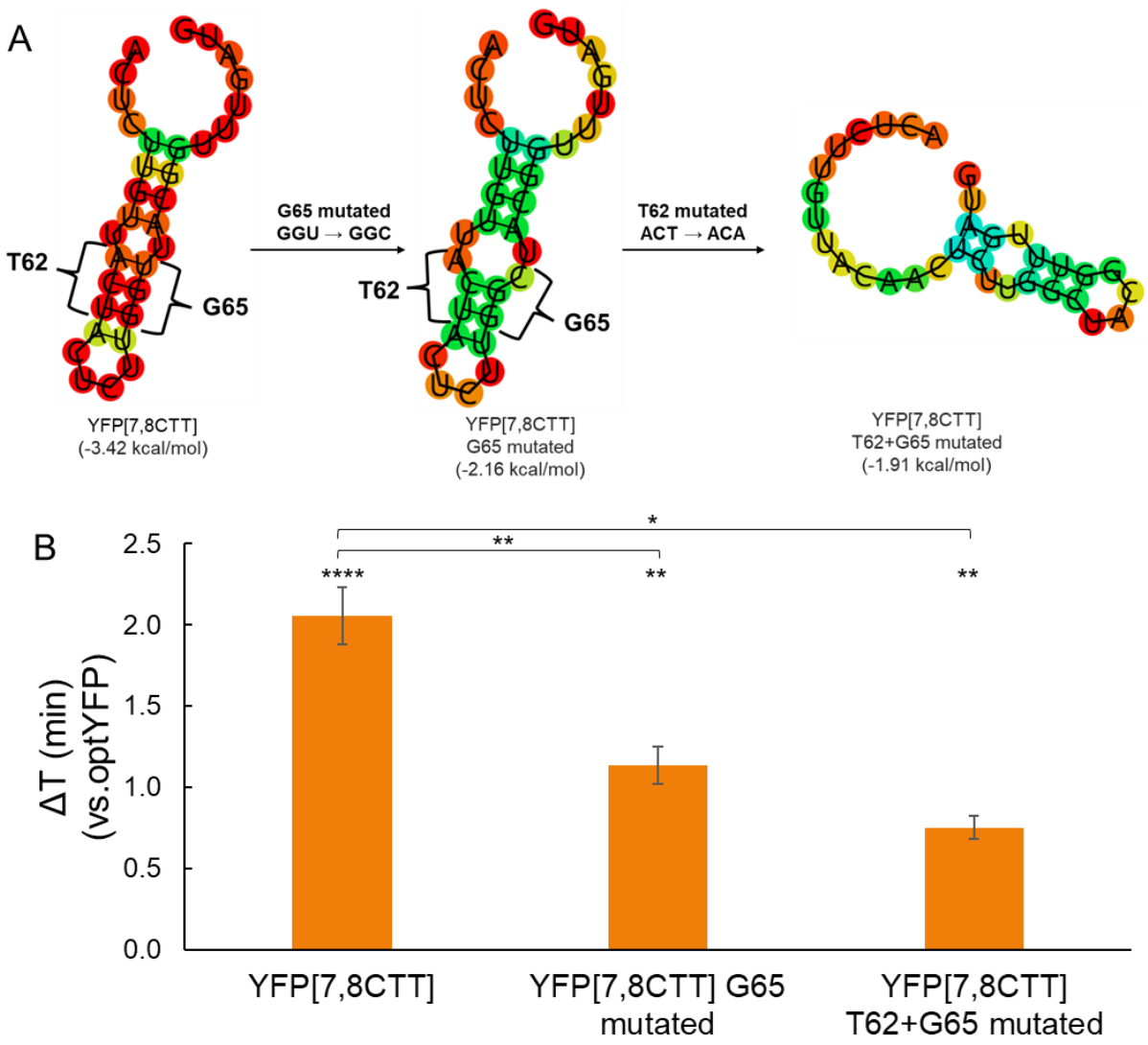

Figure 2.3.9 Point mutation rescue the elongation stall induced by YFP[7,8CTT]

A: mFold prediction, with region from bp178 to bp207. T62 and G65 mutation decreases the stabilization of the stem loop.

B: Elongation delay of YFP[7,8] constructs with point mutations compared to optYFP (n=3 for all).

All error bars indicate SEM. All statistical significances were calculated for each construct using two-tailed paired Student's t-Test against optYFP control unless otherwise specified.

2.3.4 Gene Expression in Nonoptimal Codon Constructs is Affected by Deletion of DHH1 but not HEL2

Finally, we investigated if Hel2 or other translation sensors were responsible for the negative impacts on gene expression in our nonoptimal codon substituted constructs. Of particular interest was the RNA binding protein Dhh1, a conserved DEAD-box helicase previously shown to have roles in mRNA decapping and translational repression (Carroll et al., 2011; Coller et al., 2001; Fischer, 2002; Tseng-Rogenski, 2003). Importantly, it has been shown to bind preferentially to mRNA with low codon optimality and has been proposed to slow down ribosome movement (Radhakrishnan et al., 2016; Sweet et al., 2012). We hypothesized that the negative impacts on gene expression observed in YFP[CTC] and YFP[CTT] compared to the optYFP control may be a result of either Hel2 or Dhh1 influence. To test this, we transformed our optYFP, YFP[CTC], and YFP[CTT] constructs into either a dhh1Δ or hel2Δ strain.

First, we assessed the impact of protein expression on our constructs in a dhh1Δ or hel2Δ strain deletion background (Figure 2.3.10A). Based on Dhh1's role in mediating translation repression of transcripts enriched in nonoptimal codons, we expected to see no impact in optYFP and a rescue of protein expression in YFP[CTC] and YFP[CTT]. Instead, we found differing effects for each construct; deletion of Dhh1 slightly increased protein expression in our optYFP construct, decreased protein expression in our YFP[CTC] construct, and had no statistically significant impact in our YFP[CTT] construct. We also found that Hel2 deletion had no statistically significant effect on protein expression in any of our constructs (Figure 2.3.10A). This suggests that the drop

in protein expression seen in the nonoptimal constructs was not due to a Hel2-mediated mechanism and is distinct from our acute CGA-containing constructs. Next, we examined the effect of Dhh1 on mRNA levels by comparing WT and dhh1Δ mRNA levels (Figure 2.3.10B). We found that deletion of Dhh1 decreased mRNA levels in our YFP[CTC] construct but had no statistically significant difference in the other constructs. The negative impact of Dhh1 deletion in our YFP[CTC] construct was of similar magnitude in protein and mRNA. This suggests that Dhh1 increases mRNA levels in our YFP[CTC] construct, which leads to increased protein expression.

Lastly, we wanted to determine the impact of dhh1Δ and hel2Δ backgrounds on elongation time in our substituted leucine constructs. We measured elongation delay by comparing the elongation times of our constructs in each deletion strain to WT (Figure 2.3.10C). We found that deletion of Dhh1 slightly increased the elongation delay in our optYFP and more dramatically increased the elongation delay in the YFP[CTC] strain, suggesting that Dhh1 functions to speed up elongation in these constructs. However, we found no statistically significant difference in elongation time in our YFP[CTT] construct. Additionally, we found no statistically significant difference in elongation times in our hel2Δ strains (Figure 2.3.10C). This is consistent with the hel2Δ strain protein expression data and supports the idea that a non-Hel2-mediated pathway is responsible for the negative impact on gene expression in our substituted leucine constructs.

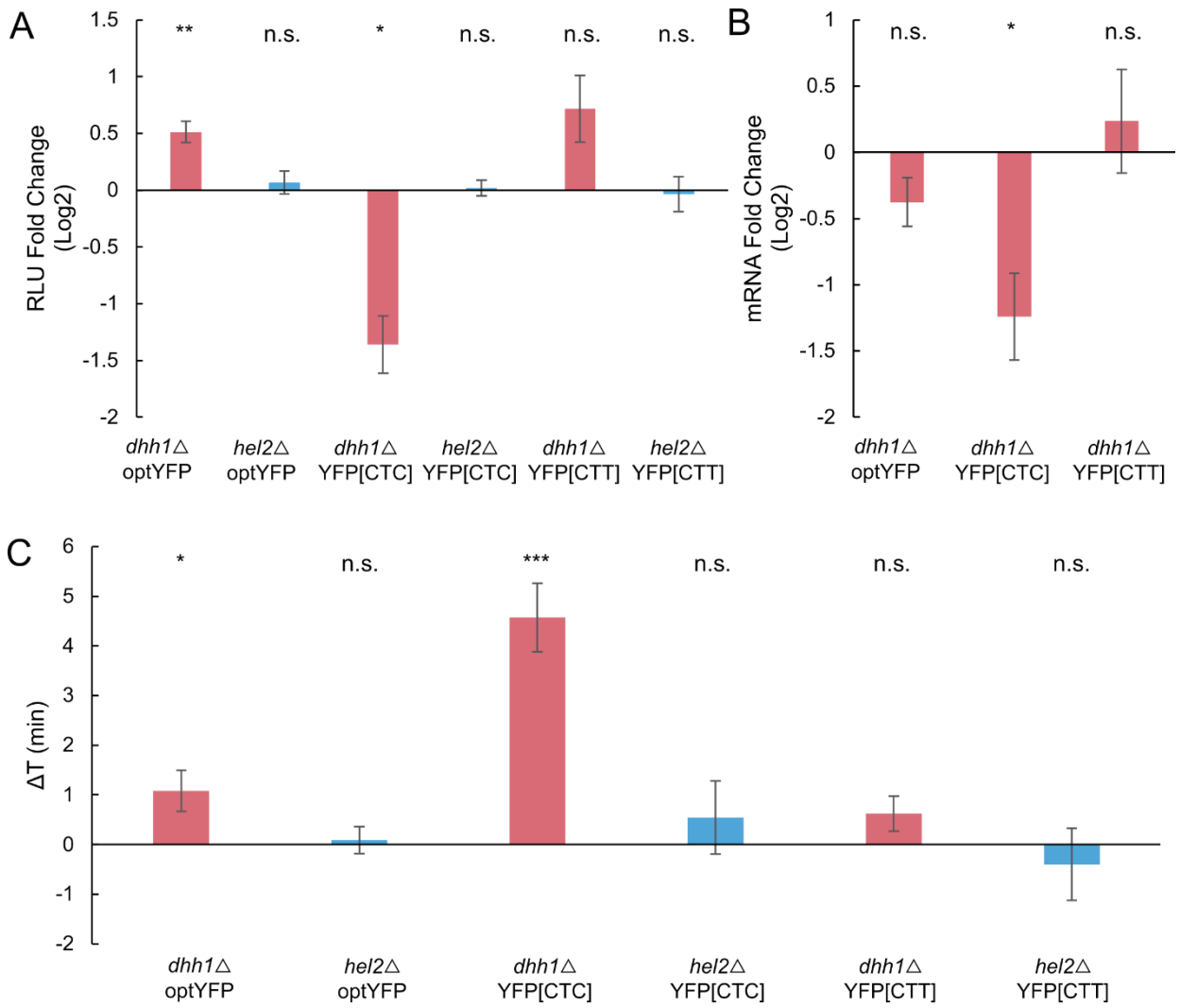

Figure 2.3.10 Dhh1 deletion, but not Hel2 deletion, affects gene expression in substitution constructs

A: Protein expression of distributed stall constructs in dhh1Δ or hel2Δ background vs WT (n=5, 4, 5, 6, 7, and 3 from left to right).

B: mRNA level fold change of distributed stall constructs in a dhh1Δ vs WT background (n = 5, 5, and 7 from left to right).

C: Elongation delay of distributed stall constructs in dhh1Δ or hel2Δ background vs WT (n= 19, 4, 18, 6, 9, and 5 from left to right). All error bars indicate SEM.

All statistical significances were calculated for each construct using two-tailed paired Student's t-Test against WT control.

2.4 Discussion

Ribosomal stall and the connected quality control pathways are important for recognizing faulty and damaged mRNAs, yet quantitative measurements of how these stalls impact translation duration have been lacking. In this study, we developed a reporter assay to quantify the in vivo elongation time of various constructs containing stalling sequences in *S. c*erevisiae. Using CGA stalling reporters we find that total elongation time increases in a dose-dependent manner corresponding with the number of tandem CGA repeats while protein expression decreases logarithmically with increasing CGA repeats. Strikingly, we find that mRNA levels stabilize upon reaching a specific stall length, suggesting that the stall-activated NGD pathway reaches a maximum decay rate at 3x CGA. Interestingly the ~50% reduction in mRNA levels is very similar to the mRNA reduction seen from a completely independently designed reporter containing 12xCGA (Veltri et al., 2022) and other reporters containing 10xAAG (rare poly-Lysine) or 8xCCG (rare polyproline codon) stalling sequences (Park & Subramaniam, 2019), further supporting NGD may be saturated at relatively shorter translational stalls.

From our synonymous leucine substitution constructs, we find that the nonoptimal codon CTT causes substantial delays in elongation time on the order of minutes, lengthening the elongation time of YFP approximately 3.5-fold. The elongation delay of ~ 150s for the CTT reporter is similar to the elongation delay for our 4xCGA stalling reporter. Yet these two reporters behave very differently as the decrease in protein expression due to CTT could be explained completely by decreased mRNA levels, while the 4xCGA decreased protein levels to an even larger extent then

the ~50% decrease in mRNA levels. This pointed to the induction of RQC, which reduces protein expression on the CGA stalls through ribosome rescue. Further supporting this induction of RQC on CGA stalls but not CTT stalls, deletion of the RQC factor Hel2 could partially rescue the mRNA levels and protein production of CGA stalls, yet it had no significant effect on protein production and elongation times due to nonoptimal CTT codons, which we believe is due to the formation of a stem-loop structure. These data point to further differentiation of ribosomal stall beyond just stall duration timing. This fits with previous reports that not all stalled ribosomes are targets for RQC, but instead the ribosomes need to be in a rotated state to be recognized by Hel2 (Ikeuchi, Tesina, et al., 2019; Matsuo et al., 2017).

While initially 20 synonymous Leu codons were changed to poor CTT codons, not all nonoptimal codons contribute equally to the elongation slowdown. Instead, we determined that two of the 20 codons were sufficient to drive the full elongation slowdown and repressed protein expression. This appears to be caused by local sequence effects and not specifically the poor codons being in the 5' end of the ORF, as adding an upstream miRFP ORF was not able to rescue the translation slowdown and reduced protein production. This argues that local sequence context is important for determining the effects of codon optimality on gene expression. This fits with reports showing that specific combinations of codons modulate translation efficiency and mRNA decay (Burke et al., 2022; Gamble et al., 2016). We find that these two CTT substitutions drive the formation of a predicted stem-loop structure and that disruption of this structure, while maintaining the two nonoptimal CTT codons partially rescues the slowed translation elongation and reporter

expression. Interestingly it was recently shown in prokaryotes that mRNA stem-loops can dock into the A site of the ribosome inhibiting translation elongation (Bao et al., 2020, 2022). These works showed that ribosome slowing was due to specific length and structure rather than just high thermodynamic stability of the stem loop. It will be interesting to explore if a similar mechanism of translation elongation slowing takes place in this context.

We found that CGA stalls added ~76s per CGA codon to the translation duration of the reporter after 3xCGAs. This led to an almost 5 minute lengthening of translation duration for a 6xCGA construct. A recent paper by Goldman and colleagues examined ribosomal clearance times on mRNA containing difficult-to-translate polyA-containing stretches and found it took approximately 10 and 13 minutes for ribosomes to clear off 50% of transcripts containing poly(A)36 and poly(A)60 stretches, respectively (Goldman et al., 2021). Their finding on delays lasting on the order of minutes is consistent with our findings and represents an intriguing observation considering that the average half-life of yeast mRNAs is ~10 minutes, suggesting that a significant portion of an mRNA's half-life can be spent engaged in a ribosomal stall (Chan et al., 2018). The long duration of stalling also fits with long queues of ribosomes 5' of the stall, as has been seen with disome-seq and in vivo translational imaging in mammalian cells (Goldman et al., 2021; P. Han et al., 2020). We believe we may be observing a cumulative effect of ribosome queuing affecting the overall translation duration.

It is well-confirmed that Hel2 is a necessary factor mediating RQC and NGD pathways however its effects on ribosomal stall have been unclear. Two non-mutually exclusive models have

been proposed (Meydan & Guydosh, 2020, 2021): first, since Hel2 is needed to promote the rescue of the stalled ribosome in a collision complex, deletion of Hel2 will slow ribosome rescue, resulting in accumulated collided ribosomes, which increases elongation delay; in the second model, as proposed by Meydan and Guydosh, Hel2 is able to sense and stabilize stalled ribosomes to prevent further translation. In this scenario, deletion of Hel2 would destabilize collided ribosomes, resulting in rescued elongation and shorter elongation delay. In this paper, we quantitatively measure the change of elongation delay after Hel2 depletion and find a reduction in the translation duration of CGA stalled sequences. This is distinct from mammalian cells, where depletion of the mammalian homolog of Hel2, ZNF598, causes further delays in the clearing of ribosomes (Goldman et al., 2021).

It has been previously reported that Dhh1 plays a role in degradation of mRNA enriched in nonoptimal codons (Radhakrishnan et al., 2016). We were surprised to find that Dhh1 deletion instead decreases the expression of the YFP[CTC] construct. As the YFP constructs used in this study are all yeast optimized except for the leucine codons, it is possible that Dhh1 deletion would only be beneficial for mRNAs more enriched in poor codons. Previous work demonstrates a negligible effect of dhh1Δ on mRNA half-life for primarily optimal mRNA (Radhakrishnan et al., 2016).

Although most studies have investigated Dhh1 with regards to its role in mRNA decay and translational repression, Dhh1 has also been shown to promote the translation of certain mRNAs. It has been previously demonstrated that a subset of mRNAs that contain highly-structured 5'UTRs

and coding sequences require Dhh1 helicase activity for efficient expression (Jungfleisch et al., 2017). Furthermore, Dhh1 can shift roles in a condition-dependent manner. During nitrogen starvation, Dhh1 is required for the efficient expression of autophagy-related proteins Atg1 and Atg13, but when nutrients are plentiful Dhh1 encourages ATG mRNA degradation (X. Liu et al., 2019). Overall, this argues that Dhh1 may play context specific roles in translation elongation and may be able to speed up elongation in specific sequence contexts.

2.5 Materials and Methods

2.5.1 Plasmid Preparation and Integration

All plasmids used in Chapter 2 are listed in Table 2.5.1 and all primers used for clone in Chapter 2 are listed in Table 2.5.3. A number of the key elongation reporter plasmids have been deposited at Addgene www.addgene.org/Brian_Zid/. Plasmids containing synonymous leucine codon substituted YFP (TTG, CTA, CTC, CTG, and CTT) and a single-copy yeast integrating plasmid containing a pTET07 promoter were provided as a kind gift from Dr. Arvind Rasi Subramaniam at the Fred Hutchinson Cancer Center in Seattle, Washington. Fragments containing pTET07, YFP variants, and yeast-optimized nanoluciferase (Promega Cat. No. N1141) were amplified using PCR and cloned into the XhoI and HindIII-digested single-copy yeast integrating plasmid using Gibson assembly.

The pAG306-pTet07-YFP[1-7CTT]-nLuc, pAG306-pTet07-YFP[1-8CTT]-nLuc, pAG306-pTet07-YFP[1-9CTT]-nLuc, pAG306-pTet07-YFP[1-10CTT]-nLuc, pAG306-pTet07-YFP[11-20CTT]-nLuc strains were generated by PCR amplification of the entire backbone of the previous pAG306-pTet07-YFP[TTG]-nLuc plasmid beginning at nLuc and ending with pTet07, and PCR amplification of the corresponding parts of the YFP[TTG] and YFP [CTT] variants (For example, YFP[1-7CTT] includes No.1-7 Leu condon part of YFP[CTT] and No.8-20 Leu codon part of YFP[TTG]) (Figure 2.3.8A). These fragments were combined using Gibson assembly.

The pAG306-pTet07-YFP[7,8CTT]-nLuc and pAG306-pTet07-YFP[8CTT] were further constructed with the same backbone of pAG306-pTet07-YFP[TTG]-nLuc plasmid, and distinct

YFP variants. YFP[7,8CTT] and YFP[8CTT] variants are constructed based on YFP[TTG] and YFP[1-8CTT]. (For example, YFP[7,8CTT] includes No.1-6 Leu condon part of YFP[TTG] and No.7-20 Leu codon part of YFP[1-8CTT]) (Figure 2.3.8A). These fragments were combined using Gibson assembly.

Plasmid variants containing two to six CGA stalls were generated using the aforementioned backbone PCR of the pAG306-pTet07-YFP[TTG] plasmid and a PCR amplified YFP[TTG] fragment containing two to six CGA repeats as a 3' overhang. These fragments were combined using Gibson assembly.

All plasmids were linearized using NotI and integrated into yeast by homologous recombination. Integrations were screened by growing transformed yeast on synthetic complete (SC) dropout plates lacking uracil. These were then frozen down for long-term storage in YPD containing 15% v/v glycerol.

2.5.2 Yeast Strains, Growth, and Media

All yeast strains used in Chapter 2 are listed in Table 2.5.2. The background yeast strain S288C (BY4741) was used for all experiments. Yeast dhh1Δ, hel2Δ, and syh1Δ strains were created by deleting the endogenous DHH1, HEL2, and SYH1 loci, respectively, using pRS315 (Addgene Plasmid #3974) and screened by growing transformed yeast on SC dropout plates lacking leucine. Specific oligos used are listed in Table 2.3.3. Yeast strains were frozen down in YPD containing 30% v/v glycerol.

For cells cultured for use in our reporter assay, cells were streaked out from frozen stocks onto YPD Agar plates and grown at 30 °C for two days. These plates were stored at 4 °C for up to one month.

2.5.3 RNA Extraction and Real Time qPCR

Yeast pellets were collected from samples 60-minutes post-ATc addition by spinning 1-1.5 mL of liquid culture at 3000 x g for 2 minutes and discarding the supernatant. These yeast pellets were then flash frozen in liquid nitrogen and stored at -80 °C until RNA extraction. RNA was extracted from yeast pellets using the MasterPure™ Yeast RNA Purification Kit (Lucigen Cat. No. MPY03100) according to the manufacturer's instructions. RNA quality and concentration was assessed using a Nanodrop.

RNA samples were subjected to DNase digestion using RQ1 RNase-free DNase (Promega) according to the manufacturer’s instructions. cDNA was prepared from equal amounts of RNA from each sample using Protoscript II Reverse Transcriptase (New England Biolabs Cat. No. M0368X) and an oligo dT(18) primer according to the manufacturer’s instructions. RT-qPCR was done using a home-brew recipe with SYBR Green at a final concentration of 0.5X (Thermo Fisher S7564). Primers specific for nanoluciferase and actin are described in Supplementary Table S2. mRNA levels were normalized to ACT1 abundance and fold change was calculated by a standard Ct analysis.

2.5.4 Luciferase-Based Elongation Reporter Assay

Liquid cultures were started from single colonies and allowed to grow overnight in YPD at 30 °C with shaking until an approximate OD600 of 0.3-0.5 after which cultures were divided into two tubes. For one of the tubes, 1 µL of a stock solution of anhydrotetracycline (250 µg/mL of ATc dissolved in EtOH) was added per mL of culture. Both tubes were returned to 30 °C with shaking for five minutes. 90 µL of each culture was added to a 96-well white flat-bottom plate (Grainger) and to each well, 10 uL of furimazine (10 mM furimazine stock solution dissolved in DMSO diluted 1:200 in YPD), was added. Immediately after sample loading, the plate was placed in a 30 °C prewarmed Tecan Infinite® 200 PRO plate reader. The following program was used and luminescence measurements were taken every 30 or 60 seconds: (1) Kinetic Cycle: [Cycle Duration: 60 minutes, Kinetic Interval: 30 or 60 seconds], (2) Shaking: [Duration: 3 seconds, Mode: Orbital, Amplitude 2 mm], (3) Luminescence: [Attenuation: Automatic, Integration Time: 1000 ms, Settle Time: 0 ms].

2.5.5 Schleif Plot and Elongation Delay Measurements

Three strains (optYFP, 4×CGA and 6×CGA) were used to run nLuc assay as an example to show data analysis method to quantify protein expression and elongation duration. Figure 2.5.1 shows the protocol of data re-processing of raw nLuc assay data.

(1) In the raw nLuc assay data, Luciferase (Luc) is plotted against Time (t), which is shown in Figure 2.5.1A. Because of the leakiness of TetO7 promoter, we could find positive nLuc expression when there isn't ATc addition (e.g. optYFP(-ATC)). To acquire the pure ATC-induced protein expression (Figure 2.5.1B), for each sample, we calculate by subtracting the samples lacking ATC from the corresponding samples with ATC across all measured timepoints. Formulas are listed below:

$$Luc = Luc\ (+ATc) - Luc(-ATc)$$

$$e.g.Luc\ (optYFP) = Luc\ (optYFP(+ATC)) - Luc(optYFP(-ATC))$$

(2) Since control for time of pre-induction steps (such as ATc absorption, activation of TetO7 promoter and transcription intiation), theoretically, we should find no nLuc induction (Luc = 0) in the beginning of the nLuc assay plot until we get the first nLuc expression. If we enlarge the beginning part of nLuc assay data (0~20 mins in Figure 2.5.1C), we find non-zero basal levels during 0~5mins (which may be induced by mechanical or technical errors). To eliminate mechanical or technical errors, all values ($Luc(t)$) were then subtracted by the "average Luc of the first 5 minutes" ($Luc(0)$) to acquire "$Luc(t) - Luc(0)$" in Figure 2.5.1D.

(3) Samples were normalized to an OD600 of 1.0 by dividing their protein expression over time by their respective ODs. Thus, in Figure 2.5.1E, we plotted the normalized ATC-induced protein expression ($Luc(t) - Luc(0)(normalized)$) against time ($Time/min$) of all samples.

Additionally, the values at 60 mins timepoints in Figure 2.5.1E were picked to evaluate relative protein expression of multiple samples.

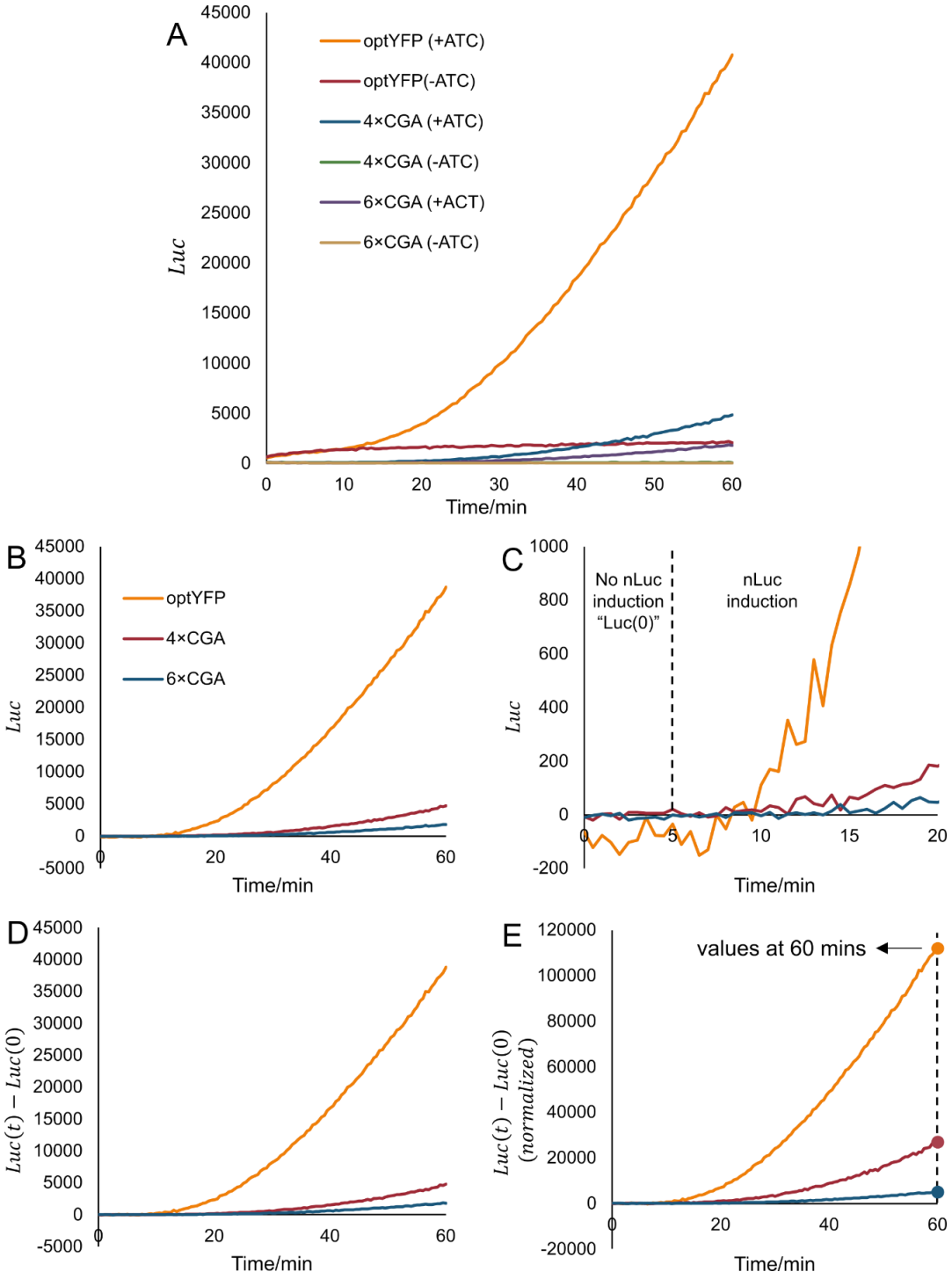

Figure 2.5.1 Data re-processing of raw nLuc assay data

A: nLuc assay data with and without ATC addition.

B: nLuc assay data with pure ATC-induced. ($Luc = Luc\ (+ATC) - Luc(-ATC)$)

C: nLuc assay data of 0~20 mins time-frame.

D: nLuc assay data with mechanical or technical errors ($Luc(0)$) subtracted.

E: nLuc assay data with OD normalized.

The Schleif Plot methodology was adapted from (Schleif et al. 1973) and slightly modified to assume a non-constant basal expression protein level. The general principle is that upon sufficient time for transcriptional induction to start there will be a proportional increase in mRNA level to time (t):

Luciferase $\propto$ mRNA level and time (t)

The increase of luciferase from a single mRNA is also proportional to DNA level which is a constant and time (t):

mRNA level $\propto$ DNA level and time (t)

As mRNA levels are also increasing with time this means that the total amount of luciferase is proportional to t2:

Luciferase $\propto$ t2 OR $\sqrt{luciferase} \propto$ t

Based on the Schleif Plot methodology, we developed the following data analysis method to acquire elongation duration. Protocol to quantify elongation duration is shown in Figure 2.5.2.

(1) For elongation duration quantification, the square root of each value in Figure 2.5.2A ($\sqrt{Luc(t) - Luc(0)}$) was calculated and plotted against time ($Time/min$) in Figure 2.5.2B.

(2) We could roughly divide Figure 2.5.2B into three regions according to the shape of curves. Region A (0~15 mins) is where we get initial nLuc expression and the nLuc induction in this region is highly variable. In region B (15~30 mins), $\sqrt{Luc(t) - Luc(0)}$ shows nice linear relationship

with time. When we go to Region C (30~60 mins), the linear increasing of curve collapses which is caused by degradation of RNA or protein. For accurate and consistent quantification of elongation duration, we selected data in region B where there are the most linear and consistent increasing curves (Figure 2.5.2C)

(3) Based on the selected data in Figure 2.5.2C, we run linear fitting and extended the fitting lines backward to get their X-intercepts (Figure 2.5.2D). Those X-intercepts describes the timepoints of initial nLuc induction of each sample. In addition, the difference between two X-intercepts describes the elongation difference (including transcription and translation) two sample. For example, the difference of X-intercepts between optYFP and 4×CGA samples includes their transcription and translation elongation time difference. One we subtracted the transcription elongation time (calculated by transcriptional elongation rate and length difference), we get translation elongation time difference between optYFP and 4×CGA samples, which depicts the elongation duration induced by 4×CGA sequence.

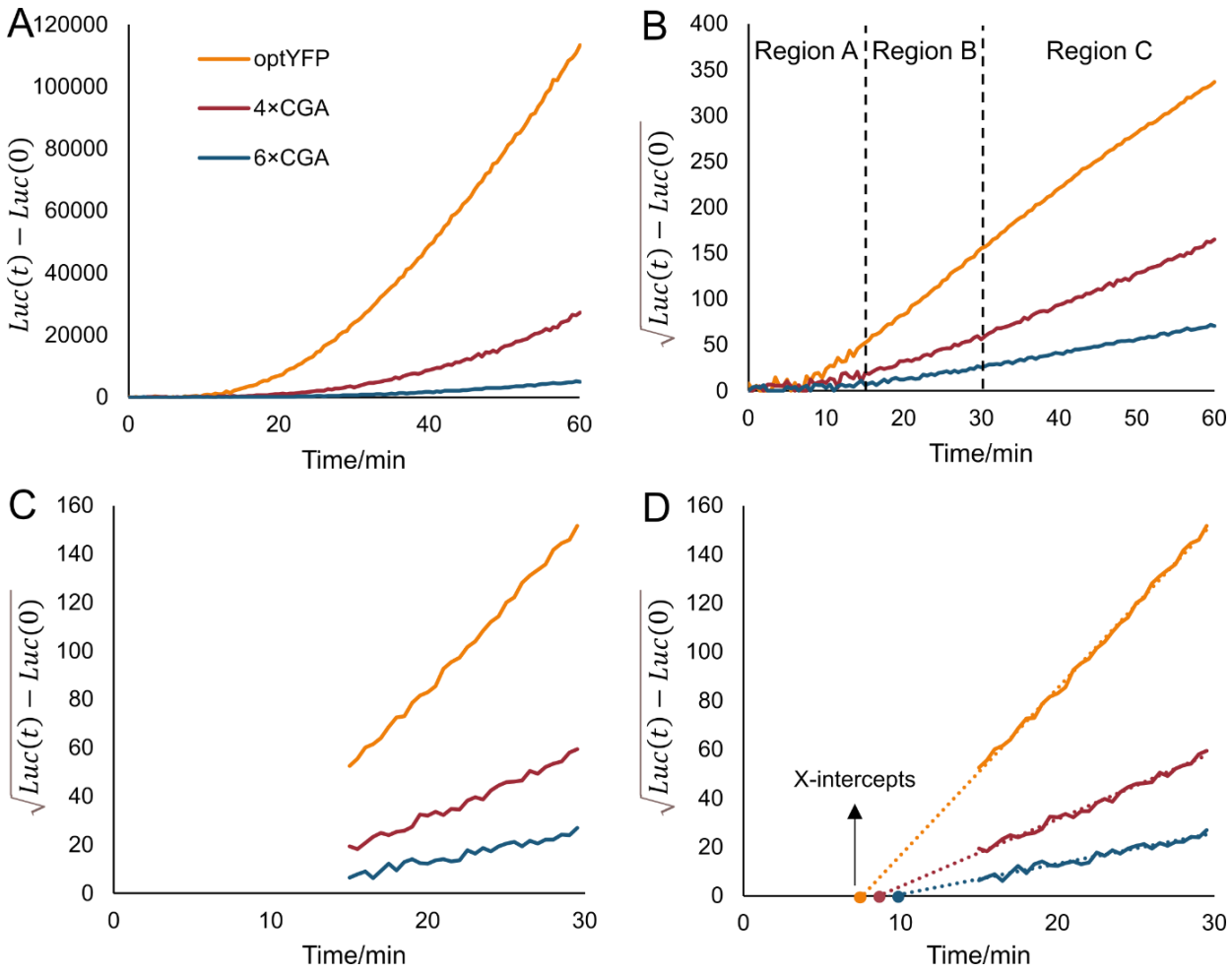

Figure 2.5.2 Schleif Plot method to quantify elongation duration

A: nLuc assay data that shows the nLuc induction of optYFP, 4×CGA and 6×CGA strains. Y-axis (luc) is normalized.

B: Square root of each luc values. The plot was divided into three regions (A, B and C) according to the shape.

C: Data selection of 15-30 mins, which shows the most linear and consistent increasing trend of curves.

D: Linear fitting and extend the fitting lines backward to get X-intercepts that describes the timepoints of initial nLuc induction of each sample.

Table 2.5.1 List of plasmids used in Chapter 2

Designation	Construct Name	Source	Identifiers
ZP404	pLLSC15	Arvind (Rasi) Subramaniam lab	pAG306-ura-rtta-yfpCTA
ZP405	pLLSC16	Arvind (Rasi) Subramaniam lab	pAG306-ura-rtta-yfpCTC
ZP406	pLLSC17	Arvind (Rasi) Subramaniam lab	pAG306-ura-rtta-yfpCTT
ZP407	pLLSC18	Arvind (Rasi) Subramaniam lab	pAG306-ura-rtta-yfpCTG
ZP408	pLLSC19	Arvind (Rasi) Subramaniam lab	pAG306-ura-rtta-yfpwt[TTG/AGA]
ZP377	nLuc source	Lab stock	TetO7-PGK1UTR-LacZ-PKTlinker-nLucPEST-MS2(v4)
ZP317	miRFP source	Lab stock	Hsp30pr-Hsp26UTR-nLuc-pKTlinker-miRFPPEST-12xMS2v6-ADH1ter
ZP191	Pringle (HPH)	Wilhelm lab	pFA6a-HphMX6
ZP145	Pringle (KAN)	Lab stock	pFA6a-Kan
ZP427	nLuc	This study	pAG306-ura-rtta-pTet-nLuc
ZP436	optYFP	This study	pAG306-ura-rtta-pTet-YFP[TTG]-nLuc
ZP464	2xCGA	This study	pAG306-ura-rtta-pTet-YFP[TTG]-2xCGA-nLuc
ZP486	3xCGA	This study	pAG306-ura-rtta-pTet-YFP[TTG]-3xCGA-nLuc
ZP465	4xCGA	This study	pAG306-ura-rtta-pTet-YFP[TTG]-4xCGA-nLuc
ZP487	5xCGA	This study	pAG306-ura-rtta-pTet-YFP[TTG]-5xCGA-nLuc
ZP466	6xCGA	This study	pAG306-ura-rtta-pTet-YFP[TTG]-6xCGA-nLuc
ZP599	6xAGA	This study	pAG306-ura-rtta-pTet-YFP[TTG]-6xAGA-nLuc
ZP432	YFP[CTA]	This study	pAG306-ura-rtta-pTet-YFP[CTA]-nLuc
ZP433	YFP[CTC]	This study	pAG306-ura-rtta-pTet-YFP[CTC]-nLuc
ZP434	YFP[CTT]	This study	pAG306-ura-rtta-pTet-YFP[CTT]-nLuc
ZP435	YFP[CTG]	This study	pAG306-ura-rtta-pTet-YFP[CTG]-nLuc
ZP616	YFP[1-7CTT]	This study	pAG306-ura-rtta-pTet-YFP[1-7CTT]-nLuc
ZP632	YFP[1-8CTT]	This study	pAG306-ura-rtta-pTet-YFP[1-8CTT]-nLuc
ZP617	YFP[1-9CTT]	This study	pAG306-ura-rtta-pTet-YFP[1-9CTT]-nLuc
ZP513	YFP[1-10CTT]	This study	pAG306-ura-rtta-pTet-YFP[1-10CTT]-nLuc
ZP515	YFP[11-20CTT]	This study	pAG306-ura-rtta-pTet-YFP[11-20CTT]-nLuc
ZP634	YFP[7,8CTT]	This study	pAG306-ura-rtta-pTet-YFP[7,8CTT]-nLuc
ZP635	YFP[8CTT]	This study	pAG306-ura-rtta-pTet-YFP[8CTT]-nLuc
ZP644	T62 mutated	This study	pAG306-ura-rtta-pTet-YFP[7,8CTT] (T62 mutated)-nLuc
ZP645	G65 mutated	This study	pAG306-ura-rtta-pTet-YFP[7,8CTT] (G65 mutated)-nLuc
ZP646	T62, G65 mutated	This study	pAG306-ura-rtta-pTet-YFP[7,8CTT] (T62, G65 mutated)-nLuc
ZP531	miRFP-optYFP	This study	pAG306-ura-rtta-pTet-miRFP-YFP[TTG]-nLuc
ZP530	miRFP-YFP[CTT]	This study	pAG306-ura-rtta-pTet-miRFP-YFP[CTT]-nLuc

Table 2.5.2 List of Yeast used in Chapter 2

Designation	Strain name	Identifiers
ZY8	ZY8	BY4741
ZY549	ZY8 hel2△	BY4741, hel2△
ZY501	ZY8 dhh1 △	BY4741, dhh1△
ZY803	ZY8 syh1 △	BY4741, syh1△
ZY478	nLuc	BY4741, pAG306-ura-rtta-pTet-nLuc
ZY483	optYFP	BY4741, pAG306-ura-rtta-pTet-YFP[TTG]-nLuc
ZY532	2xCGA	BY4741, pAG306-ura-rtta-pTet-YFP[TTG]-2xCGA-nLuc
ZY578	3xCGA	BY4741, pAG306-ura-rtta-pTet-YFP[TTG]-3xCGA-nLuc
ZY533	4xCGA	BY4741, pAG306-ura-rtta-pTet-YFP[TTG]-4xCGA-nLuc
ZY579	5xCGA	BY4741, pAG306-ura-rtta-pTet-YFP[TTG]-5xCGA-nLuc
ZY534	6xCGA	BY4741, pAG306-ura-rtta-pTet-YFP[TTG]-6xCGA-nLuc
ZY836	6xAGA	BY4741, pAG306-ura-rtta-pTet-YFP[TTG]-6xAGA-nLuc
ZY484	YFP[CTA]	BY4741, pAG306-ura-rtta-pTet-YFP[CTA]-nLuc
ZY480	YFP[CTC]	BY4741, pAG306-ura-rtta-pTet-YFP[CTC]-nLuc
ZY481	YFP[CTT]	BY4741, pAG306-ura-rtta-pTet-YFP[CTT]-nLuc
ZY482	YFP[CTG]	BY4741, pAG306-ura-rtta-pTet-YFP[CTG]-nLuc
ZY870	YFP[1-7CTT]	BY4741, pAG306-ura-rtta-pTet-YFP[1-7CTT]-nLuc
ZY871	YFP[1-8CTT]	BY4741, pAG306-ura-rtta-pTet-YFP[1-8CTT]-nLuc
ZY872	YFP[1-9CTT]	BY4741, pAG306-ura-rtta-pTet-YFP[1-9CTT]-nLuc
ZY624	YFP[1-10CTT]	BY4741, pAG306-ura-rtta-pTet-YFP[1-10CTT]-nLuc
ZY626	YFP[11-20CTT]	BY4741, pAG306-ura-rtta-pTet-YFP[11-20CTT]-nLuc
ZY877	YFP[7,8CTT]	BY4741, pAG306-ura-rtta-pTet-YFP[7,8CTT]-nLuc
ZY878	YFP[8CTT]	BY4741, pAG306-ura-rtta-pTet-YFP[8CTT]-nLuc
ZY987	T62 mutated	BY4741, pAG306-ura-rtta-pTet-YFP[7,8CTT] (T62 mutated)-nLuc
ZY898	G65 mutated	BY4741, pAG306-ura-rtta-pTet-YFP[7,8CTT] (G65 mutated)-nLuc
ZY989	T62 + G65 mutated	BY4741, pAG306-ura-rtta-pTet-YFP[7,8CTT] (T62 + G65 mutated)-nLuc
ZY692	miRFP-optYFP	BY4741, pAG306-ura-rtta-pTet-miRFP-YFP[TTG]-nLuc
ZY691	miRFP-YFP[CTT]	BY4741, pAG306-ura-rtta-pTet-miRFP-YFP[CTT]-nLuc
ZY553	optYFP hel2△	BY4741, hel2△, pAG306-ura-rtta-pTet-YFP[TTG]-nLuc
ZY566	2xCGA hel2△	BY4741, hel2△, pAG306-ura-rtta-pTet-YFP[TTG]-2xCGA-nLuc
ZY567	4xCGA hel2△	BY4741, hel2△, pAG306-ura-rtta-pTet-YFP[TTG]-4xCGA-nLuc
ZY568	6xCGA hel2△	BY4741, hel2△, pAG306-ura-rtta-pTet-YFP[TTG]-6xCGA-nLuc
ZY550	YFP[CTC] hel2△	BY4741, hel2△, pAG306-ura-rtta-pTet-YFP[CTC]-nLuc
ZY551	YFP[CTT] hel2△	BY4741, hel2△, pAG306-ura-rtta-pTet-YFP[CTT]-nLuc
ZY519	optYFP dhh1△	BY4741, dhh1△, pAG306-ura-rtta-pTet-YFP[TTG]-nLuc
ZY516	YFP[CTC] dhh1△	BY4741, dhh1△, pAG306-ura-rtta-pTet-YFP[CTC]-nLuc
ZY522	YFP[CTT] dhh1△	BY4741, dhh1△, pAG306-ura-rtta-pTet-YFP[CTT]-nLuc
ZY808	optYFP syh1△	BY4741, syh1△, pAG306-ura-rtta-pTet-YFP[TTG]-nLuc
ZY809	6xCGA syh1△	BY4741, syh1△, pAG306-ura-rtta-pTet-YFP[TTG]-6xCGA-nLuc
ZY807	YFP[CTT] syh1△	BY4741, syh1△, pAG306-ura-rtta-pTet-YFP[CTT]-nLuc

Table 2.5.3 List of primers used in Chapter 2

Identifier	Primer Name	Purpose	Sequence
ZO1186	Hel2 Deletion Fwd	Hel2 endogenous deletion	CTAATGCTATTGTCAGTTACAGGTTAGAAATAT ATTTCCAA CGG ATC CCC GGG TTA ATT AA
ZO1187	Hel2 Deletion Rev		CGAAAAAATAGTGGCTATACTTCTTTTCAAGA ATTAGG GAA TTC GAG CTC GTT TAA AC
ZO1192	Hel2 Check Fwd	qPCR to check Hel2 endogenous deletion	TCTCAACCTACCTCAACTACC
ZO1193	Hel2 Check Rev		GCTGCTTTTGTTTGCCTTTC
ZO113	Dhh1 Deletion Fwd	Dhh1 endogenous deletion	ATCCCAGGCCTAAAATACGACAAGAAAGAAA ATAGTAGTA CGG ATC CCC GGG TTA ATT AA
ZO114	Dhh1 Deletion Rev		GCGTATCTCACCACAGTAGTTATTTTTTCTTAG ATATTCT GAA TTC GAG CTC GTT TAA AC
ZO131	Dhh1 Check Fwd	qPCR to check Dhh1 endogenous deletion	ACAGCCGCATTTGTTATTCC
ZO130	Dhh1 Check Rev		ACGACTTGGGAAGTTTGCAG
ZO117	Dom34 Deletion Fwd	Dom34 endogenous deletion	AAATGTAATTTAATGAAGATCCCAAAAAATTA AGCATTCG CGG ATC CCC GGG TTA ATT AA
ZO118	Dom34 Deletion Rev		AAATTTTATGTGTACATTACTTTTTTCTTACATA GTAAAT GAA TTC GAG CTC GTT TAA AC
ZO127	Dom34 Check Fwd	qPCR to check Dom34 endogenous deletion	AGAGCAATGGAGGAAAAGCA
ZO126	Dom34 Check Rev		CCTCACCATCGTCTTCATCA
ZO1331	Syh1 Deletion Fwd	Syh1 endogenous deletion	TTTGCCACAGCTTGCACAAGATTGGCAGTGG CAGTAAGTG CGG ATC CCC GGG TTA ATT AA
ZO1332	Syh1 Deletion Rev		GCGTAGTAAACAACTACTATGGAACAAAAAG GCT GAA TTC GAG CTC GTT TAA AC
ZO1335	Syh1 Check Fwd	qPCR to check Syh1 endogenous deletion	TAATTTGGCGCCTTGGGCTA
ZO1336	Syh1 Check Rev		AGATGGGGAAGGCGTTCTTG
ZO83	Actin Fwd	RT-qPCR	CTGCCGGTATTGACCAAACT
ZO84	Actin Rev		CGGTGATTTCCTTTTGCATT
ZO553	nLuc Fwd	RT-qPCR	TGGTGATCAAATGGGTCAAA
ZO544	nLuc Rev		CCTTCATAAGGACGACCAAA
ZO1452	pTet07_F	PCR pTet for ZP436 clone	GGAATTGACGAGTACGGTGGGTAGCTCGAG CCACTTCTAAATAAGCGAATTTC
ZO1453	pTet07_R		AATTGATCCGGTAATTTAGTGTG
ZO1459	yfp-nLucPEST_F	PCR nLuc for ZP436 clone	CACGGTATGGACGAATTGTACAAG ATGGTTTTTACTTTAGAAGATTTTG
ZO1463	Cyc1term-nLuc_R		GAATGTAAGCGTGACATAACTAATAAGCTTTT A AAAACCATGAGAATTAGCTAAAATACG
ZO1455	optYFP_F	PCR optYFP for ZP436 clone	ACTAAATTACCGGATCAATT ATGTCTAAGGGTGAAGAATTG
ZO1456	optYFP_R		TCTTCTAAAGTAAAAACCAT CTTGTACAATTCGTCCATAC
ZO463	NLuc+PestR	PCR pAG306 vector (including nLuc and pTet) (commonly used)	ATGGTTTTTACTTTAGAAGATTTTG
ZO1453	pTet07_R		AATTGATCCGGTAATTTAGTGTG
ZO1464	pTet-synYFP_F	PCR YFP for ZP432~ZP435 clone	ACTAAATTACCGGATCAATT ATGTCTAAGGGTGAAGAA
ZO1465	nLuc-synYFP_R		CAACAAAATCTTCTAAAGTAAAAACCAT CTTGTACAATTCGTCCATAC

Table 2.5.4 List of primers used in Chapter 2 (Continued)

ZO1464	pTet-synYFP_F	PCR YFP[TTG]-2CGA for ZP464 clone	ACTAAATTACCGGATCAATT ATGTCTAAGGGTGAAGAA
ZO1468	2xArgCGA-synYFP_R		CAACAAAATCTTCTAAAGTAAAAACCAT TCGTCG CTTGTACAATTCGTCCATAC
ZO1464	pTet-synYFP_F	PCR YFP[TTG]-3CGA for ZP465 clone	ACTAAATTACCGGATCAATT ATGTCTAAGGGTGAAGAA
ZO1469	3xArgCGA-synYFP_R		CAACAAAATCTTCTAAAGTAAAAACCAT TCGTCGTCG CTTGTACAATTCGTCCATAC
ZO1464	pTet-synYFP_F	PCR YFP[TTG]-4CGA for ZP466 clone	ACTAAATTACCGGATCAATT ATGTCTAAGGGTGAAGAA
ZO1470	4xArgCGA-synYFP_R		CAACAAAATCTTCTAAAGTAAAAACCAT TCGTCGTCGTCG CTTGTACAATTCGTCCATAC
ZO1464	pTet-synYFP_F	PCR YFP[TTG]-5CGA for ZP467 clone	ACTAAATTACCGGATCAATT ATGTCTAAGGGTGAAGAA
ZO1471	5xArgCGA-synYFP_R		CAACAAAATCTTCTAAAGTAAAAACCAT TCGTCGTCGTCGTCG CTTGTACAATTCGTCCATAC
ZO1464	pTet-synYFP_F	PCR YFP[TTG]-6CGA for ZP468 clone	ACTAAATTACCGGATCAATT ATGTCTAAGGGTGAAGAA
ZO1472	6xArgCGA-synYFP_R		CAACAAAATCTTCTAAAGTAAAAACCAT TCGTCGTCGTCGTCGTCG CTTGTACAATTCGTCCATAC
ZO1464	pTet-synYFP_F	PCR 5'part of YFP[1-7CTT] for ZP616 clone	ACTAAATTACCGGATCAATT ATGTCTAAGGGTGAAGAA
ZO1543	LeuYFP-07_R		CCGTAACCCAAAGTAGTAACAAGAGT
ZO1542	LeuYFP-07_F	PCR 3'part of YFP[1-7CTT] for ZP616 clone	ACTCTTGTTACTACTTTGGGTTACGG
ZO1465	nLuc-synYFP_R		CAACAAAATCTTCTAAAGTAAAAACCAT CTTGTACAATTCGTCCATAC
ZO1464	pTet-synYFP_F	PCR 5'part of YFP[1-8CTT] for ZP632 clone	ACTAAATTACCGGATCAATT ATGTCTAAGGGTGAAGAA
ZO1650	LeuYFP-08_R V2		GCGAAACACATCAAACCGTAACC
ZO1544	LeuYFP-08_F	PCR 3'part of YFP[1-8CTT] for ZP632 clone	ACTCTTGTTACTACTCTTGGTTACGG
ZO1465	nLuc-synYFP_R		CAACAAAATCTTCTAAAGTAAAAACCAT CTTGTACAATTCGTCCATAC
ZO1464	pTet-synYFP_F	PCR 5'part of YFP[1-9CTT] for ZP617 clone	ACTAAATTACCGGATCAATT ATGTCTAAGGGTGAAGAA
ZO1560	LeuYFP-09_R		GGCATAGCAGACTTGAAGAAGTCG
ZO1559	LeuYFP-09_F	PCR 3'part of YFP[1-9CTT] for ZP617 clone	CGACTTCTTCAAGTCTGCTATGCC
ZO1465	nLuc-synYFP_R		CAACAAAATCTTCTAAAGTAAAAACCAT CTTGTACAATTCGTCCATAC
ZO1464	pTet-synYFP_F	PCR 5'part of YFP[1-10CTT] for ZP513 clone	ACTAAATTACCGGATCAATT ATGTCTAAGGGTGAAGAA
ZO1486	FirstHalfYFP_R		CCGTCTTCCTTGAAGTCGATACCC
ZO1487	SecondHalfYFP_F	PCR 3'part of YFP[1-10CTT] for ZP513 clone	GGGTATCGACTTCAAGGAAGACGG
ZO1465	nLuc-synYFP_R		CAACAAAATCTTCTAAAGTAAAAACCAT CTTGTACAATTCGTCCATAC

Table 2.5.5 List of primers used in Chapter 2 (Continued)

ZO1464	pTet-synYFP_F	PCR 5'part of YFP[11-20CTT] for ZP515 clone	ACTAAATTACCGGATCAATT ATGTCTAAGGGTGAAGAA
ZO1486	FirstHalfYFP_R		CCGTCTTCCTTGAAGTCGATACCC
ZO1487	SecondHalfYFP_F	PCR 3'part of YFP[11-20CTT] for ZP515 clone	GGGTATCGACTTCAAGGAAGACGG
ZO1465	nLuc-synYFP_R		CAACAAAATCTTCTAAAGTAAAAACCAT CTTGTACAATTCGTCCATAC
ZO1464	pTet-synYFP_F	PCR 5'part of YFP[7,8CTT] for ZP634 clone	ACTAAATTACCGGATCAATT ATGTCTAAGGGTGAAGAA
ZO1652	LeuYFP[7,8 CTT]_R		AGTTGGCCATGGAACTGG
ZO1651	LeuYFP[7,8 CTT]_F	PCR 3'part of YFP[7,8CTT] for ZP634 clone	CCAGTTCCATGGCCAACT
ZO1465	nLuc-synYFP_R		CAACAAAATCTTCTAAAGTAAAAACCAT CTTGTACAATTCGTCCATAC
ZO1464	pTet-synYFP_F	PCR 5'part of YFP[8CTT] for ZP635 clone	ACTAAATTACCGGATCAATT ATGTCTAAGGGTGAAGAA
ZO1654	LeuYFP[8 CTT]_R		ACCGTAACCAAGAGTAGTAAC
ZO1653	LeuYFP[8 CTT]_F	PCR 3'part of YFP[8CTT] for ZP635 clone	GTTACTACTCTTGGTTACGGT
ZO1465	nLuc-synYFP_R		CAACAAAATCTTCTAAAGTAAAAACCAT CTTGTACAATTCGTCCATAC
ZO1464	pTet-synYFP_F	PCR 5'part of YFP[7,8CTT](T62 mutated) for ZP644 clone	ACTAAATTACCGGATCAATT ATGTCTAAGGGTGAAGAA
ZO1679	YFP point mutation (ACT to ACA)_R		CAAACCGTAACCAAGAGTTGTAAC
ZO1678	YFP point mutation (ACT to ACA)_F	PCR 3'part of YFP[7,8CTT](T62 mutated) for ZP644 clone	GTTACAACTCTTGGTTACGGTTTG
ZO1465	nLuc-synYFP_R		CAACAAAATCTTCTAAAGTAAAAACCAT CTTGTACAATTCGTCCATAC
ZO1464	pTet-synYFP_F	PCR 5'part of YFP[7,8CTT](G65 mutated) for ZP645 clone	ACTAAATTACCGGATCAATT ATGTCTAAGGGTGAAGAA
ZO1681	YFP point mutation (GGT to GGC)_R		CAAACCGTAGCCAAGAGTAGTAAC
ZO1680	YFP point mutation (GGT to GGC)_F	PCR 3'part of YFP[7,8CTT](G65 mutated) for ZP645 clone	GTTACTACTCTTGGCTACGGTTTG
ZO1465	nLuc-synYFP_R		CAACAAAATCTTCTAAAGTAAAAACCAT CTTGTACAATTCGTCCATAC
ZO1464	pTet-synYFP_F	PCR 5'part of YFP[7,8CTT](T62, G65 mutated) for ZP646 clone	ACTAAATTACCGGATCAATT ATGTCTAAGGGTGAAGAA
ZO1683	YFP point mutation (ACT to ACA) (GGT to GGC)_R		CAAACCGTAGCCAAGAGTTGTAAC
ZO1682	YFP point mutation (ACT to ACA) (GGT to GGC)_F	PCR 3'part of YFP[7,8CTT](T62, G65 mutated) for ZP646 clone	GTTACAACTCTTGGCTACGGTTTG
ZO1465	nLuc-synYFP_R		CAACAAAATCTTCTAAAGTAAAAACCAT CTTGTACAATTCGTCCATAC
ZO1493	pTet-miRFP_F	PCR miRFP for ZP530/ZP531	ACTAAATTACCGGATCAATT ATGGTAGCAGGCCATGCAAG
ZO1494	synYFP_miRFP_R		TTCTTCACCCTTAGACAT GCTTTCCAGAGCTGTAATCC

2.6 Acknowledgements

Chapter 2, in full, is prepared for publication: Harjono, V, Hou, W, Harvey, AT, Subramaniam, AR, and Zid, BM. Quantification of elongation stalls and impact on gene expression in yeast. The dissertation author is the first author of this publication.

We would like to thank the Zid lab for helpful feedback on the manuscript. We thank Claes Andréasson for sharing the yeast optimized Nanoluciferase. This work was supported, in part, by the National Institutes of Health R35GM128798 (BMZ), funding from the UCSD Molecular Genetics Training grant (VH) and a training grant in Quantitative Integrative Biology from UCSD's qBio Program (ATH)

Chapter 3 Effects of Translation on Co-translational Import of Mitoproteins and Its Import Stress

3.1 Background

Mitochondria, vital organelles in eukaryotic cells, contain hundreds of proteins essential for metabolic processes, and damage to mitochondria can lead to various human diseases. While mitochondrial DNA encodes a limited number of MIM proteins intended for the electron transport chain and oxidative phosphorylation, most mitochondrial proteins are encoded by nuclear DNA and are synthesized in the cytosol before being translocated to distinct compartments within the mitochondrion. Mitochondrial proteins can be imported post-translationally or co-translationally, with various mechanisms involved, including recruitment of distinct chaperones to keep precursor proteins import-competent with unfolded state. Furthermore, binding of chaperones is guided by specific targeting signals, such as MTS, and facilitates targeting of precursor proteins to the TOM complex for translocation.

Investigations on co-translational import of nuclear encoded mitoproteins could trace back to 1970s, when scientists found the alignment of ribosome-like particles along the MOM with electron microscopic examination (Kellems et al., 1974). In recent years, the co-translational manner of mitoprotein import has gained support from various analyses, such as fluorescent microscopy, APEX-Seq, ribosome profiling, and more (Fazal et al., 2019; Garcia et al., 2007; Williams et al., 2014). Further investigations demonstrated the effects of 3’UTR and MTS from

the coding region on facilitating mRNA localization. Puf3, an RNA-binding protein from MOM, binds to 3'UTR to tether mRNA to the mitochondrion (García-Rodríguez et al., 2007; Saint-Georges et al., 2008). Meanwhile, the NAC chaperone, which binds to ribosomes and nascent polypeptides, can associate with Om14 from MOM to target precursor proteins to the TOM complex (Gamerdinger et al., 2019; Lesnik et al., 2014). These observations propose a mechanism for co-translational protein import into mitochondria specifically applicable to a subset of nuclear-encoded mitochondrial mRNAs.

Although mRNA localization is an effective means of controlling gene expression (K. C. Martin & Ephrussi, 2009), and there is compelling evidence for the localization of mRNAs to mitochondria, its potential for mediating the mitochondrial composition remains under explored. Tatsuhisa Tsuboi, a post-doctoral scholar in Zid's lab, discovered that the interactions between mitochondria and mRNA/nascent-peptide (MTS) complexes can be influenced by the kinetics of protein synthesis (Tsuboi et al., 2020). In this study, Dr. Tsuboi investigated Tim50, which is an essential component of the TIM23 (translocase of the inner mitochondrial membrane) complex. He found that within the TIM50 CDS, there exists a series of 7 consecutive proline codons, positioned roughly 60 amino acids downstream of the MTS. Upon removing these polyproline residues, it was observed that the localization of TIM50 mRNA became more susceptible to changes in environmental conditions. Since polyproline stretches have been previously demonstrated to induce ribosomal stall (Huter et al., 2017; Pavlov et al., 2009), Dr. Tsuboi's findings propose a possible mechanism, which suggests that this local deceleration of ribosomes

at polyproline site could enhance the likelihood of mitochondria identifying the TIM50 MTS and subsequently facilitating its binding with the mitochondrial surface.

3.2 Results

3.2.1 Quantification of Elongation Stalls Induced by Polyproline in Mitoproteins

To verify the effects of the polyproline sequence on translational elongation stalling, Dr. Tsuboi conducted further examination of the amino acid sequence of Tim50 WT. As a result, he identified a proline-rich region located between 174 to 188 amino acids from N-terminus. We constructed a Tim50 (-P14) strain with deletion of "P14" containing the whole proline-rich region (PPFPDLLPPPPPPP), and a Tim50 (-P7) strains with deletion of "P7" containing the 7 consecutive prolines (PPPPPPP) in the proline-rich region (Figure 3.2.1A). Using the in-vivo elongation reporter discussed in Chapter 2, we quantified elongation time of all three Tim50 variants (Tim50 WT in Figure 3.2.1B) and calculated elongation delay of "P7" and "P14" (Figure 3.2.1C). Thus, we could evaluate the "stalling effects" of polyproline sequence by comparison of its "elongation time ratio" and "length ratios" in Tim50. The calculative processes and results are shown blow:

Length ratio of "P14" in Tim50 = $\frac{length\ of\ "P14"}{length\ of\ Tim50\ WT} = \frac{14\ aa}{476\ aa} \approx 3\%$

Elongation time ratio of "P14" in Tim50 = $\frac{ELongation\ delay\ of\ "P14"}{ELongation\ time\ of\ Tim50\ WT} = \frac{0.527\ min}{1.55\ min} \approx 34\%$

The calculative results shows that the "P14" spends about 34% of elongation time of Tim50 CDS, while it only takes up about 3% of the size of Tim50 CDS, which demonstrates a strong "stalling effect".

Similarly, we investigated another polyproline-induced "stalling effects" in YTA12, which is also a nuclear encoded mitochondrial protein and inserted into MIM after co-translational import.

We examined YTA12 and found a proline-rich region with 9 consecutive prolines (P9), which located between 154 to 163 amino acids from N-terminus. We constructed a YTA12(-P9) strain with deletion of the whole “P9” sequence (Figure 3.2.1D), then quantified elongation time both YTA12 variants (Figure 3.2.1E) and calculated elongation delay of “P9” (Figure 3.2.1F). Similarly, we finally evaluate the “stalling effects” of polyproline sequence in YTA12 using the calculative processes and results are shown blow:

Length ratio of “P9” in YTA12 = $\frac{length\ of\ "P9"}{length\ of\ YTA12\ WT} = \frac{9\ aa}{825\ aa} \approx 1\%$

Elongation time ratio of “P9” in YTA12 = $\frac{ELongation\ delay\ of\ "P9"}{ELongation\ time\ of\ YTA12\ WT} = \frac{3.76\ min}{9.05\ min} \approx 42\%$

The calculative results shows that the “P9” spends about 42% of elongation time of YTA12 CDS, while it only takes up about 1% of the size of YTA12 CDS, which demonstrates even a stronger “stalling effect”.

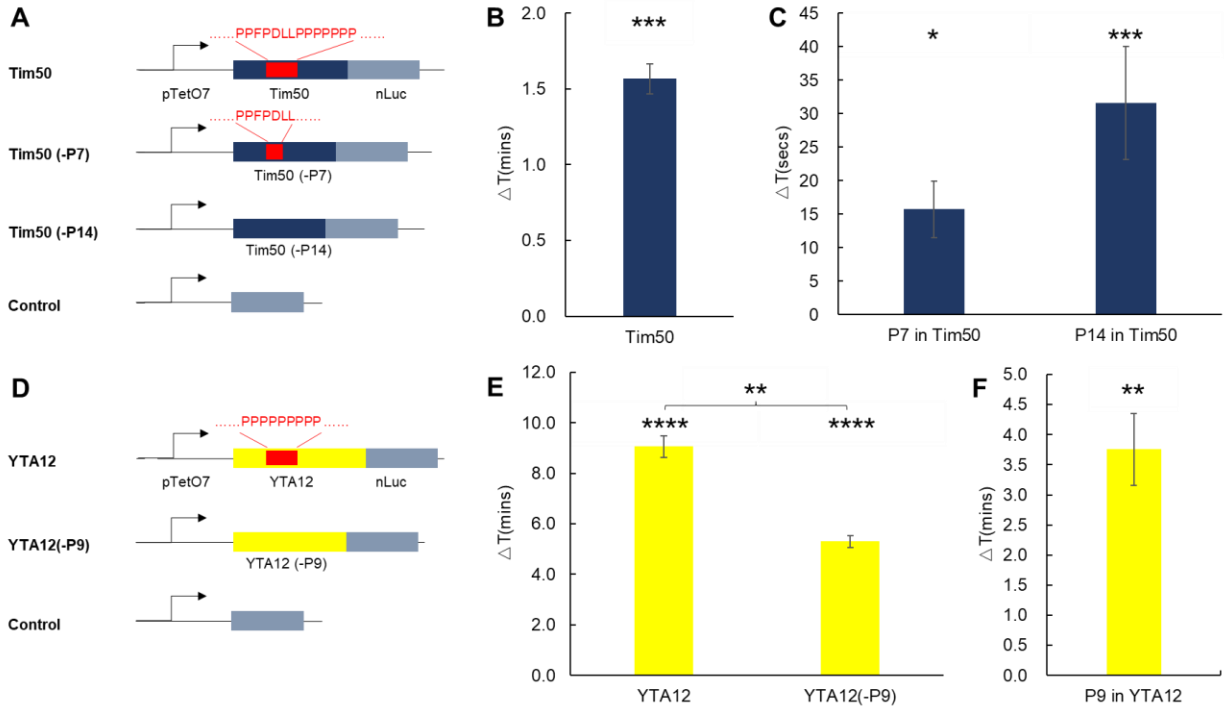

Figure 3.2.1 Polyproline sequence induces ribosomal stall which impedes translational elongation.

A: Diagram of Tim50 constructs with/without polyproline depletion. "-P7" means depletion of "PPPPPPP" sequence, and "-P14" means depletion of "PPFPDLLPPPPPPP" sequence.

B: Elongation time of Tim50. (n=7)

C: Elongation delay of polyproline sequence. △T is quantified through elongation time of Tim50 subtracted by elongation time of Tim50 (-P7) or Tim50 (-P14). (n=14)

D: Diagram of YTA12 constructs with/without polyproline depletion. "-P9" means depletion of "PPPPPPPPP" sequence.

E: Elongation time of YTA12. (n=3)

F: Elongation delay of polyproline sequence. △T is quantified through elongation time of YTA12 subtracted by elongation time of YTA12 (-P9). (n=3)

All error bars indicate SEM. Statistical significances in Figure B and E were calculated for each construct using two-tailed paired Student's t-Test against Control strain. Statistical significances in Figure C were calculated for each construct using two-tailed paired Student's t-Test against Tim50 strain. Statistical significances in Figure F was calculated using two-tailed paired Student's t-Test against YTA12 strain.

3.2.2 Translation of Polyproline Sequence is Mediated by eIF5A, whose Depletion Induces MitoCPR.

Eukaryotic translation initiation factor 5A (eIF5A) is a vital and highly conserved protein that plays crucial roles throughout the translation process. It is coded by two closely related but differentially expressed paralog genes, TIF51A/TIF51B in yeast and EIF5A1/EIF5A2 in humans. Notably, eIF5A is believed to be a critical factor in mitigating ribosomal stall induced by proline-rich sequences. Upon activation, eIF5A interacts with ribosomes, facilitating the translation of peptide motifs containing consecutive prolines or combinations of prolines with glycine and charged amino acids (Gutierrez et al., 2013).

Marina Barba Aliaga, a PhD exchange student in the Zid lab, was interested in studying the functions of the translation factor eIF5A in cellular metabolism and transcriptional control (Barba Aliaga, 2023). We collaborated to study the effects of eIF5A on translation of Tim50, including both the protein synthesis time (Figure 3.2.2 top) and protein expression (Figure 3.2.2 bottom) using in-vivo elongation reporter. With the eIF5A depletion (37℃), we found significant delay of protein synthesis time (Figure 3.2.2 A) and decreasing of protein expression (Figure 3.2.2 D) for Tim50 WT. Once the polyproline sequence is deleted from Tim50, both protein synthesis time and protein expression show significant change in after eIF5A depletion (Figure 3.2.2 B, C, E and F), which proposed the essential function of eIF5A on facilitating translation of proline-rich motif in Tim50. Furthermore, in 2017, Schuller et al showed the distribution of ribosome reads after eIF5A depletion, providing evidence of ribosomal stall near the site of a polyproline motif in Tim50

(Schuller et al., 2017). Taken together, these data demonstrate that translation of the polyproline motif in Tim50 is mediated by eIF5A. Deletion of eIF5A can trigger ribosomal stall caused by polyprolines, which impedes the translation of Tim50.

Cells can respond in various ways to cope with the stress caused by mitochondrial defects when the translocation and import of mitoproteins are affected. These responses are crucial in maintaining cellular homeostasis. Dr. Marina's studies proposed that the MitoCPR, a mitochondrial import stress response, will be triggered once elongation stalling at polyproline motif is induced by eIF5A depletion (Barba Aliaga, 2023). In Figure 3.2.3A, we tested the induction of PDR5, a MitoCPR-responsive gene, after eIF5A depletion. The increased expression under restrictive temperature (37°C) indicated the activation of MitoCPR. Then, we assumed that the mitochondrial import stress induced by elongation stalling may hinder the co-translational import of other Tim50-dependent proteins, ultimately affecting their production. To verify that, we tested the expression of Cyc1, a Tim50-dependent protein, and the significantly lower Cyc1 production under restrictive temperature in the tif51A-1 strain confirms our assumption (Figure 3.2.3B).

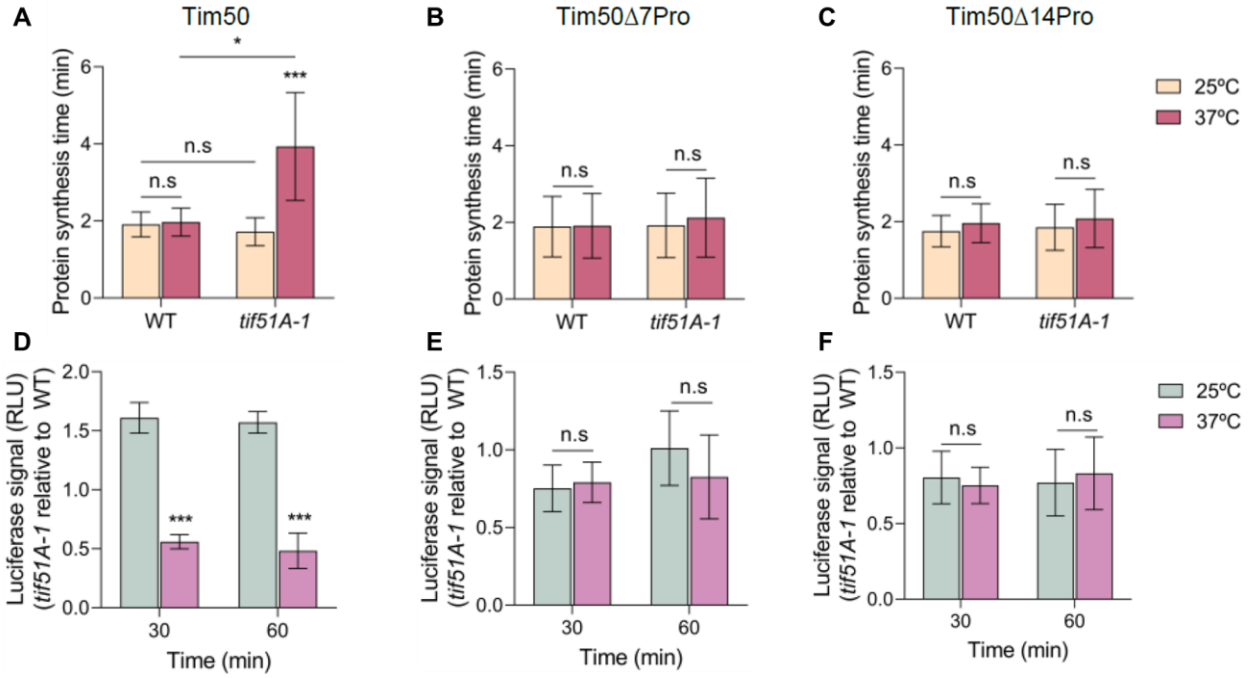

Figure 3.2.2 Tim50 translation depends on eIF5A due to its proline-rich sequence (Barba Aliaga, 2023)

A: Protein synthesis time of wild-type Tim50 in wild-type and tif51A-1 strains.

B: Protein synthesis time of Tim50Δ7Pro [or Tim50 (-P7)] in wild-type and tif51A-1 strains.

C: Protein synthesis time of Tim50Δ14Pro [or Tim50 (-P14)] in wild-type and tif51A-1 strains.

D: Protein expression (or Luciferase Signal) of wild-type Tim50 in wild-type and tif51A-1 strains.

E: Protein expression (or Luciferase Signal) of Tim50Δ7Pro [or Tim50 (-P7)] in wild-type and tif51A-1 strains.

F: Protein expression (or Luciferase Signal) of Tim50Δ14Pro [or Tim50 (-P14)] in wild-type and tif51A-1 strains.

Results are presented as mean ± SD from at least three independent experiments. The statistical significance was measured by using a two-tailed paired Student t-test relative to 25ºC. *$p < 0.05$, **$p < 0.01$, ***$p < 0.001$. n.s indicates no significant differences.

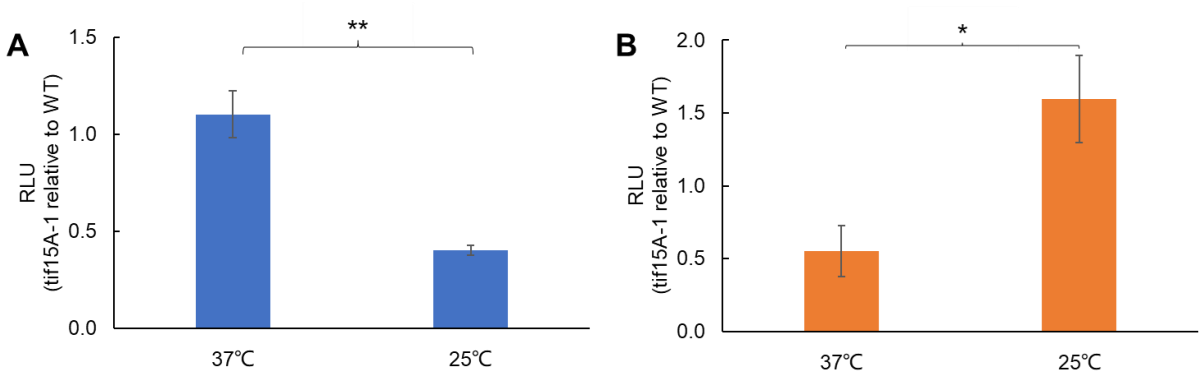

Figure 3.2.3 Depletion of eIF5A triggers mitochondrial import stress response

A: Protein expression (or RLU) induced by PDR5p in wild-type and tif51A-1 strains.

B: Protein expression (or RLU) of Cyc1 in wild-type and tif51A-1 strains.

All error bars indicate SEM. Statistical significances were calculated using two-tailed paired Student's t-Test.

3.3 Discussion

In this chapter, our investigations provide valuable insights into the effects of polyproline sequences on translational elongation stalling in two mitochondrial proteins, Tim50 and YTA12. By systematically examining the impact of specific proline-rich regions, such as "P14" in Tim50 and "P9" in YTA12, on the elongation process (Figure 3.2.1), the study sheds light on the potential regulatory role of these sequences in protein synthesis, significantly slowing down the protein synthesis process. In combination with previous studies (Tsuboi et al., 2020), we propose that these stalling effects might be critical for the proper folding and functioning of these mitochondrial proteins. The existence of a proline-rich stalling motif located near the mitochondrial targeting signal (MTS) facilitates the folding of MTS and recruitment of relevant chaperones (such as NAC), which drives mRNA localization and co-translational import of mitoproteins. Meanwhile, the elongation delay caused by the proline-rich motif also potentially extends the time of mRNA localization on the mitochondrion, ultimately reducing mRNA half-life. Thus, the presence of such proline-rich regions may provide an additional layer of regulation in protein synthesis, allowing the cell to fine-tune the expression and activity of these mitochondrial proteins.

The collaborative research between Dr. Marina and the Zid lab focused on studying the effects of eIF5A on the translation of Tim50, a protein crucial for mitochondrial import. The depletion of eIF5A resulted in a significant delay in protein synthesis time and a decrease in protein expression for Tim50 (Figure 3.2.2). However, when the polyproline sequence in Tim50 was deleted, the

effect of eIF5A depletion on protein synthesis time and expression was mitigated, suggesting that eIF5A facilitates the translation of the proline-rich motif in Tim50 (Figure 3.2.2).

The study also explored how cells respond to mitochondrial defects affecting the translocation and import of mitoproteins. The results indicated the activation of MitoCPR, as evidenced by the induction of PDR5, when elongation stalling at the polyproline motif is induced by eIF5A depletion in Figure 3.2.4A. In addition, the significantly lower production of the Tim50-dependent protein Cyc1 after eIF5A depletion represents how import stress causes mitochondrial defects by hindering mitoproteins import and expression (Figure 3.2.4B).

3.4 Materials and Methods

3.4.1 Plasmid Preparation and Integration

All plasmids used in Chapter 3 are listed in Table 3.4.1 and all primers used for clone in Chapter 3 are listed in Table 3.4.3. The Tim50, Tim50(-P7) and Tim50(-P14) constructs were generated by restriction digestion (SacI and NotI) of the entire backbone of the ZP24 plasmid, and PCR amplification of the corresponding parts of the TetO7 promoter, Tim50 5'UTR, nLucPEST and distinct Tim50 variants. These fragments were combined using Gibson assembly.

The YTA12 and YTA12(-P9) constructs were generated by PCR of the entire backbone of the ZO436 plasmid (from Chapter 2), and PCR amplification of the corresponding YTA12 variants. These fragments were combined using Gibson assembly.

The pRG206MX-PDR5p-nLuc construct were generated by restriction digestion (BamHI and HindIII) of the entire backbone of the pRG206 (Plasmid #64527) from Addgene, and PCR amplification of the corresponding parts of the PDR5 promoter and nLuc. These fragments were combined using Gibson assembly.

3.4.2 Yeast Strains, Growth, and Media

All yeast strains used in Chapter 3 are listed in Table 3.4.2. The background yeast strain S288C (BY4741) was used for all experiments. Yeast hel2Δ, and strains were created by deleting the endogenous HEL2 loci, using pRS315 (Addgene Plasmid #3974) and screened by growing

transformed yeast on SC dropout plates lacking leucine. Specific oligos used are listed in Table 3.4.3. Yeast strains were frozen down in YPD containing 30% v/v glycerol.

For cells cultured for use in our reporter assay, cells were streaked out from frozen stocks onto YPD Agar plates and grown at 30 °C for two days. These plates were stored at 4 °C for up to one month.

3.4.3 Luciferase-Based Elongation Reporter Assay

Liquid cultures were started from single colonies and allowed to grow overnight in YPD at 30 °C with shaking until an approximate OD600 of 0.3-0.5 after which cultures were divided into two tubes. For one of the tubes, 1 µL of a stock solution of anhydrotetracycline (250 µg/mL of ATc dissolved in EtOH) was added per mL of culture. Both tubes were returned to 30 °C with shaking for five minutes. 90 µL of each culture was added to a 96-well white flat-bottom plate (Grainger) and to each well, 10 uL of furimazine (10 mM furimazine stock solution dissolved in DMSO diluted 1:200 in YPD), was added. Immediately after sample loading, the plate was placed in a 30 °C prewarmed Tecan Infinite® 200 PRO plate reader. The following program was used and luminescence measurements were taken every 30 or 60 seconds: (1) Kinetic Cycle: [Cycle Duration: 60 minutes, Kinetic Interval: 30 or 60 seconds], (2) Shaking: [Duration: 3 seconds, Mode: Orbital, Amplitude 2 mm], (3) Luminescence: [Attenuation: Automatic, Integration Time: 1000 ms, Settle Time: 0 ms].

Table 3.4.1 List of plasmids used in Chapter 3

Designation	Construct Name	Source	Identifiers
ZP42	rtTA	Lab Stock	pRS306-Perv14-rtTA(S2)
ZP15	Backbone	Lab Stock	pRS305-12xMS2 v4
ZP35	TetO7 source	Lab Stock	TetO7-lacZ
ZP256	nLucPEST source	Lab Stock	305-HSP30prUTR-nLuc-pest-(v6) 12XMS2
TTP155	Tim50 source	Lab Stock	TIM50p-TIM50orf-flagyoGF
TTP174	Tim50(-P7) source	Lab Stock	TIM50p-TIM50-delPolyPx7-flayyoGFP
TTP169	Tim50(-P14) source	Lab Stock	TIM50p-TIM50-delPolyP-flayyoGFP
ZP603	Cyc1	Lab Stock	pAG306-pTet07-Tim50 5'UTR-CYC1-nLuc
ZP270	pRG206	Addgene	pRG206
ZP378	Tim50	This study	pRS305-pTetO7-Tim50 5’UTR-Tim50-nLucPEST-12xMS2 v4
ZP379	Tim50(-P7)	This study	pRS305-pTetO7-Tim50 5’UTR-Tim50(-P7)-nLucPEST-12xMS2 v4
ZP380	Tim50(-P14)	This study	pRS305-pTetO7-Tim50 5’UTR-Tim50(-P14)-nLucPEST-12xMS2 v4
ZP402	Control	This study	pRS305-pTetO7-Tim50 5’UTR-nLucPEST-12xMS2 v4
ZP652	YTA12	This study	pAG306 pTetO7-Tim50 5'UTR-YTA12-nLuc-CYC1ter
ZP653	YTA12(-P9)	This study	pAG306 pTetO7-Tim50 5'UTR-YTA12(-9Pro)-nLuc-CYC1ter
ZP446	Control	This study	pAG306-TetO7p-Tim50 5'UTR-nLuc-CYC1 terminator
ZP663	PDR5	This study	pRG206MX-PDR5p-nLuc

Table 3.4.2 List of Yeast used in Chapter 3

Designation	Strain name	Source	Identifiers
MY6	WT Yta12-GFP Su9	Lab stock	WT YTA12-GFP-HIS3 Su9-mCherry
MY13	WT Yta12Δ9Pro	Lab stock	WT YTA12Δ9Pro-GFP-HIS3
ZY411	rtTA	Lab stock	Perv14-rtTA
ZY8	BY4741	Lab stock	BY4741
ZY549	Hel2 deletion	Lab stock	Hel2 deletion
MY2	hyp2-1	Lab stock	eIF5A temperature sensitive mutant
MY59	hyp2-1 hel2Δ	Lab stock	hyp2-1 hel2::HIS3
ZY417	Tim50	This study	TetO7-Tim50-nLuc; Perv14-rtTA
ZY418	Tim50(-P7)	This study	TetO7-Tim50(-7 polyproline)-nLuc; Perv14-rtTA
ZY419	Tim50(-P14)	This study	TetO7-Tim50(-14 polyproline)-nLuc; Perv14-rtTA
ZY467	Control	This study	TetO7-Tim50UTR-nLuc; Perv14-rtTA
ZY895	YTA12	This study	pAG306 pTetO7-Tim50 5'UTR-YTA12-nLuc-CYC1ter
ZY896	YTA12(-P9)	This study	pAG306 pTetO7-Tim50 5'UTR-YTA12(-9Pro)-nLuc-CYC1ter
ZY528	Control	This study	pAG306-pTet07-Tim50 5'UTR-nLuc;
ZY926	PDR5 WT	This study	pRG206MX-PDR5-nLuc
ZY927	PDR5 Hel2△	This study	pRG206MX-PDR5-nLuc, Hel2△
ZY930	PDR5 eIF5A mutant	This study	pRG206MX-PDR5-nLuc, hyp2-1
ZY931	PDR5 Hel2△ eIF5A mutant	This study	pRG206MX-PDR5-nLuc, hyp2-1, Hel2△
ZY969	CYC1 WT	This study	Tim50, pAG306-pTet07-Tim50 5'UTR-CYC1-nLuc
ZY959	CYC1 eIF5A mutant	This study	hyp2-1 Tim50, pAG306-pTet07-Tim50 5'UTR-CYC1-nLuc

Table 3.4.3 List of primers used in Chapter 3

Designation	Primer Name	Purpose	Sequence
ZO993	TetO7pr-TIM50UTR_F	PCR Tim50, Tim50(-P7) and Tim50(-P14) with Tim50 5'UTR	CATTAGGTCCTTTGTAGCATAAAT GTAATTTCTAGCATCCACTCAATT
ZO994	nLucPEST-TIM50_R		CAACAAAATCTTCTAAAGTAAAAACCAT TTTGGATTCAGCAATCTTCTTCT
ZO982	ZP15H-TetO7B-Gib_F v2	PCR TetO7 promoter	GGGCGAATTGGAGCTCCACCGC CCACTTCTAAATAAGCGAATTTC
ZO992	TetO7_R		ATTTATGCTACAAAGGACCTAATG
ZO993	TetO7pr-TIM50UTR_F	PCR Tim50 5'UTR	CATTAGGTCCTTTGTAGCATAAAT GTAATTTCTAGCATCCACTCAATT
TTO377			TGCAAGCGGGTGATTTTTGGAAGTTTATTCTAGC
ZO463	yNLucF	PCR nLucPEST	ATGGTTTTTACTTTAGAAGATTTTG
ZO928	ZP24H-nLucPESTB-Gib_R		AGGATCCACTAGTTCTAGAGCGGCC TTAAACATTAATACGAGCAGAAGC
ZO982	ZP15H-TetO7B-Gib_F v2	PCT TetO7p-Tim50 5'UTR	GGGCGAATTGGAGCTCCACCGC CCACTTCTAAATAAGCGAATTTC
ZO1087	Tim50UTR-nLuc_R		CCAACAAAATCTTCTAAAGTAAAAACCAT TGCAAGCGGGTGATTTTTGG
ZO1416	YTA12_F	PCR YTA12 and YTA12(-P9)	CCAAAAATCACCCGCTTGCAATGTTGCTACTTTC TTGGTCAAGAATTGCT
ZO1417	YTA12_R		CAACAAAATCTTCTAAAGTAAAAACCATGTTTG TAGATGGCTTAGGCTCATTA
ZO463	yNLucF	PCR Backbone for YTA12 constructs	ATGGTTTTTACTTTAGAAGATTTTG
ZO1037	Tim50UTR_R		TGCAAGCGGGTGATTTTTGGAAGTTTATTCTAGC
ZO1750	PDR5_F	PCR PDR5p-PDR5 ORF	GCGGTGGCTCTAGAACTAGTGGATCCGTTAACG TAAATATGTCTTCCTCTTTG
ZO1751	PDR5 5'UTR-nLuc_R		CAAAATCTTCTAAAGTAAAAACCATTTTTGTCTA AAGTCTTTCGAACGAGCG
ZO463	yNLucF	PCR nLuc-CYC1t	ATGGTTTTTACTTTAGAAGATTTTG
ZO1733	CYCt_R		TCGAGGTCGACGGTATCGATAAGCTGCAAATTA AAGCCTTCGAGC
ZO1186	Hel2 Deletion Fwd	Hel2 endogenous deletion	CTAATGCTATTGTCAGTTACAGGTTAGAAATATAT TTCCAA CGG ATC CCC GGG TTA ATT AA
ZO1187	Hel2 Deletion Rev		CGAAAAAATAGTGGCTATACTTCTTTTCAAGAAT TAGG GAA TTC GAG CTC GTT TAA AC

3.5 Acknowledgement

Chapter 3 consists of both published and unpublished material. Section 3.2.1 and part of Section 3.2.2 are unpublished material. Figure 3.2.2 in Section 3.2.2 is quoted from published PhD dissertation of Marina Barba Aliaga: Barba Aliaga, M. Functions of the translation factor eIF5A in cellular metabolism and transcriptional control [Doctoral thesis]

We would like to thank the Zid lab for helpful feedback on the manuscript, especially Tatsuhisa Tsuboi, for sharing Tim50 variants. We thank Dr. Marina for sharing YTA12 variants and Tif51A-1 strain. We thank Claes Andréasson for sharing the yeast optimized Nanoluciferase. This work was supported, in part, by the National Institutes of Health R35GM128798 (BMZ), funding from the UCSD Molecular Genetics Training grant (VH) and a training grant in Quantitative Integrative Biology from UCSD's qBio Program (ATH)

Chapter 4 Rvb1/Rvb2 Proteins Couple Transcription and Translation during Glucose Starvation

4.1 Background

Cells are constantly exposed to fluctuating and challenging environmental conditions, necessitating rapid adaptive responses to ensure survival. The cellular stress response is a complex phenomenon involving gene expression modifications that maintain internal stability while suppressing overall protein synthesis. During stress, cells form membrane-less RNA-protein granules, known as stress granules (SGs) and processing bodies (PBs), through a process called liquid-liquid phase separation. These granules are composed of RNA-binding proteins (RBPs) and non-translating mRNAs (Begovich & Wilhelm, 2020; Guzikowski et al., 2019). In recent years, a variety of research are done to understand the mechanism of stress-induced granules formation and their relations with translation and translation. For example, impaired translation initiation serves as a common trigger for granule formation (Khong et al., 2017; Matheny et al., 2019). The obstructive presence of ribosomes during elongation may hinder RNA-RNA interactions, allowing free transcripts to engage in RNA-RNA interactions and initiate their formation (Khong et al., 2017; Van Treeck et al., 2018). In yeast, mRNAs induced by stress display distinct localization patterns (Zid & O'Shea, 2014). In our previous studies, we figured out two distinct classes of mRNA that are both transcriptionally induced under stress (Zid & O'Shea, 2014). Class I mRNAs (such as HSP30 and HSP26) are translationally induced and remain dispersed throughout the cytoplasm,

while class II mRNAs (such as GSY1, GLC3 and HXK1) localize to both PBs and SGs, showing reduced translation activity. In addition, it has been reported that promoter sequences and co-transcriptional loading of factors onto mRNA may determine its fate within the cytoplasm. These observations suggest a connection between transcription, translatability, and mRNA localization during stress. Further studies are needed to unravel the mechanisms underlying mRNA localization and granule formation, as well as the functional consequences of these processes in the cellular stress response.

Sophie Chan, a PHD graduate from Brian Zid's lab, developed an innovative proteomics-based screening method that allowed us to identify Rvb1/Rvb2 proteins, which are conserved ATPases involved in protein assembly chaperoning and chromatin remodeling (Chen et al., 2022). These proteins were found to interact with the promoters of class II genes related to alternative glucose metabolism, such as GLC3. Dr. Chan's findings revealed that Rvb1 and Rvb2 were highly enriched at the promoters and mRNAs of class II genes (Chen et al., 2022). Furthermore, by engineering Rvb1/Rvb2 binding to class I mRNAs, it was possible to sequester the mRNAs into mRNP granules and inhibit their translation (Chen et al., 2022). Interestingly, this tethering of Rvb proteins to the mRNA also led to a further increase in the transcriptional upregulation of the target genes (Chen et al., 2022).

To be exact, Dr. Chan first developed a novel screening technique called Co-Transcriptional ImmunoPrecipitation (CoTrIP) to identify protein factors involved in the regulation of mRNA fate during stress (Chen et al., 2022). This technique involves modifying a yeast plasmid with LacO-

binding sites and adding a uniform cyan fluorescent protein (CFP) open-reading frame (ORF) and different promoters of interest (Unnikrishnan et al., 2010, 2012). By comparing the protein enrichment on different promoters (GLC3 vs HSP30 and HSP26), it is identified that distinct protein factors associated with specific classes of promoters (Chen et al., 2022). Notably, the ATP-dependent DNA helicase Rvb1 showed a tenfold higher enrichment on the GLC3 promoter compared to HSP30/HSP26 promoters. Rvb1 and its counterpart Rvb2 are highly conserved AAA+ family proteins involved in nuclear pathways (Jha & Dutta, 2009). Although they primarily act on DNA, they have also been found as core components of cytoplasmic stress granules (Jain et al., 2016; Kakihara et al., 2014; Rizzolo et al., 2017). Microscopic observations showed that while Rvb1/Rvb2 are mainly located in the nucleus under normal conditions, a fraction of them translocates to distinct cytoplasmic granules upon 30 minutes of glucose starvation (Chen et al., 2022). Similar findings have been observed in 2-deoxyglucose-driven glucose starvation, where Rvb1 formed cytoplasmic foci independent of P-bodies and stress granules (Rizzolo et al., 2017). These observations suggest that Rvb1/Rvb2 have the ability to shuttle between the nucleus and cytoplasm, indicating their potential involvement in diverse cellular processes.

To validate the CoTrIP findings and investigate the DNA binding patterns of Rvb1 and Rvb2 during stress, Chromatin Immunoprecipitation sequencing (ChIP-seq) was performed (Chen et al., 2022). The ChIP-seq results demonstrated that Rvb1 and Rvb2 were enriched from the -500 bp region to the transcription start site (TSS) across the genome during 10 minutes of glucose starvation, whereas the negative control Pgk1 did not show enrichment in the promoter region

(Chen et al., 2022). The enrichment of Rvb1 and Rvb2 on promoters is consistent with their role as chromatin remodelers (Zhou et al., 2017). Notably, Rvb1 and Rvb2 showed significantly higher enrichment on the proximal promoters of class II genes compared to class I genes and the average genome (Chen et al., 2022).

While Rvb1 and Rvb2 are primarily known for their involvement in DNA processes, they have also been found to interact with various mRNAs, influencing mRNA translation and stability (Izumi et al., 2012; Mu et al., 2015). To investigate their mRNA binding patterns, RNA Immunoprecipitation (RIP) was performed on Rvb1, Rvb2, followed by RT-qPCR analysis under stress conditions. The results consistently showed that during glucose starvation, Rvb1 and Rvb2 were significantly more enriched on the mRNAs of class II alternative glucose metabolism genes compared to class I heat shock genes (Chen et al., 2022). In addition, studies of reporter mRNAs, designed with a uniform CFP ORF driven by either the GLC3 or HSP26 promoter, showed significantly higher enrichment of Rvb1 and Rvb2 on the mRNA driven by the GLC3 promoter compared to the HSP26 promoter during glucose starvation (Chen et al., 2022). This suggests that the promoter itself determines the interaction of transcribed mRNA with Rvb1 and Rvb2, indicating that these proteins are likely loaded onto nascent mRNAs co-transcriptionally from the promoters (Zid & O'Shea, 2014).

As Rvb1/Rvb2 were found to be located at both promoters in the nucleus and associated with mRNAs in the cytoplasm, Dr. Chan further investigated the influence of Rvb1 and Rvb2 proteins on the fate of mRNAs in the cytoplasm (Chen et al., 2022). Dr. Chan specifically studied the

mRNAs from class I heat shock genes and engineered interactions between Rvb1/Rvb2 and these mRNAs. Interestingly, binding of Rvb1 and Rvb2 caused the class I heat shock mRNAs to behave similarly to class II alternative glucose metabolism mRNAs, including induced transcription, repressed translation and granular localization after glucose starvation (Chen et al., 2022). In addition, when glucose was replenished in starved cells, the translation of class II genes was rapidly induced, indicating the potential role of the granules as repositories for translationally repressed mRNAs during stress, which suggest that once the stress is removed, the mRNAs held in the granules can be quickly released and translated (Chen et al., 2022).

To further validate the impact of Rvb1/Rvb2 binding on gene expression regulation and granule localization, we aimed to reduce the function of RVB proteins in cells. In section 4.2, we employed CRISPRi to suppress the expression of Rvb1/Rvb2 and subsequently examined the transcriptional and translational efficiency of class II mRNAs. Our findings demonstrated increased protein expression but decreased mRNA abundance during glucose starvation when Rvb2 was knocked down, providing additional support for the interconnectedness of Rvb1/Rvb2 in coupling transcription, mRNA granular localization, and translational efficiency of mRNAs under glucose starvation conditions.

4.2 RVB2 Knockdown Drives Decreased mRNA Induction but Enhanced Protein Production of Rvb1/Rvb2 Target Genes

To further test the role of RVB1/RVB2 in regulating gene expression during glucose starvation,

we sought to reduce RVB function in cells. RVB1/RVB2 deletions are inviable (Jónsson et al., 2001) so we aimed to identify gRNA targets that would temporally reduce RVB expression through inducible gRNAs and dCas9-MXi (Smith et al., 2016). We found an RVB2 gRNA that gave an ~20-fold reduction in RVB2 expression 8 hr after treatment with anhydrotetracycline (ATc) (Figure 4.2A and B). To investigate the necessity of Rvb1/Rvb2 in the translational repression of class II genes during glucose starvation, we C-terminal tagged two class II genes (GSY1 and HXK1) and one class I gene (HSP30) and then quantified their protein induction after 30 min glucose starvation. While both class II genes had robust mRNA induction upon glucose starvation in the control samples (Figure 4.2), this was associated with no significant upregulation of protein production (Figure 4.2C). Upon RVB2 knockdown, we find a significant increase in the stress induction of the class II proteins Gsy1 and Hxk1, while we find no significant difference in the protein induction of the class I protein Hsp30 (Figure 4.2C). While the higher protein induction could be because of even further increases in mRNA levels, we instead find that RVB2 knockdown causes a greater than twofold decrease in GSY1 and HXK1 mRNA induction (Figure 4.2D). This is consistent with previous findings (Jónsson et al., 2001) as well as our tethering data that Rvb1/Rvb2 have a role in transcriptional induction. Together this data further supports the role for Rvb1/Rvb2 repressing the translatability of target mRNAs during glucose starvation.

Figure 4.2.1 Knockdown of RVB2 drives enhances protein production of Rvb target genes during glucose starvation.

(A) A schematic view of CRISPRi repression of RVB2 transcription. The RVB2 gRNA was placed under the control of a TetOn promoter. Upon anhydrotetracycline (ATc) treatment, this induces RVB2 gRNA expression, targeting dCas9-MXi to the upstream region of RVB2 and repressing transcription.

(B) mRNA levels of RVB2 and ACT1 were determined in log-phase cultures expressing either an RVB1 or RVB2 gRNA. RVB2 mRNA levels were normalized to ACT1. Statistical significance was achieved by two-sample t-test. RVB1 gRNA (n = 2); RVB2 gRNA (n = 5).

(C) Endogenous genes tagged with nLuc and luciferase was quantified during log-phase growth and 30 min after glucose starvation in ±ATc cultures. Statistical significance was achieved by two-sample t-test (GSY1, HXK1 n = 4, HSP30 n = 3).

(D) mRNA levels of the genes of interest were tested in log phase and 30 min of glucose starvation ±ATc. The log2 fold change -Glu/+Glu in the RVB2 knockdown was subtracted from the control mRNA fold change. Statistical significance was assessed by a one-sample t-test to test whether the mean fold change differs from 0 (no change from -ATc control) (GSY1, HXK1 n = 4, HSP30 n = 3) (*$p<0.05$, **$p<0.01$, **$p<0.001$).

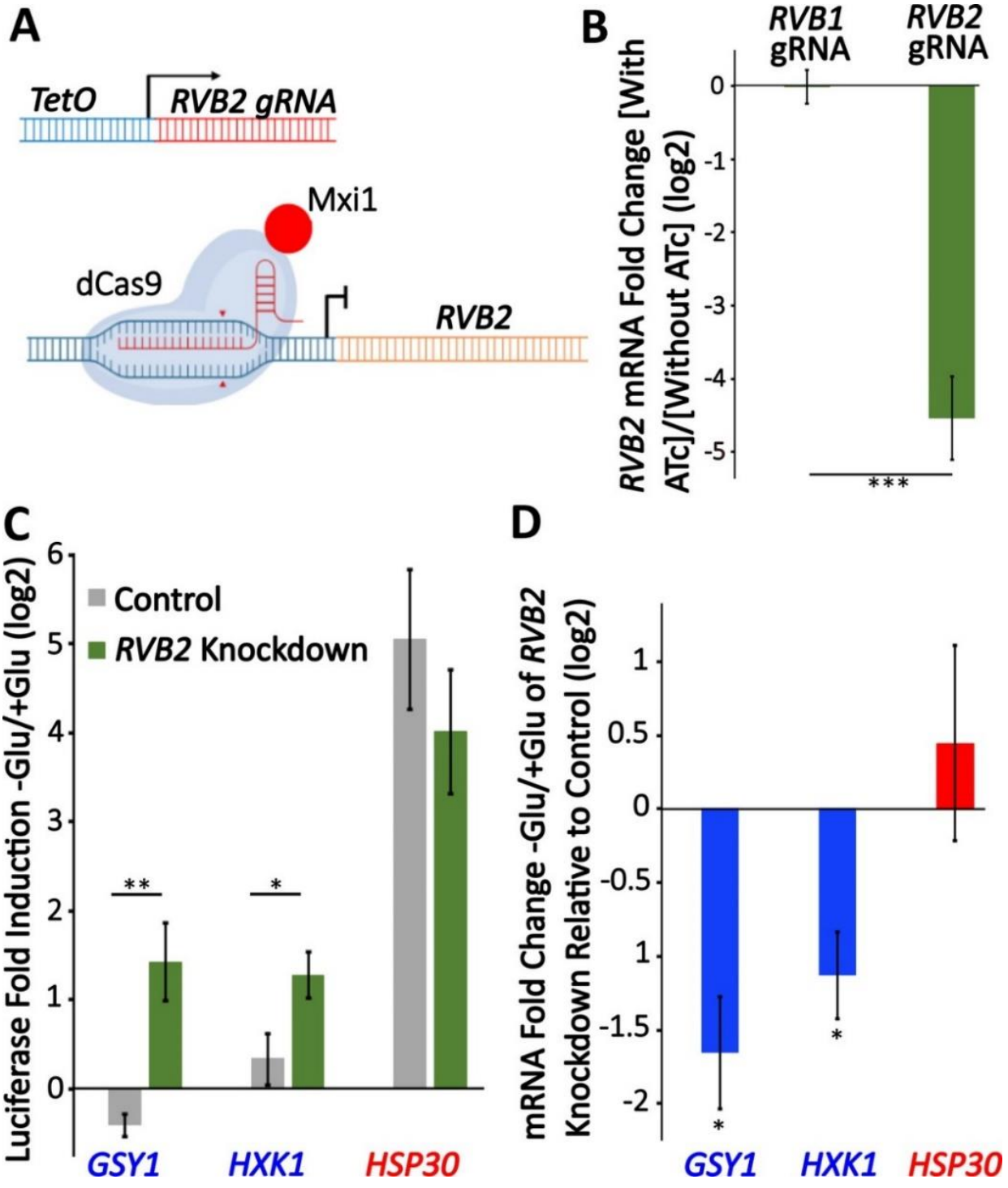
A
TetO
RVB2 gRNA
Mxi1
dCas9
RVB2
B
RVB1 gRNA
RVB2 gRNA
RVB2 mRNA Fold Change [With ATc]/[Without ATc] (log2)
0
-1
-2
-3
-4
-5
***
C
Control
RVB2 Knockdown
Luciferase Fold Induction -Glu/+Glu (log2)
6
5
4
3
2
1
0
**
*
GSY1
HXK1
HSP30
D
mRNA Fold Change -Glu/+Glu of RVB2 Knockdown Relative to Control (log2)
1
0.5
0
-0.5
-1
-1.5
-2
*
*
GSY1
HXK1
HSP30

4.3 Discussion

In fluctuating environments, cells must quickly adjust the expression of different genes dependent upon cellular needs. Here, our results demonstrate a novel function of the AAA+ATPases Rvb1/Rvb2 in the cytoplasm, and a novel mechanism of Rvb1/Rvb2 in coupling the transcription, mRNA cytoplasmic localization, and translation of specific genes (Figure 4.3). We identified Rvb1/Rvb2 as enriched protein factors on the promoters of the class II alternative glucose metabolism genes that are upregulated in transcription but downregulated in translation during glucose starvation. Results showed that Rvb1/Rvb2 have a strong preferred interaction with both promoters and mRNAs of these genes, suggesting that Rvb1/Rvb2 are loaded from enriched promoters to the nascent mRNAs. More interestingly, when we tethered Rvb1/Rvb2 to the mRNAs, the binding of Rvb1/Rvb2 had a strong impact on reducing mRNA translation and increasing the mRNA granular localization. We are uncertain whether Rvb1/Rvb2 tethering represses translation, which directs mRNAs to mRNP granules; or Rvb1/Rvb2 binding directly targets the mRNA to the granule, which represses translation; or some combination of both – as these are very hard to disentangle. Either way, these data, along with our RVB2 depletion data, suggest the potential co-transcriptional loading of Rvb1/Rvb2 directs post-transcriptional mRNA fate in the cytoplasm, which further indicates that Rvb1/Rvb2 couple the transcription and translation of the interacting genes.

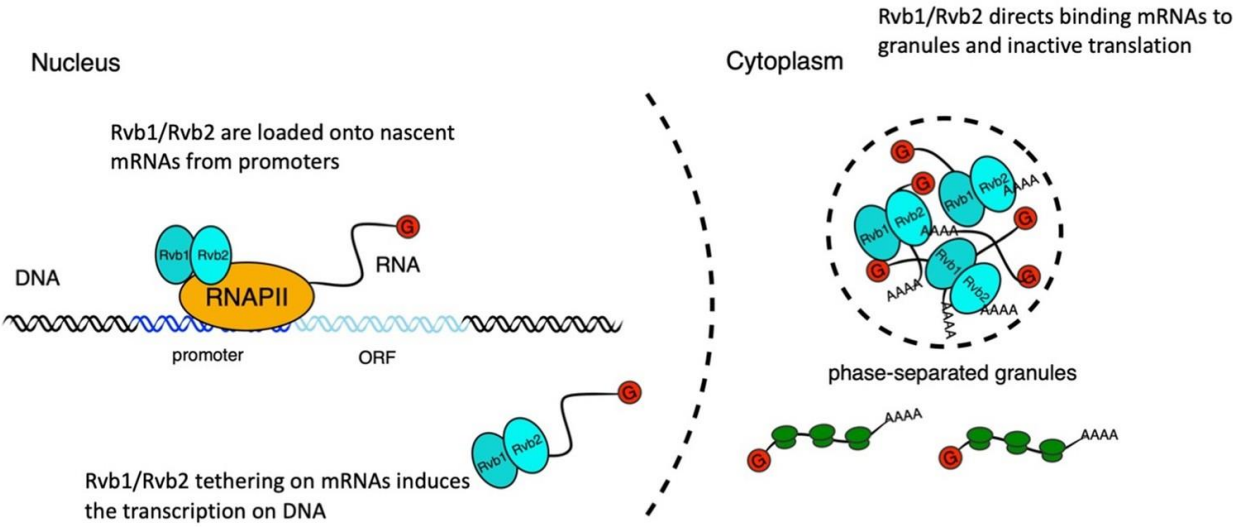

Figure 4.3.1 A working illustration of Rvb1/Rvb2's mechanism in coupling the transcription and translation of interacting genes.

First, Rvb1/Rvb2 are recruited by specific promoters and loaded onto the nascent mRNAs during glucose starvation. Then Rvb1/Rvb2 escort the interacting mRNAs to the cytoplasm and cause repressed translation and localization to cytoplasmic granules. Also, forced Rvb binding on an mRNA drives an increase in the transcription of the corresponding genes, further showing the coupling of transcription and translation.

4.4 Materials and Methods

4.4.1 RVB2 CRISPRi Knockdown

RVB2 gRNA forward and reverse complement oligos were annealed together and then further extended using NM637 and NM636. This PCR product was inserted into the TetO gRNA vector pNTI661 by digesting this vector with BamHI/HindIII as described previously (McGlincy et al., 2021). The final plasmid construct for expressing gRNA is ZP577, which was further linearized and integrated into yeast by homologous recombination. To swap the selection marker of ZP577 from Leucine to Uracil, we run restriction digestion to ZP577 using SacI and EcorV and PCR Ura marker from ZP522. gRNA fragment of ZP577 was acquired and purified using gel extraction, followed by Gibsom Assembly to assemble these fragments. Final plasmid construct for gRNA expression is ZP633, which was further linearized using EcorV and integrated into yeast by homologous recombination. Integrations was screened by growing transformed yeast on synthetic complete (SC) dropout plates lacking uracil. These were then frozen down for long-term storage in YPD containing 15% v/v glycerol.

4.4.2 Yeast Strains, Growth, and Media

Cells were grown overnight in SC-Leu+Glu media to low OD < 0.5. Cells were diluted and 250 ng/L of ATc was added to the experimental sample and control and experimental samples were

allowed to grow for 8 hr to an OD ~0.4. Yeast were either prepped for assays or glucose-starved for 30 min and then prepped for nLuc and RT-qPCR assays.

4.4.3 RNA Extraction and Real Time qPCR

The RT-qPCR protocol was adapted from Tsuboi et al., 2020. RNA was extracted using the MasterPure Yeast RNA Purification Kit (Epicentre). cDNA was prepared using ProtoScript II Reverse Transcriptase (NEB #M0368X) with a 1:1 combination of oligodT 18 primers and random hexamers (NEB) according to the manufacturer's instructions. mRNA abundance was determined by qPCR using a home-brew recipe with SYBR Green at a final concentration of 0.5× (Thermo Fisher #S7564). Primers specific for each transcript are described in Key resources table. The mRNA levels were normalized to ACT1 abundance, and the fold change between samples was calculated by a standard ΔΔCt analysis. All data were included except for one sample that had high technical variation, and another that had very high ACT1 CT values. Both samples were flagged as analysis began.

4.4.4 Luciferase-Based Elongation Reporter Assay

The nanoluciferase (nLuc) assay was adapted from methods previously described by Masser et al., 2016. Cells were grown to an OD660 to ~0.4 in SCD medium at 30°C and glucose-starved in SC-G medium for 30 min. Then, 90 µL of cell culture was loaded onto a Cellstar non-transparent

white 96-well flat-bottom plate (Sigma-Aldrich). OD_{660} of cells was taken for each sample. For cells treated with cycloheximide (CHX), CHX was added to a final concentration of 100 μg/mL to stop the translation for 5 min. To measure the nanoluciferase signal, 11 μL of substrate mix (10 μL of Promega Nano-Glo Luciferase Assay Buffer, 0.1 μL of Promega NanoLuc luciferase substrate, and 1 μL of 10 mg/mL CHX) was added and mixed with the samples by pipetting. Measurements were taken immediately after addition of substrate mix by Tecan Infinite Lumi plate reader. Data analysis method is same as Chapter 2.5.5.

Table 4.4.1 List of plasmids used in Chapter 4

Designation	Construct Name	Source	Identifiers
ZP479	pNTI661	Ingolia lab CRISPR sgRNA vector	pNTI661 pRPR1(TetO)-sgRNA
ZP480	dCas9-Mxi1	Ingolia lab CRISPR effector	pNTI647 dCas9-Mxi1 TetR KanMX
ZP577	Rvb2gRNA(Leu)	This study	pNTI661 pRPR1(TetO)-sgRNA (Rvb2gRNA_i04) (Leu Marker)
ZP633	Rvb2gRNA(Ura)	This study	pNTI661 pRPR1(TetO)-sgRNA (Rvb2gRNA_i04) (Ura Marker)
ZP522	Ura provider	This study	pRS416-dCas9-Mxi1 + TetR + pRPR1(TetO)-NotI-gRNA

Table 4.4.2 List of Yeast used in Chapter 4

Designation	Strain name	Identifiers
ZY854	dCas9	Dcp2-iRFP-NAT, MCP-2xGFP, GSY1pr-nLuc-MS2, dCas9-Mxi1 TetR
ZY873	Rvb2 gRNA	pNTI661 pRPR1(TetO)-sgRNA (Rvb2gRNA_i04), Dcp2-iRFP-NAT, MCP-2xGFP, GSY1pr-nLuc-MS2, dCas9-Mxi1 TetR

Table 4.4.3 List of primers used in Chapter 4

Designation	Primer Name	Purpose	Sequence
ZO1379	Rvb2gRNA_i04	Anneal to get Rvb2gRNA	tctgggagctgcgattggcaTGAAGACTGTACATTCACACgttttagagctagaaatagc
ZO1388	Rvb2gRNA_i04rc		gctatttctagctctaaaacGTGTGAATGTACAGTCTTCAtgccaatcgcagctcccaga
ZO1397	NM636	extend gRNA oligos for gibson assembly into ZP479	gccttattttaacttgctatttctagctctaaaac
ZO1398	NM637		ggctgggaacgaaactctgggagctgcgattggca
ZO1626	UraR2	Pcr Ura Marker from ZP522	TCACGCATGCTCAAGAGCTGTATTTTCTCCTTACGCATCTG
ZO1627	UraF2		CCAGTTATCCAAGTAGATGTACTGAGAGTGCACCATAC

4.5 Acknowledgements

Chapter 4 is part of a published paper: Yang S Chen, Wanfu Hou, Sharon Tracy, Alex T Harvey, Vince Harjono, Fan Xu, James J Moresco John R Yates III, Brian M Zid. Rvb1/Rvb2 proteins couple transcription and translation during glucose starvation. The dissertation author is the second author of this publication.

We thank the Zid lab especially Anna R Guzikowski and Tatsuhisa Tsuboi for helpful feedback on this manuscript. We also thank Toshio Tsukiyama for sharing the LacI-Flag and pUC-TalO8 plasmids. We also thank the Ingolia lab for sharing the dCas9-Mxi pNTI647 and gRNA base vector pNTI661. This work was in part supported by the National Institutes of Health R35GM128798 (to BMZ) and the Yeast Resource Center P41GM103533 (JJM and JRY).

Chapter 5 Future Directions and Concluding Remarks

5.1 Future Directions

The development of the in-vivo elongation reporter in *Saccharomyces cerevisiae* represents a significant advancement in tools to study translational kinetics in eukaryotic cell. Compared with transitional methods (such as ribosome profiling or single molecular imaging), this reporter allows us to quantitatively monitor translation elongation change in a living *Saccharomyces cerevisiae* organism. In Chapters 2 and 3, we utilized the elongation reporter to quantitatively understand the effects of genetic elements, including codons, amino acids, and mRNA secondary structure, on translational kinetics. By quantifying translational kinetics, we were able to further study how these factors influence co-translational pathways, such as ribosome quality control (RQC) and protein import. Moreover, our in-vivo elongation reporter holds the potential for extensive use in investigations related to the translation process. For instance, it has been reported that translation kinetics of cells can respond to various extracellular environmental factors, such as nutrient changes, to maintain cellular homeostasis (Gameiro & Struhl, 2018). Furthermore, numerous intracellular regulatory factors, such as translational factors and microRNAs, mediate the translation process (Fabian et al., 2010; Xu et al., 2022). Our elongation reporter presents a powerful tool to quantitatively study how translation is affected by these diverse factors. Additionally, the in-vivo elongation reporter has the potential to elucidate more intracellular phenomena related to translation, such as co-translational folding.

One major area for improvement is to minimize the variability in the collected data from the luciferase assay across replicates, as we will calculate the elongation speed from the time-course luciferase induction curve. While we have established a series of standard procedures to minimize deviations resulting from manual actions, such as reagent addition, mixing, and potential extracellular stress, we still encounter instrumental errors, especially from the luciferase reader, which can impact our final quantifications. In addition to the data collection, the data analysis, specifically using the Schleif Plot, may not be straightforward for new users. In a standard elongation induction curve (Section 2.5.5), the relatively low luciferase signal during the early stage can be overwhelmed by systematic errors in the reader. Additionally, data from the late stage will be invalid due to decaying of luciferase, as per the mechanism of the Schleif Plot. For these reasons, we usually avoid taking data during both the very early and late time periods to ensure accurate and consistent quantification. Furthermore, seeking ways to extend survival of active luciferase may be a valuable improvement of the in-vivo elongation reporter.

Until now, we have only built the in-vivo elongation reporter in *Saccharomyces cerevisiae*, so another valuable future direction is to construct this elongation reporter in more species, especially mammalian cells. Notably, mammalian cells represent a distinct and more complicated intracellular environment. Fortunately, both the tetracycline (Tet)-controlled gene expression system and luciferase are universally used in mammalian cells (Kanai et al., 2019; Yamada et al., 2018).

In chapter 3, our investigations provide valuable insights into the effects of proline-rich motifs on translational elongation stalling in two mitochondrial proteins and their effects on translational elongation stalling. Further investigations could explore other polyproline sequences in different proteins and their functional significance or other stalling motifs from more nuclear-encoded mitochondrial proteins. Additionally, understanding the underlying molecular mechanisms that lead to elongation stalling upon encountering polyproline sequences could provide deeper insights into the regulation of protein synthesis in eukaryotic cells. Another significant direction in Chapter 3 is to understand the effects of eIF5A on facilitating the elongation of the proline-rich motif during co-translational import, and our further investigations demonstrate the induction of MitoCPR after eIF5A depletion. Considering the intricate mitochondrial import system and numerous mitochondrial stress response, one area of further study is to reveal the mechanisms of MitoCPR, such as the way cells sense import stress. An interesting direction is to understand the function of Tim50 in mediating import stress, since a series of nuclear-encoded proteins, including Tim50 itself, are imported with Tim50-dependent manner. Thus, it is unclear whether the stalled Tim50 precursors at the translocase or the shortage of Tim Complex directly triggers import stress.

In the context of examining the relationships among transcription, mRNA translatability, and mRNA granule formation under glucose starvation, our research has demonstrated that Rvb1/Rvb2 play a pivotal role in coupling gene regulation from the nucleus to the cytosol. This project focuses on investigating the cellular stress response during glucose starvation. A promising area for future exploration involves studying other types of extracellular stress, such as nutrient deprivation or re-

addition, heat shock, and oxidative stress. Another area of investigation pertains to the functions of Rvb1/Rvb2, which serve as ATP-dependent DNA helicases. In Chapter 4, our findings reveal that Rvb1/Rvb2 are co-transcriptionally loaded onto nascent mRNAs during glucose starvation, subsequently translocating to the cytosol to mediate mRNA translation and localization. Detailed elucidation of the translocation mechanisms from the nucleus to the cytosol and the protein-nucleic acid interactions will enhance our comprehension of the effects of Rvb1/Rvb2 under stress conditions. Moreover, within mammalian cells, the upregulation of RUVBL1/RUVBL2, the homologs of Rvb1/Rvb2, has been correlated with various cancer types. Delving deeper into the functions of these proteins is important for understanding their role in connecting gene expression across diverse conditions and their potential impact on cancer progression in mammalian cells.

5.2 Concluding Remarks

Regulation of Translational kinetics and post-transcriptional activities plays essential roles in mediating gene expression and maintain cellular homeostasis under varies conditions. In this dissertation, we have used *S. cer*evisiae as a model organism to construct an in-vivo translation elongation reporter. Based on this reporter, we are able to quantitatively study how translational kinetics is fine-tuned by factors from nucleic acid sequence and explore how distinct translational kinetics mediates various co-translational pathways. We find distinct stalling factors can trigger distinct co-translational outcomes, even though they harbor similar elongation duration. At the same time, we also use the elongation reporter to study an endogenous and functional stalling motif in nuclear-encoded mitochondrial proteins and figure out its effects on mediating co-translational import. Finally, we have studied the relationship among transcription, mRNA translation and localization. Using genome editing, we demonstrated it is the Rvb1/Rvb2 that couples links between translation and mRNA localization under glucose starvation.

5.3 References

Alagar Boopathy, L. R., Jacob-Tomas, S., Alecki, C., & Vera, M. (2022). Mechanisms tailoring the expression of heat shock proteins to proteostasis challenges. *Journal of Biological Chemistry*, *298*(5), 101796. https://doi.org/10.1016/j.jbc.2022.101796

Alhusaini, N., & Coller, J. (2016). The deadenylase components Not2p, Not3p, and Not5p promote mRNA decapping. *RNA*, *22*(5), 709–721. https://doi.org/10.1261/rna.054742.115

Arpat, A. B., Liechti, A., De Matos, M., Dreos, R., Janich, P., & Gatfield, D. (2020). Transcriptome-wide sites of collided ribosomes reveal principles of translational pausing. *Genome Research*, *30*(7), 985–999. https://doi.org/10.1101/gr.257741.119

Arribere, J. A., Doudna, J. A., & Gilbert, W. V. (2011). Reconsidering Movement of Eukaryotic mRNAs between Polysomes and P Bodies. *Molecular Cell*, *44*(5), 745–758. https://doi.org/10.1016/j.molcel.2011.09.019

Ashe, M. P., De Long, S. K., & Sachs, A. B. (2000). Glucose Depletion Rapidly Inhibits Translation Initiation in Yeast. *Molecular Biology of the Cell*, *11*(3), 833–848. https://doi.org/10.1091/mbc.11.3.833

Backes, S., Hess, S., Boos, F., Woellhaf, M. W., Gödel, S., Jung, M., Mühlhaus, T., & Herrmann, J. M. (2018). Tom70 enhances mitochondrial preprotein import efficiency by binding to internal targeting sequences. *Journal of Cell Biology*, *217*(4), 1369–1382. https://doi.org/10.1083/jcb.201708044

Bae, H., & Coller, J. (2022). Codon optimality-mediated mRNA degradation: Linking translational elongation to mRNA stability. *Molecular Cell*, *82*(8), 1467–1476. https://doi.org/10.1016/j.molcel.2022.03.032

Balaban, R. S., Nemoto, S., & Finkel, T. (2005). Mitochondria, Oxidants, and Aging. *Cell*, *120*(4), 483–495. https://doi.org/10.1016/j.cell.2005.02.001

Bao, C., Loerch, S., Ling, C., Korostelev, A. A., Grigorieff, N., & Ermolenko, D. N. (2020). MRNA stem-loops can pause the ribosome by hindering A-site tRNA binding. *ELife*, *9*, e55799. https://doi.org/10.7554/eLife.55799

Bao, C., Zhu, M., Nykonchuk, I., Wakabayashi, H., Mathews, D. H., & Ermolenko, D. N. (2022). Specific length and structure rather than high thermodynamic stability enable regulatory mRNA stem-loops to pause translation. *Nature Communications*, *13*(1), Article 1. https://doi.org/10.1038/s41467-022-28600-5

Barba Aliaga, M. (2023). *Functions of the translation factor eIF5A in cellular metabolism and transcriptional control* [Doctoral thesis]. https://roderic.uv.es/handle/10550/88612

Barba-Aliaga, M., & Alepuz, P. (2022). Role of eIF5A in Mitochondrial Function. *International Journal of Molecular Sciences*, *23*(3), 1284. https://doi.org/10.3390/ijms23031284

Begovich, K., & Wilhelm, J. E. (2020). An In Vitro Assembly System Identifies Roles for RNA Nucleation and ATP in Yeast Stress Granule Formation. *Molecular Cell*, *79*(6), 991-1007.e4. https://doi.org/10.1016/j.molcel.2020.07.017

Boersma, S., Khuperkar, D., Verhagen, B. M. P., Sonneveld, S., Grimm, J. B., Lavis, L. D., & Tanenbaum, M. E. (2019). Multi-Color Single-Molecule Imaging Uncovers Extensive Heterogeneity in mRNA Decoding. *Cell*, *178*(2), 458-472.e19. https://doi.org/10.1016/j.cell.2019.05.001

Bogorodskiy, A., Okhrimenko, I., Burkatovskii, D., Jakobs, P., Maslov, I., Gordeliy, V., Dencher, N. A., Gensch, T., Voos, W., Altschmied, J., Haendeler, J., & Borshchevskiy, V. (2021). Role of Mitochondrial Protein Import in Age-Related Neurodegenerative and Cardiovascular Diseases. *Cells*, *10*(12), 3528. https://doi.org/10.3390/cells10123528

Boos, F., Mühlhaus, T., & Herrmann, J. M. (2018). Detection of Internal Matrix Targeting Signal-like Sequences (iMTS-Ls) in Mitochondrial Precursor Proteins Using the TargetP Prediction Tool. *Bio-Protocol*, *8*(17), e2474. https://doi.org/10.21769/BioProtoc.2474

Brandman, O., Stewart-Ornstein, J., Wong, D., Larson, A., Williams, C. C., Li, G.-W., Zhou, S., King, D., Shen, P. S., Weibezahn, J., Dunn, J. G., Rouskin, S., Inada, T., Frost, A., & Weissman, J. S. (2012). A Ribosome-Bound Quality Control Complex Triggers Degradation of Nascent Peptides and Signals Translation Stress. *Cell*, *151*(5), 1042–1054. https://doi.org/10.1016/j.cell.2012.10.044

Buchan, J. R., Muhlrad, D., & Parker, R. (2008). P bodies promote stress granule assembly in Saccharomyces cerevisiae. *Journal of Cell Biology*, *183*(3), 441–455. https://doi.org/10.1083/jcb.200807043

Burke, P. C., Park, H., & Subramaniam, A. R. (2022). A nascent peptide code for translational control of mRNA stability in human cells. *Nature Communications*, *13*(1), 6829. https://doi.org/10.1038/s41467-022-34664-0

Buschauer, R., Matsuo, Y., Sugiyama, T., Chen, Y.-H., Alhusaini, N., Sweet, T., Ikeuchi, K., Cheng, J., Matsuki, Y., Nobuta, R., Gilmozzi, A., Berninghausen, O., Tesina, P., Becker, T., Coller, J., Inada, T., & Beckmann, R. (2020). The Ccr4-Not complex monitors the translating ribosome for codon optimality. *Science*, *368*(6488), eaay6912. https://doi.org/10.1126/science.aay6912

Caponigro, G., & Parker, R. (1995). Multiple functions for the poly(A)-binding protein in mRNA decapping and deadenylation in yeast. *Genes & Development*, *9*(19), 2421–2432. https://doi.org/10.1101/gad.9.19.2421

Carroll, J. S., Munchel, S. E., & Weis, K. (2011). The DExD/H box ATPase Dhh1 functions in translational repression, mRNA decay, and processing body dynamics. *Journal of Cell Biology*, *194*(4), 527–537. https://doi.org/10.1083/jcb.201007151

Chan, L. Y., Mugler, C. F., Heinrich, S., Vallotton, P., & Weis, K. (2018). Non-invasive measurement of mRNA decay reveals translation initiation as the major determinant of mRNA stability. *ELife*, *7*, e32536. https://doi.org/10.7554/eLife.32536

Chao, J. A., Yoon, Y. J., & Singer, R. H. (2012). Imaging Translation in Single Cells Using Fluorescent Microscopy. *Cold Spring Harbor Perspectives in Biology*, *4*(11), a012310. https://doi.org/10.1101/cshperspect.a012310

Charneski, C. A., & Hurst, L. D. (2013). Positively Charged Residues Are the Major Determinants of Ribosomal Velocity. *PLOS Biology*, *11*(3), e1001508. https://doi.org/10.1371/journal.pbio.1001508

Chen, Y. S., Hou, W., Tracy, S., Harvey, A. T., Harjono, V., Xu, F., Moresco, J. J., Yates, J. R., III, & Zid, B. M. (2022). Rvb1/Rvb2 proteins couple transcription and translation during glucose starvation. *ELife*, *11*, e76965. https://doi.org/10.7554/eLife.76965

Chiabudini, M., Tais, A., Zhang, Y., Hayashi, S., Wölfle, T., Fitzke, E., & Rospert, S. (2014). Release Factor eRF3 Mediates Premature Translation Termination on Polylysine-Stalled Ribosomes in Saccharomyces cerevisiae. *Molecular and Cellular Biology*, *34*(21), 4062–4076. https://doi.org/10.1128/MCB.00799-14

Choi, J., Grosely, R., Prabhakar, A., Lapointe, C. P., Wang, J., & Puglisi, J. D. (2018). How Messenger RNA and Nascent Chain Sequences Regulate Translation Elongation. *Annual Review of Biochemistry*, *87*(1), 421–449. https://doi.org/10.1146/annurev-biochem-060815-014818

Chu, D., Kazana, E., Bellanger, N., Singh, T., Tuite, M. F., & von der Haar, T. (2014). Translation elongation can control translation initiation on eukaryotic mRNAs. *The EMBO Journal*, *33*(1), 21–34. https://doi.org/10.1002/embj.201385651

Cichocki, B. A., Krumpe, K., Vitali, D. G., & Rapaport, D. (2018). Pex19 is involved in importing dually targeted tail-anchored proteins to both mitochondria and peroxisomes. *Traffic*, *19*(10), 770–785. https://doi.org/10.1111/tra.12604

Collart, M. A., & Weiss, B. (2020). Ribosome pausing, a dangerous necessity for co-translational events. *Nucleic Acids Research*, *48*(3), 1043–1055. https://doi.org/10.1093/nar/gkz763

Coller, J. M., Tucker, M., Sheth, U., Valencia-Sanchez, M. A., & Parker, R. (2001). The DEAD box helicase, Dhh1p, functions in mRNA decapping and interacts with both the decapping and deadenylase complexes. *RNA*, *7*(12), 1717–1727. https://doi.org/10.1017/S135583820101994X

Dang, Y., Kedersha, N., Low, W.-K., Romo, D., Gorospe, M., Kaufman, R., Anderson, P., & Liu, J. O. (2006). Eukaryotic Initiation Factor 2α-independent Pathway of Stress Granule Induction by the Natural Product Pateamine A*. *Journal of Biological Chemistry*, *281*(43), 32870–32878. https://doi.org/10.1074/jbc.M606149200

Defenouillère, Q., Yao, Y., Mouaikel, J., Namane, A., Galopier, A., Decourty, L., Doyen, A., Malabat, C., Saveanu, C., Jacquier, A., & Fromont-Racine, M. (2013). Cdc48-associated complex bound to 60S particles is required for the clearance of aberrant translation products. *Proceedings of the National Academy of Sciences*, *110*(13), 5046–5051. https://doi.org/10.1073/pnas.1221724110

Defenouillère, Q., Zhang, E., Namane, A., Mouaikel, J., Jacquier, A., & Fromont-Racine, M. (2016). Rqc1 and Ltn1 Prevent C-terminal Alanine-Threonine Tail (CAT-tail)-induced Protein Aggregation by Efficient Recruitment of Cdc48 on Stalled 60S Subunits*. *Journal of Biological Chemistry*, *291*(23), 12245–12253. https://doi.org/10.1074/jbc.M116.722264

Deshaies, R. J., Koch, B. D., Werner-Washburne, M., Craig, E. A., & Schekman, R. (1988). A subfamily of stress proteins facilitates translocation of secretory and mitochondrial precursor polypeptides. *Nature*, *332*(6167), Article 6167. https://doi.org/10.1038/332800a0

Doma, M. K., & Parker, R. (2006). Endonucleolytic cleavage of eukaryotic mRNAs with stalls in translation

elongation. *Nature*, *440*(7083), Article 7083. https://doi.org/10.1038/nature04530

D'Orazio, K. N., Wu, C. C.-C., Sinha, N., Loll-Krippleber, R., Brown, G. W., & Green, R. (2019). The endonuclease Cue2 cleaves mRNAs at stalled ribosomes during No Go Decay. *ELife*, *8*, e49117. https://doi.org/10.7554/eLife.49117

dos Reis, M., Wernisch, L., & Savva, R. (2003). Unexpected correlations between gene expression and codon usage bias from microarray data for the whole Escherichia coli K-12 genome. *Nucleic Acids Research*, *31*(23), 6976–6985. https://doi.org/10.1093/nar/gkg897

Edwards, A. M., Kane, C. M., Young, R. A., & Kornberg, R. D. (1991). Two dissociable subunits of yeast RNA polymerase II stimulate the initiation of transcription at a promoter in vitro. *Journal of Biological Chemistry*, *266*(1), 71–75. https://doi.org/10.1016/S0021-9258(18)52403-0

Eisenack, T. J., & Trentini, D. B. (2023). Ending a bad start: Triggers and mechanisms of co-translational protein degradation. *Frontiers in Molecular Biosciences*, *9*. https://www.frontiersin.org/articles/10.3389/fmolb.2022.1089825

Eshraghi, M., Karunadharma, P. P., Blin, J., Shahani, N., Ricci, E. P., Michel, A., Urban, N. T., Galli, N., Sharma, M., Ramírez-Jarquín, U. N., Florescu, K., Hernandez, J., & Subramaniam, S. (2021). Mutant Huntingtin stalls ribosomes and represses protein synthesis in a cellular model of Huntington disease. *Nature Communications*, *12*(1), Article 1. https://doi.org/10.1038/s41467-021-21637-y

F. LACROUTE & G. S. STENT. (1968). Two regulatory models involving variable growth periods of β-galactosidase. *Journal of Molecular Biology*, *35*(1), 172–173. https://doi.org/10.1016/S0022-2836(68)80045-2

Fabian, M. R., Sonenberg, N., & Filipowicz, W. (2010). Regulation of mRNA Translation and Stability by microRNAs. *Annual Review of Biochemistry*, *79*(1), 351–379. https://doi.org/10.1146/annurev-biochem-060308-103103

Fazal, F. M., Han, S., Parker, K. R., Kaewsapsak, P., Xu, J., Boettiger, A. N., Chang, H. Y., & Ting, A. Y. (2019). Atlas of Subcellular RNA Localization Revealed by APEX-Seq. *Cell*, *178*(2), 473-490.e26. https://doi.org/10.1016/j.cell.2019.05.027

Fischer, N. (2002). The DEAD box protein Dhh1 stimulates the decapping enzyme Dcp1. *The EMBO Journal*, *21*(11), 2788–2797. https://doi.org/10.1093/emboj/21.11.2788

Fleiss, A., & Sarkisyan, K. S. (2019). A brief review of bioluminescent systems (2019). *Current Genetics*, *65*(4), 877–882. https://doi.org/10.1007/s00294-019-00951-5

Foury, F., Roganti, T., Lecrenier, N., & Purnelle, B. (1998). The complete sequence of the mitochondrial genome of Saccharomyces cerevisiae. *FEBS Letters*, *440*(3), 325–331. https://doi.org/10.1016/S0014-5793(98)01467-7

Francis Crick. (1958). *On Protein Synthesis*. Francis Crick - Profiles in Science. https://profiles.nlm.nih.gov/spotlight/sc/catalog/nlm:nlmuid-101584582X404-doc

Franks, A., Airoldi, E., & Slavov, N. (2017). Post-transcriptional regulation across human tissues. *PLOS Computational Biology*, *13*(5), e1005535. https://doi.org/10.1371/journal.pcbi.1005535

Gadir, N., Haim-Vilmovsky, L., Kraut-Cohen, J., & Gerst, J. E. (2011). Localization of mRNAs coding for mitochondrial proteins in the yeast Saccharomyces cerevisiae. *RNA*, *17*(8), 1551–1565. https://doi.org/10.1261/rna.2621111

Gamble, C. E., Brule, C. E., Dean, K. M., Fields, S., & Grayhack, E. J. (2016). Adjacent Codons Act in Concert to Modulate Translation Efficiency in Yeast. *Cell*, *166*(3), 679–690. https://doi.org/10.1016/j.cell.2016.05.070

Gameiro, P. A., & Struhl, K. (2018). Nutrient Deprivation Elicits a Transcriptional and Translational Inflammatory Response Coupled to Decreased Protein Synthesis. *Cell Reports*, *24*(6), 1415–1424. https://doi.org/10.1016/j.celrep.2018.07.021

Gamerdinger, M., Kobayashi, K., Wallisch, A., Kreft, S. G., Sailer, C., Schlömer, R., Sachs, N., Jomaa, A., Stengel, F., Ban, N., & Deuerling, E. (2019). Early Scanning of Nascent Polypeptides inside the Ribosomal Tunnel by NAC. *Molecular Cell*, *75*(5), 996-1006.e8. https://doi.org/10.1016/j.molcel.2019.06.030

Garcia, M., Darzacq, X., Delaveau, T., Jourdren, L., Singer, R. H., & Jacq, C. (2007). Mitochondria-associated Yeast mRNAs and the Biogenesis of Molecular Complexes. *Molecular Biology of the Cell*, *18*(2), 362–368. https://doi.org/10.1091/mbc.e06-09-0827

García-Rodríguez, L. J., Gay, A. C., & Pon, L. A. (2007). Puf3p, a Pumilio family RNA binding protein, localizes to mitochondria and regulates mitochondrial biogenesis and motility in budding yeast. *Journal of Cell Biology*, *176*(2), 197–207. https://doi.org/10.1083/jcb.200606054

Gardin, J., Yeasmin, R., Yurovsky, A., Cai, Y., Skiena, S., & Futcher, B. (2014). Measurement of average decoding rates of the 61 sense codons in vivo. *ELife*, *3*, e03735. https://doi.org/10.7554/eLife.03735

Gatsing, K. (1972). Efficiency of protein and messenger RNA synthesis in bacteriophage T4-infected cells of Escherichia coli. *Journal of Molecular Biology*, *71*(3), 529–545. https://doi.org/10.1016/S0022-2836(72)80021-4

Gilks, N., Kedersha, N., Ayodele, M., Shen, L., Stoecklin, G., Dember, L. M., & Anderson, P. (2004). Stress Granule Assembly Is Mediated by Prion-like Aggregation of TIA-1. *Molecular Biology of the Cell*, *15*(12), 5383–5398. https://doi.org/10.1091/mbc.e04-08-0715

Glover, M. L., Burroughs, A. Max., Monem, P. C., Egelhofer, T. A., Pule, M. N., Aravind, L., & Arribere, J. A. (2020). NONU-1 Encodes a Conserved Endonuclease Required for mRNA Translation Surveillance. *Cell Reports*, *30*(13), 4321-4331.e4. https://doi.org/10.1016/j.celrep.2020.03.023

Gold, V. A., Chroscicki, P., Bragoszewski, P., & Chacinska, A. (2017). Visualization of cytosolic ribosomes on the surface of mitochondria by electron cryo-tomography. *EMBO Reports*, *18*(10), 1786–1800. https://doi.org/10.15252/embr.201744261

Goldman, D. H., Livingston, N. M., Movsik, J., Wu, B., & Green, R. (2021). Live-cell imaging reveals kinetic determinants of quality control triggered by ribosome stalling. *Molecular Cell*, *81*(8), 1830-1840.e8. https://doi.org/10.1016/j.molcel.2021.01.029

Griffiths, K. K., & Levy, R. J. (2017). Evidence of Mitochondrial Dysfunction in Autism: Biochemical Links,

Genetic-Based Associations, and Non-Energy-Related Mechanisms. *Oxidative Medicine and Cellular Longevity*, *2017*, e4314025. https://doi.org/10.1155/2017/4314025

Gutierrez, E., Shin, B.-S., Woolstenhulme, C. J., Kim, J.-R., Saini, P., Buskirk, A. R., & Dever, T. E. (2013). EIF5A Promotes Translation of Polyproline Motifs. *Molecular Cell*, *51*(1), 35–45. https://doi.org/10.1016/j.molcel.2013.04.021

Guzikowski, A. R., Chen, Y. S., & Zid, B. M. (2019). Stress-induced mRNP granules: Form and function of processing bodies and stress granules. *WIREs RNA*, *10*(3), e1524. https://doi.org/10.1002/wrna.1524

Halstead, J. M., Lionnet, T., Wilbertz, J. H., Wippich, F., Ephrussi, A., Singer, R. H., & Chao, J. A. (2015). An RNA biosensor for imaging the first round of translation from single cells to living animals. *Science*, *347*(6228), 1367–1671. https://doi.org/10.1126/science.aaa3380

Han, K., Jaimovich, A., Dey, G., Ruggero, D., Meyuhas, O., Sonenberg, N., & Meyer, T. (2014). Parallel measurement of dynamic changes in translation rates in single cells. *Nature Methods*, *11*(1), Article 1. https://doi.org/10.1038/nmeth.2729

Han, P., Shichino, Y., Schneider-Poetsch, T., Mito, M., Hashimoto, S., Udagawa, T., Kohno, K., Yoshida, M., Mishima, Y., Inada, T., & Iwasaki, S. (2020). Genome-wide Survey of Ribosome Collision. *Cell Reports*, *31*(5), 107610. https://doi.org/10.1016/j.celrep.2020.107610

Hansen, K. G., Aviram, N., Laborenz, J., Bibi, C., Meyer, M., Spang, A., Schuldiner, M., & Herrmann, J. M. (2018). An ER surface retrieval pathway safeguards the import of mitochondrial membrane proteins in yeast. *Science*, *361*(6407), 1118–1122. https://doi.org/10.1126/science.aar8174

Hansen, K. G., & Herrmann, J. M. (2019). Transport of Proteins into Mitochondria. *The Protein Journal*, *38*(3), 330–342. https://doi.org/10.1007/s10930-019-09819-6

Hanson, G., Alhusaini, N., Morris, N., Sweet, T., & Coller, J. (2018). Translation elongation and mRNA stability are coupled through the ribosomal A-site. *RNA*, *24*(10), 1377–1389. https://doi.org/10.1261/rna.066787.118

Hanson, G., & Coller, J. (2018). Codon optimality, bias and usage in translation and mRNA decay. *Nature Reviews Molecular Cell Biology*, *19*(1), 20–30. https://doi.org/10.1038/nrm.2017.91

Harigaya, Y., & Parker, R. (2010). No-go decay: A quality control mechanism for RNA in translation. *WIREs RNA*, *1*(1), 132–141. https://doi.org/10.1002/wrna.17

Hashimoto, S., Sugiyama, T., Yamazaki, R., Nobuta, R., & Inada, T. (2020). Identification of a novel trigger complex that facilitates ribosome-associated quality control in mammalian cells. *Scientific Reports*, *10*(1), Article 1. https://doi.org/10.1038/s41598-020-60241-w

Hershberg, R., & Petrov, D. A. (2008). Selection on Codon Bias. *Annual Review of Genetics*, *42*(1), 287–299. https://doi.org/10.1146/annurev.genet.42.110807.091442

Hickey, K. L., Dickson, K., Cogan, J. Z., Replogle, J. M., Schoof, M., D'Orazio, K. N., Sinha, N. K., Hussmann, J. A., Jost, M., Frost, A., Green, R., Weissman, J. S., & Kostova, K. K. (2020). GIGYF2 and 4EHP Inhibit Translation Initiation of Defective Messenger RNAs to Assist Ribosome-Associated Quality Control. *Molecular Cell*, *79*(6), 950-962.e6. https://doi.org/10.1016/j.molcel.2020.07.007

Hilal, T., Yamamoto, H., Loerke, J., Bürger, J., Mielke, T., & Spahn, C. M. T. (2016). Structural insights into ribosomal rescue by Dom34 and Hbs1 at near-atomic resolution. *Nature Communications*, *7*(1), Article 1. https://doi.org/10.1038/ncomms13521

Hood, H. M., Neafsey, D. E., Galagan, J., & Sachs, M. S. (2009). Evolutionary Roles of Upstream Open Reading Frames in Mediating Gene Regulation in Fungi. *Annual Review of Microbiology*, *63*(1), 385–409. https://doi.org/10.1146/annurev.micro.62.081307.162835

Huter, P., Arenz, S., Bock, L. V., Graf, M., Frister, J. O., Heuer, A., Peil, L., Starosta, A. L., Wohlgemuth, I., Peske, F., Nováček, J., Berninghausen, O., Grubmüller, H., Tenson, T., Beckmann, R., Rodnina, M. V., Vaiana, A. C., & Wilson, D. N. (2017). Structural Basis for Polyproline-Mediated Ribosome Stalling and Rescue by the Translation Elongation Factor EF-P. *Molecular Cell*, *68*(3), 515-527.e6. https://doi.org/10.1016/j.molcel.2017.10.014

Hüttelmaier, S., Zenklusen, D., Lederer, M., Dictenberg, J., Lorenz, M., Meng, X., Bassell, G. J., Condeelis, J., & Singer, R. H. (2005). Spatial regulation of β-actin translation by Src-dependent phosphorylation of ZBP1. *Nature*, *438*(7067), Article 7067. https://doi.org/10.1038/nature04115

Ikemura, T. (1985). Codon usage and tRNA content in unicellular and multicellular organisms. *Molecular Biology and Evolution*, *2*(1), 13–34. https://doi.org/10.1093/oxfordjournals.molbev.a040335

Ikeuchi, K., Izawa, T., & Inada, T. (2019). Recent Progress on the Molecular Mechanism of Quality Controls Induced by Ribosome Stalling. *Frontiers in Genetics*, *9*. https://www.frontiersin.org/articles/10.3389/fgene.2018.00743

Ikeuchi, K., Tesina, P., Matsuo, Y., Sugiyama, T., Cheng, J., Saeki, Y., Tanaka, K., Becker, T., Beckmann, R., & Inada, T. (2019). Collided ribosomes form a unique structural interface to induce Hel2-driven quality control pathways. *The EMBO Journal*, *38*(5), e100276. https://doi.org/10.15252/embj.2018100276

Ingolia, N. T., Ghaemmaghami, S., Newman, J. R. S., & Weissman, J. S. (2009). Genome-Wide Analysis in Vivo of Translation with Nucleotide Resolution Using Ribosome Profiling. *Science*, *324*(5924), 218–223. https://doi.org/10.1126/science.1168978

Ingolia, N. T., Lareau, L. F., & Weissman, J. S. (2011). Ribosome Profiling of Mouse Embryonic Stem Cells Reveals the Complexity and Dynamics of Mammalian Proteomes. *Cell*, *147*(4), 789–802. https://doi.org/10.1016/j.cell.2011.10.002

Ishimura, R., Nagy, G., Dotu, I., Zhou, H., Yang, X.-L., Schimmel, P., Senju, S., Nishimura, Y., Chuang, J. H., & Ackerman, S. L. (2014). Ribosome stalling induced by mutation of a CNS-specific tRNA causes neurodegeneration. *Science*, *345*(6195), 455–459. https://doi.org/10.1126/science.1249749

Izumi, N., Yamashita, A., & Ohno, S. (2012). Integrated regulation of PIKK-mediated stress responses by AAA+ proteins RUVBL1 and RUVBL2. *Nucleus*, *3*(1), 29–43. https://doi.org/10.4161/nucl.18926

Jackson, R. J., Hellen, C. U. T., & Pestova, T. V. (2010). The mechanism of eukaryotic translation initiation and principles of its regulation. *Nature Reviews Molecular Cell Biology*, *11*(2), Article 2. https://doi.org/10.1038/nrm2838

Jain, S., Wheeler, J. R., Walters, R. W., Agrawal, A., Barsic, A., & Parker, R. (2016). ATPase-Modulated Stress

Granules Contain a Diverse Proteome and Substructure. *Cell*, *164*(3), 487–498. https://doi.org/10.1016/j.cell.2015.12.038

Jha, S., & Dutta, A. (2009). RVB1/RVB2: Running Rings around Molecular Biology. *Molecular Cell*, *34*(5), 521–533. https://doi.org/10.1016/j.molcel.2009.05.016

Jónsson, Z. O., Dhar, S. K., Narlikar, G. J., Auty, R., Wagle, N., Pellman, D., Pratt, R. E., Kingston, R., & Dutta, A. (2001). Rvb1p and Rvb2p Are Essential Components of a Chromatin Remodeling Complex That Regulates Transcription of over 5% of Yeast Genes*. *Journal of Biological Chemistry*, *276*(19), 16279–16288. https://doi.org/10.1074/jbc.M011523200

Jores, T., Lawatscheck, J., Beke, V., Franz-Wachtel, M., Yunoki, K., Fitzgerald, J. C., Macek, B., Endo, T., Kalbacher, H., Buchner, J., & Rapaport, D. (2018). Cytosolic Hsp70 and Hsp40 chaperones enable the biogenesis of mitochondrial β-barrel proteins. *Journal of Cell Biology*, *217*(9), 3091–3108. https://doi.org/10.1083/jcb.201712029

Jungfleisch, J., Nedialkova, D. D., Dotu, I., Sloan, K. E., Martinez-Bosch, N., Brüning, L., Raineri, E., Navarro, P., Bohnsack, M. T., Leidel, S. A., & Díez, J. (2017). Corrigendum: A novel translational control mechanism involving RNA structures within coding sequences. *Genome Research*, *27*(4), 663–663. https://doi.org/10.1101/gr.222133.117

Juszkiewicz, S., Speldewinde, S. H., Wan, L., Svejstrup, J. Q., & Hegde, R. S. (2020). The ASC-1 Complex Disassembles Collided Ribosomes. *Molecular Cell*, *79*(4), 603-614.e8. https://doi.org/10.1016/j.molcel.2020.06.006

Kakihara, Y., Makhnevych, T., Zhao, L., Tang, W., & Houry, W. A. (2014). Nutritional status modulates box C/D snoRNP biogenesis by regulated subcellular relocalization of the R2TP complex. *Genome Biology*, *15*(7), 404. https://doi.org/10.1186/s13059-014-0404-4

Kanai, Y., Kawagishi, T., Matsuura, Y., & Kobayashi, T. (2019). In Vivo Live Imaging of Oncolytic Mammalian Orthoreovirus Expressing NanoLuc Luciferase in Tumor Xenograft Mice. *Journal of Virology*, *93*(14), e00401-19. https://doi.org/10.1128/JVI.00401-19

Karpinets, T. V., Greenwood, D. J., Sams, C. E., & Ammons, J. T. (2006). RNA:protein ratio of the unicellular organism as a characteristic of phosphorous and nitrogen stoichiometry and of the cellular requirement of ribosomes for protein synthesis. *BMC Biology*, *4*(1), 30. https://doi.org/10.1186/1741-7007-4-30

Kedersha, N., Cho, M. R., Li, W., Yacono, P. W., Chen, S., Gilks, N., Golan, D. E., & Anderson, P. (2000). Dynamic Shuttling of Tia-1 Accompanies the Recruitment of mRNA to Mammalian Stress Granules. *Journal of Cell Biology*, *151*(6), 1257–1268. https://doi.org/10.1083/jcb.151.6.1257

Kedersha, N. L., Gupta, M., Li, W., Miller, I., & Anderson, P. (1999). RNA-Binding Proteins Tia-1 and Tiar Link the Phosphorylation of Eif-2α to the Assembly of Mammalian Stress Granules. *Journal of Cell Biology*, *147*(7), 1431–1442. https://doi.org/10.1083/jcb.147.7.1431

Kellems, R. E., Allison, V. F., & Butow, R. A. (1974). Cytoplasmic Type 80 S Ribosomes Associated with Yeast Mitochondria: II. EVIDENCE FOR THE ASSOCIATION OF CYTOPLASMIC RIBOSOMES WITH THE OUTER MITOCHONDRIAL MEMBRANE IN SITU. *Journal of Biological Chemistry*,

249(10), 3297–3303. https://doi.org/10.1016/S0021-9258(19)42672-0

Khong, A., Matheny, T., Jain, S., Mitchell, S. F., Wheeler, J. R., & Parker, R. (2017). The Stress Granule Transcriptome Reveals Principles of mRNA Accumulation in Stress Granules. *Molecular Cell*, *68*(4), 808-820.e5. https://doi.org/10.1016/j.molcel.2017.10.015

Kim, S. J., Yoon, J. S., Shishido, H., Yang, Z., Rooney, L. A., Barral, J. M., & Skach, W. R. (2015). Protein folding. Translational tuning optimizes nascent protein folding in cells. *Science (New York, N.Y.)*, *348*(6233), 444–448. https://doi.org/10.1126/science.aaa3974

Klaips, C. L., Jayaraj, G. G., & Hartl, F. U. (2017). Pathways of cellular proteostasis in aging and disease. *Journal of Cell Biology*, *217*(1), 51–63. https://doi.org/10.1083/jcb.201709072

Komar, A. A. (2019). [Synonymous Codon Usage-a Guide for Co-Translational Protein Folding in the Cell]. *Molekuliarnaia Biologiia*, *53*(6), 883–898. https://doi.org/10.1134/S0026898419060090

Komar, A. A., Lesnik, T., & Reiss, C. (1999). Synonymous codon substitutions affect ribosome traffic and protein folding during in vitro translation. *FEBS Letters*, *462*(3), 387–391. https://doi.org/10.1016/S0014-5793(99)01566-5

Kostova, K. K., Hickey, K. L., Osuna, B. A., Hussmann, J. A., Frost, A., Weinberg, D. E., & Weissman, J. S. (2017). CAT-tailing as a fail-safe mechanism for efficient degradation of stalled nascent polypeptides. *Science*, *357*(6349), 414–417. https://doi.org/10.1126/science.aam7787

Lemaux, P. G., Herendeen, S. L., Bloch, P. L., & Neidhardt, F. C. (1978). Transient rates of synthesis of individual polypeptides in E. coli following temperature shifts. *Cell*, *13*(3), 427–434. https://doi.org/10.1016/0092-8674(78)90317-3

Lesnik, C., Cohen, Y., Atir-Lande, A., Schuldiner, M., & Arava, Y. (2014). OM14 is a mitochondrial receptor for cytosolic ribosomes that supports co-translational import into mitochondria. *Nature Communications*, *5*(1), Article 1. https://doi.org/10.1038/ncomms6711

Letzring, D. P., Dean, K. M., & Grayhack, E. J. (2010). Control of translation efficiency in yeast by codon–anticodon interactions. *RNA*, *16*(12), 2516–2528. https://doi.org/10.1261/rna.2411710

Li, G.-W., Burkhardt, D., Gross, C., & Weissman, J. S. (2014). Quantifying Absolute Protein Synthesis Rates Reveals Principles Underlying Allocation of Cellular Resources. *Cell*, *157*(3), 624–635. https://doi.org/10.1016/j.cell.2014.02.033

Li, G.-W., Oh, E., & Weissman, J. S. (2012). The anti-Shine–Dalgarno sequence drives translational pausing and codon choice in bacteria. *Nature*, *484*(7395), Article 7395. https://doi.org/10.1038/nature10965

Lian, X., Guo, J., Gu, W., Cui, Y., Zhong, J., Jin, J., He, Q.-Y., Wang, T., & Zhang, G. (2016). Genome-Wide and Experimental Resolution of Relative Translation Elongation Speed at Individual Gene Level in Human Cells. *PLOS Genetics*, *12*(2), e1005901. https://doi.org/10.1371/journal.pgen.1005901

Liu, X., Yao, Z., Jin, M., Namkoong, S., Yin, Z., Lee, J. H., & Klionsky, D. J. (2019). Dhh1 promotes autophagy-related protein translation during nitrogen starvation. *PLOS Biology*, *17*(4), e3000219. https://doi.org/10.1371/journal.pbio.3000219

Liu, Y. (2020). A code within the genetic code: Codon usage regulates co-translational protein folding. *Cell*

Communication and Signaling, *18*(1), 145. https://doi.org/10.1186/s12964-020-00642-6

Liu, Y., Yang, Q., & Zhao, F. (2021). Synonymous but Not Silent: The Codon Usage Code for Gene Expression and Protein Folding. *Annual Review of Biochemistry*, *90*(1), 375–401. https://doi.org/10.1146/annurev-biochem-071320-112701

Lu, B., & Guo, S. (2020). Mechanisms Linking Mitochondria Dysfunction and Proteostasis Failure. *Trends in Cell Biology*, *30*(4), 317–328. https://doi.org/10.1016/j.tcb.2020.01.008

Majmundar, A. J., Wong, W. J., & Simon, M. C. (2010). Hypoxia-Inducible Factors and the Response to Hypoxic Stress. *Molecular Cell*, *40*(2), 294–309. https://doi.org/10.1016/j.molcel.2010.09.022

Martin, K. C., & Ephrussi, A. (2009). mRNA Localization: Gene Expression in the Spatial Dimension. *Cell*, *136*(4), 719–730. https://doi.org/10.1016/j.cell.2009.01.044

Martin, P. B., Kigoshi-Tansho, Y., Sher, R. B., Ravenscroft, G., Stauffer, J. E., Kumar, R., Yonashiro, R., Müller, T., Griffith, C., Allen, W., Pehlivan, D., Harel, T., Zenker, M., Howting, D., Schanze, D., Faqeih, E. A., Almontashiri, N. A. M., Maroofian, R., Houlden, H., … Cox, G. A. (2020). NEMF mutations that impair ribosome-associated quality control are associated with neuromuscular disease. *Nature Communications*, *11*(1), Article 1. https://doi.org/10.1038/s41467-020-18327-6

Mason, P. B., & Struhl, K. (2005). Distinction and Relationship between Elongation Rate and Processivity of RNA Polymerase II In Vivo. *Molecular Cell*, *17*(6), 831–840. https://doi.org/10.1016/j.molcel.2005.02.017

Masser, A. E., Kandasamy, G., Kaimal, J. M., & Andréasson, C. (2016). Luciferase NanoLuc as a reporter for gene expression and protein levels in *Saccharomyces cerevisiae*. *Yeast*, *33*(5), 191–200. https://doi.org/10.1002/yea.3155

Matheny, T., Rao, B. S., & Parker, R. (2019). Transcriptome-Wide Comparison of Stress Granules and P-Bodies Reveals that Translation Plays a Major Role in RNA Partitioning. *Molecular and Cellular Biology*, *39*(24), e00313-19. https://doi.org/10.1128/MCB.00313-19

Matsuo, Y., Ikeuchi, K., Saeki, Y., Iwasaki, S., Schmidt, C., Udagawa, T., Sato, F., Tsuchiya, H., Becker, T., Tanaka, K., Ingolia, N. T., Beckmann, R., & Inada, T. (2017). Ubiquitination of stalled ribosome triggers ribosome-associated quality control. *Nature Communications*, *8*(1), Article 1. https://doi.org/10.1038/s41467-017-00188-1

Matsuo, Y., Tesina, P., Nakajima, S., Mizuno, M., Endo, A., Buschauer, R., Cheng, J., Shounai, O., Ikeuchi, K., Saeki, Y., Becker, T., Beckmann, R., & Inada, T. (2020). RQT complex dissociates ribosomes collided on endogenous RQC substrate SDD1. *Nature Structural & Molecular Biology*, *27*(4), Article 4. https://doi.org/10.1038/s41594-020-0393-9

Mazroui, R., Sukarieh, R., Bordeleau, M.-E., Kaufman, R. J., Northcote, P., Tanaka, J., Gallouzi, I., & Pelletier, J. (2006). Inhibition of Ribosome Recruitment Induces Stress Granule Formation Independently of Eukaryotic Initiation Factor 2α Phosphorylation. *Molecular Biology of the Cell*, *17*(10), 4212–4219. https://doi.org/10.1091/mbc.e06-04-0318

McGlincy, N. J., Meacham, Z. A., Reynaud, K. K., Muller, R., Baum, R., & Ingolia, N. T. (2021). A genome-

scale CRISPR interference guide library enables comprehensive phenotypic profiling in yeast. *BMC Genomics*, *22*(1), 205. https://doi.org/10.1186/s12864-021-07518-0

Meydan, S., & Guydosh, N. R. (2020). Disome and Trisome Profiling Reveal Genome-wide Targets of Ribosome Quality Control. *Molecular Cell*, *79*(4), 588-602.e6. https://doi.org/10.1016/j.molcel.2020.06.010

Meydan, S., & Guydosh, N. R. (2021). A cellular handbook for collided ribosomes: Surveillance pathways and collision types. *Current Genetics*, *67*(1), 19–26. https://doi.org/10.1007/s00294-020-01111-w

Mokas, S., Mills, J. R., Garreau, C., Fournier, M.-J., Robert, F., Arya, P., Kaufman, R. J., Pelletier, J., & Mazroui, R. (2009). Uncoupling Stress Granule Assembly and Translation Initiation Inhibition. *Molecular Biology of the Cell*, *20*(11), 2673–2683. https://doi.org/10.1091/mbc.e08-10-1061

Morisaki, T., Lyon, K., DeLuca, K. F., DeLuca, J. G., English, B. P., Zhang, Z., Lavis, L. D., Grimm, J. B., Viswanathan, S., Looger, L. L., Lionnet, T., & Stasevich, T. J. (2016). Real-time quantification of single RNA translation dynamics in living cells. *Science*, *352*(6292), 1425–1429. https://doi.org/10.1126/science.aaf0899

Mu, X., Fu, Y., Zhu, Y., Wang, X., Xuan, Y., Shang, H., Goff, S. P., & Gao, G. (2015). HIV-1 Exploits the Host Factor RuvB-like 2 to Balance Viral Protein Expression. *Cell Host & Microbe*, *18*(2), 233–242. https://doi.org/10.1016/j.chom.2015.06.018

Münch, C., & Harper, J. W. (2016). Mitochondrial unfolded protein response controls matrix pre-RNA processing and translation. *Nature*, *534*(7609), Article 7609. https://doi.org/10.1038/nature18302

Narula, A., Ellis, J., Taliaferro, J. M., & Rissland, O. S. (2019). Coding regions affect mRNA stability in human cells. *RNA*, *25*(12), 1751–1764. https://doi.org/10.1261/rna.073239.119

Neelagandan, N., Lamberti, I., Carvalho, H. J. F., Gobet, C., & Naef, F. (2020). What determines eukaryotic translation elongation: Recent molecular and quantitative analyses of protein synthesis. *Open Biology*, *10*(12), 200292. https://doi.org/10.1098/rsob.200292

Nyathi, Y., Wilkinson, B. M., & Pool, M. R. (2013). Co-translational targeting and translocation of proteins to the endoplasmic reticulum. *Biochimica et Biophysica Acta (BBA) - Molecular Cell Research*, *1833*(11), 2392–2402. https://doi.org/10.1016/j.bbamcr.2013.02.021

O'Farrell, P. H. (1975). High Resolution Two-Dimensional Electrophoresis of Proteins. *The Journal of Biological Chemistry*, *250*(10), 4007–4021.

Opaliński, Ł., Song, J., Priesnitz, C., Wenz, L.-S., Oeljeklaus, S., Warscheid, B., Pfanner, N., & Becker, T. (2018). Recruitment of Cytosolic J-Proteins by TOM Receptors Promotes Mitochondrial Protein Biogenesis. *Cell Reports*, *25*(8), 2036-2043.e5. https://doi.org/10.1016/j.celrep.2018.10.083

Panas, M. D., Ivanov, P., & Anderson, P. (2016). Mechanistic insights into mammalian stress granule dynamics. *Journal of Cell Biology*, *215*(3), 313–323. https://doi.org/10.1083/jcb.201609081

Park, H., & Subramaniam, A. R. (2019). Inverted translational control of eukaryotic gene expression by ribosome collisions. *PLOS Biology*, *17*(9), e3000396. https://doi.org/10.1371/journal.pbio.3000396

Passmore, L. A., & Coller, J. (2022). Roles of mRNA poly(A) tails in regulation of eukaryotic gene expression.

Nature Reviews Molecular Cell Biology, *23*(2), Article 2. https://doi.org/10.1038/s41580-021-00417-y

Pavlov, M. Y., Watts, R. E., Tan, Z., Cornish, V. W., Ehrenberg, M., & Forster, A. C. (2009). Slow peptide bond formation by proline and other N-alkylamino acids in translation. *Proceedings of the National Academy of Sciences*, *106*(1), 50–54. https://doi.org/10.1073/pnas.0809211106

Pechmann, S., & Frydman, J. (2013). Evolutionary conservation of codon optimality reveals hidden signatures of cotranslational folding. *Nature Structural & Molecular Biology*, *20*(2), 237–243. https://doi.org/10.1038/nsmb.2466

Pedersen, S. (1984). Escherichia coli ribosomes translate in vivo with variable rate. *The EMBO Journal*, *3*(12), 2895–2898. https://doi.org/10.1002/j.1460-2075.1984.tb02227.x

Pfeffer, S., Woellhaf, M. W., Herrmann, J. M., & Förster, F. (2015). Organization of the mitochondrial translation machinery studied in situ by cryoelectron tomography. *Nature Communications*, *6*(1), Article 1. https://doi.org/10.1038/ncomms7019

Pisareva, V. P., Skabkin, M. A., Hellen, C. U. T., Pestova, T. V., & Pisarev, A. V. (2011). Dissociation by Pelota, Hbs1 and ABCE1 of mammalian vacant 80S ribosomes and stalled elongation complexes. *The EMBO Journal*, *30*(9), 1804–1817. https://doi.org/10.1038/emboj.2011.93

Plotkin, J. B., & Kudla, G. (2011). Synonymous but not the same: The causes and consequences of codon bias. *Nature Reviews Genetics*, *12*(1), Article 1. https://doi.org/10.1038/nrg2899

Presnyak, V., Alhusaini, N., Chen, Y.-H., Martin, S., Morris, N., Kline, N., Olson, S., Weinberg, D., Baker, K. E., Graveley, B. R., & Coller, J. (2015). Codon Optimality Is a Major Determinant of mRNA Stability. *Cell*, *160*(6), 1111–1124. https://doi.org/10.1016/j.cell.2015.02.029

Protter, D. S. W., & Parker, R. (2016). Principles and Properties of Stress Granules. *Trends in Cell Biology*, *26*(9), 668–679. https://doi.org/10.1016/j.tcb.2016.05.004

Proud, C. G. (2019). Phosphorylation and Signal Transduction Pathways in Translational Control. *Cold Spring Harbor Perspectives in Biology*, *11*(7), a033050. https://doi.org/10.1101/cshperspect.a033050

Radhakrishnan, A., Chen, Y.-H., Martin, S., Alhusaini, N., Green, R., & Coller, J. (2016). The DEAD-Box Protein Dhh1p Couples mRNA Decay and Translation by Monitoring Codon Optimality. *Cell*, *167*(1), 122-132.e9. https://doi.org/10.1016/j.cell.2016.08.053

Riba, A., Di Nanni, N., Mittal, N., Arhné, E., Schmidt, A., & Zavolan, M. (2019). Protein synthesis rates and ribosome occupancies reveal determinants of translation elongation rates. *Proceedings of the National Academy of Sciences*, *116*(30), 15023–15032. https://doi.org/10.1073/pnas.1817299116

Richter, K., Haslbeck, M., & Buchner, J. (2010). The Heat Shock Response: Life on the Verge of Death. *Molecular Cell*, *40*(2), 253–266. https://doi.org/10.1016/j.molcel.2010.10.006

Rizzolo, K., Huen, J., Kumar, A., Phanse, S., Vlasblom, J., Kakihara, Y., Zeineddine, H. A., Minic, Z., Snider, J., Wang, W., Pons, C., Seraphim, T. V., Boczek, E. E., Alberti, S., Costanzo, M., Myers, C. L., Stagljar, I., Boone, C., Babu, M., & Houry, W. A. (2017). Features of the Chaperone Cellular Network Revealed through Systematic Interaction Mapping. *Cell Reports*, *20*(11), 2735–2748. https://doi.org/10.1016/j.celrep.2017.08.074

Rodnina, M. V., & Wintermeyer, W. (2016). Protein Elongation, Co-translational Folding and Targeting. *Journal of Molecular Biology*, *428*(10, Part B), 2165–2185. https://doi.org/10.1016/j.jmb.2016.03.022

Rojas-Duran, M. F., & Gilbert, W. V. (2012). Alternative transcription start site selection leads to large differences in translation activity in yeast. *RNA*, *18*(12), 2299–2305. https://doi.org/10.1261/rna.035865.112

Rosenzweig, R., Nillegoda, N. B., Mayer, M. P., & Bukau, B. (2019). The Hsp70 chaperone network. *Nature Reviews Molecular Cell Biology*, *20*(11), Article 11. https://doi.org/10.1038/s41580-019-0133-3

Russell, R. C., Yuan, H.-X., & Guan, K.-L. (2014). Autophagy regulation by nutrient signaling. *Cell Research*, *24*(1), Article 1. https://doi.org/10.1038/cr.2013.166

Sachs, A. B., & Davis, R. W. (1989). The poly(A) binding protein is required for poly(A) shortening and 60S ribosomal subunit-dependent translation initiation. *Cell*, *58*(5), 857–867. https://doi.org/10.1016/0092-8674(89)90938-0

Saint-Georges, Y., Garcia, M., Delaveau, T., Jourdren, L., Crom, S. L., Lemoine, S., Tanty, V., Devaux, F., & Jacq, C. (2008). Yeast Mitochondrial Biogenesis: A Role for the PUF RNA-Binding Protein Puf3p in mRNA Localization. *PLOS ONE*, *3*(6), e2293. https://doi.org/10.1371/journal.pone.0002293

Schleif, R., Hess, W., Finkelstein, S., & Ellis, D. (1973). Induction Kinetics of the L -Arabinose Operon of *Escherichia coli*. *Journal of Bacteriology*, *115*(1), 9–14. https://doi.org/10.1128/jb.115.1.9-14.1973

Schmidt, C., Becker, T., Heuer, A., Braunger, K., Shanmuganathan, V., Pech, M., Berninghausen, O., Wilson, D. N., & Beckmann, R. (2016). Structure of the hypusinylated eukaryotic translation factor eIF-5A bound to the ribosome. *Nucleic Acids Research*, *44*(4), 1944–1951. https://doi.org/10.1093/nar/gkv1517

Schuller, A. P., & Green, R. (2018). Roadblocks and resolutions in eukaryotic translation. *Nature Reviews Molecular Cell Biology*, *19*(8), Article 8. https://doi.org/10.1038/s41580-018-0011-4

Schuller, A. P., Wu, C. C.-C., Dever, T. E., Buskirk, A. R., & Green, R. (2017). EIF5A Functions Globally in Translation Elongation and Termination. *Molecular Cell*, *66*(2), 194-205.e5. https://doi.org/10.1016/j.molcel.2017.03.003

Schwanhäusser, B., Gossen, M., Dittmar, G., & Selbach, M. (2009). Global analysis of cellular protein translation by pulsed SILAC. *PROTEOMICS*, *9*(1), 205–209. https://doi.org/10.1002/pmic.200800275

Shah, K. H., Zhang, B., Ramachandran, V., & Herman, P. K. (2013). Processing Body and Stress Granule Assembly Occur by Independent and Differentially Regulated Pathways in Saccharomyces cerevisiae. *Genetics*, *193*(1), 109–123. https://doi.org/10.1534/genetics.112.146993

Shao, S., Brown, A., Santhanam, B., & Hegde, R. S. (2015). Structure and Assembly Pathway of the Ribosome Quality Control Complex. *Molecular Cell*, *57*(3), 433–444. https://doi.org/10.1016/j.molcel.2014.12.015

Shen, P. S., Park, J., Qin, Y., Li, X., Parsawar, K., Larson, M. H., Cox, J., Cheng, Y., Lambowitz, A. M., Weissman, J. S., Brandman, O., & Frost, A. (2015). Rqc2p and 60S ribosomal subunits mediate mRNA-independent elongation of nascent chains. *Science*, *347*(6217), 75–78.

https://doi.org/10.1126/science.1259724

Sherman, M. Y., & Qian, S.-B. (2013). Less is more: Improving proteostasis by translation slow down. *Trends in Biochemical Sciences*, *38*(12), 585–591. https://doi.org/10.1016/j.tibs.2013.09.003

Shoemaker, C. J., Eyler, D. E., & Green, R. (2010). Dom34:Hbs1 Promotes Subunit Dissociation and Peptidyl-tRNA Drop-Off to Initiate No-Go Decay. *Science*, *330*(6002), 369–372. https://doi.org/10.1126/science.1192430

Simms, C. L., Yan, L. L., & Zaher, H. S. (2017). Ribosome Collision Is Critical for Quality Control during No-Go Decay. *Molecular Cell*, *68*(2), 361-373.e5. https://doi.org/10.1016/j.molcel.2017.08.019

Smith, J. D., Suresh, S., Schlecht, U., Wu, M., Wagih, O., Peltz, G., Davis, R. W., Steinmetz, L. M., Parts, L., & St.Onge, R. P. (2016). Quantitative CRISPR interference screens in yeast identify chemical-genetic interactions and new rules for guide RNA design. *Genome Biology*, *17*(1), 45. https://doi.org/10.1186/s13059-016-0900-9

Somero, G. N. (2020). The cellular stress response and temperature: Function, regulation, and evolution. *Journal of Experimental Zoology Part A: Ecological and Integrative Physiology*, *333*(6), 379–397. https://doi.org/10.1002/jez.2344

Starosta, A. L., Lassak, J., Jung, K., & Wilson, D. N. (2014). The bacterial translation stress response. *FEMS Microbiology Reviews*, *38*(6), 1172–1201. https://doi.org/10.1111/1574-6976.12083

Stein, K. C., & Frydman, J. (2019). The stop-and-go traffic regulating protein biogenesis: How translation kinetics controls proteostasis. *Journal of Biological Chemistry*, *294*(6), 2076–2084. https://doi.org/10.1074/jbc.REV118.002814

Sundaramoorthy, E., Leonard, M., Mak, R., Liao, J., Fulzele, A., & Bennett, E. J. (2017). ZNF598 and RACK1 Regulate Mammalian Ribosome-Associated Quality Control Function by Mediating Regulatory 40S Ribosomal Ubiquitylation. *Molecular Cell*, *65*(4), 751-760.e4. https://doi.org/10.1016/j.molcel.2016.12.026

Sweet, T., Kovalak, C., & Coller, J. (2012). The DEAD-Box Protein Dhh1 Promotes Decapping by Slowing Ribosome Movement. *PLoS Biology*, *10*(6), e1001342. https://doi.org/10.1371/journal.pbio.1001342

Tanenbaum, M. E., Gilbert, L. A., Qi, L. S., Weissman, J. S., & Vale, R. D. (2014). A Protein-Tagging System for Signal Amplification in Gene Expression and Fluorescence Imaging. *Cell*, *159*(3), 635–646. https://doi.org/10.1016/j.cell.2014.09.039

Tatavarty, V., Ifrim, M. F., Levin, M., Korza, G., Barbarese, E., Yu, J., & Carson, J. H. (2012). Single-molecule imaging of translational output from individual RNA granules in neurons. *Molecular Biology of the Cell*, *23*(5), 918–929. https://doi.org/10.1091/mbc.E11-07-0622

Tauber, D., Tauber, G., & Parker, R. (2020). Mechanisms and Regulation of RNA Condensation in RNP Granule Formation. *Trends in Biochemical Sciences*, *45*(9), 764–778. https://doi.org/10.1016/j.tibs.2020.05.002

Teixeira, D., Sheth, U., Valencia-Sanchez, M. A., Brengues, M., & Parker, R. (2005). Processing bodies require RNA for assembly and contain nontranslating mRNAs. *RNA*, *11*(4), 371–382.

https://doi.org/10.1261/rna.7258505

Tesina, P., Ebine, S., Buschauer, R., Thoms, M., Matsuo, Y., Inada, T., & Beckmann, R. (2023). Molecular basis of eIF5A-dependent CAT tailing in eukaryotic ribosome-associated quality control. *Molecular Cell*, *83*(4), 607-621.e4. https://doi.org/10.1016/j.molcel.2023.01.020

Tesina, P., Lessen, L. N., Buschauer, R., Cheng, J., Wu, C. C., Berninghausen, O., Buskirk, A. R., Becker, T., Beckmann, R., & Green, R. (2020). Molecular mechanism of translational stalling by inhibitory codon combinations and poly(A) tracts. *The EMBO Journal*, *39*(3). https://doi.org/10.15252/embj.2019103365

Tomomatsu, S., Watanabe, A., Tesina, P., Hashimoto, S., Ikeuchi, K., Li, S., Matsuo, Y., Beckmann, R., & Inada, T. (2023). Two modes of Cue2-mediated mRNA cleavage with distinct substrate recognition initiate no-go decay. *Nucleic Acids Research*, *51*(1), 253–270. https://doi.org/10.1093/nar/gkac1172

Tseng-Rogenski, S. S.-I. (2003). Functional conservation of Dhh1p, a cytoplasmic DExD/H-box protein present in large complexes. *Nucleic Acids Research*, *31*(17), 4995–5002. https://doi.org/10.1093/nar/gkg712

Tsuboi, T., Kuroha, K., Kudo, K., Makino, S., Inoue, E., Kashima, I., & Inada, T. (2012). Dom34:Hbs1 Plays a General Role in Quality-Control Systems by Dissociation of a Stalled Ribosome at the 3′ End of Aberrant mRNA. *Molecular Cell*, *46*(4), 518–529. https://doi.org/10.1016/j.molcel.2012.03.013

Tsuboi, T., Viana, M. P., Xu, F., Yu, J., Chanchani, R., Arceo, X. G., Tutucci, E., Choi, J., Chen, Y. S., Singer, R. H., Rafelski, S. M., & Zid, B. M. (2020). Mitochondrial volume fraction and translation duration impact mitochondrial mRNA localization and protein synthesis. *ELife*, *9*, e57814. https://doi.org/10.7554/eLife.57814

Ude, S., Lassak, J., Starosta, A. L., Kraxenberger, T., Wilson, D. N., & Jung, K. (2013). Translation Elongation Factor EF-P Alleviates Ribosome Stalling at Polyproline Stretches. *Science*, *339*(6115), 82–85. https://doi.org/10.1126/science.1228985

Unnikrishnan, A., Akiyoshi, B., Biggins, S., & Tsukiyama, T. (2012). An Efficient Purification System for Native Minichromosome from Saccharomyces cerevisiae. In R. H. Morse (Ed.), *Chromatin Remodeling: Methods and Protocols* (pp. 115–123). Humana Press. https://doi.org/10.1007/978-1-61779-477-3_8

Unnikrishnan, A., Gafken, P. R., & Tsukiyama, T. (2010). Dynamic changes in histone acetylation regulate origins of DNA replication. *Nature Structural & Molecular Biology*, *17*(4), Article 4. https://doi.org/10.1038/nsmb.1780

van den Elzen, A. M. G., Henri, J., Lazar, N., Gas, M. E., Durand, D., Lacroute, F., Nicaise, M., van Tilbeurgh, H., Séraphin, B., & Graille, M. (2010). Dissection of Dom34–Hbs1 reveals independent functions in two RNA quality control pathways. *Nature Structural & Molecular Biology*, *17*(12), Article 12. https://doi.org/10.1038/nsmb.1963

Van Treeck, B., Protter, D. S. W., Matheny, T., Khong, A., Link, C. D., & Parker, R. (2018). RNA self-assembly contributes to stress granule formation and defining the stress granule transcriptome.

Proceedings of the National Academy of Sciences, *115*(11), 2734–2739. https://doi.org/10.1073/pnas.1800038115

Veltri, A. J., D'Orazio, K. N., Lessen, L. N., Loll-Krippleber, R., Brown, G. W., & Green, R. (2022). Distinct elongation stalls during translation are linked with distinct pathways for mRNA degradation. *ELife*, *11*, e76038. https://doi.org/10.7554/eLife.76038

Verma, R., Oania, R. S., Kolawa, N. J., & Deshaies, R. J. (2013). Cdc48/p97 promotes degradation of aberrant nascent polypeptides bound to the ribosome. *ELife*, *2*, e00308. https://doi.org/10.7554/eLife.00308

Verma, R., Reichermeier, K. M., Burroughs, A. M., Oania, R. S., Reitsma, J. M., Aravind, L., & Deshaies, R. J. (2018). Vms1 and ANKZF1 peptidyl-tRNA hydrolases release nascent chains from stalled ribosomes. *Nature*, *557*(7705), Article 7705. https://doi.org/10.1038/s41586-018-0022-5

Walsh, I. M., Bowman, M. A., Soto Santarriaga, I. F., Rodriguez, A., & Clark, P. L. (2020). Synonymous codon substitutions perturb cotranslational protein folding in vivo and impair cell fitness. *Proceedings of the National Academy of Sciences*, *117*(7), 3528–3534. https://doi.org/10.1073/pnas.1907126117

Wang, X., & Chen, X. J. (2015). A cytosolic network suppressing mitochondria-mediated proteostatic stress and cell death. *Nature*, *524*(7566), Article 7566. https://doi.org/10.1038/nature14859

Wang, X., Chi, H., Zhou, B., Li, W., Li, Z., & Xia, Z. (n.d.). Bacterial Luciferase Gene Cassette as a Real-time Bioreporter for Infection Model and Drug Evaluation. *Current Pharmaceutical Design*, *24*(8), 952–958.

Wang, Z., Gaba, A., & Sachs, M. S. (1999). A Highly Conserved Mechanism of Regulated Ribosome Stalling Mediated by Fungal Arginine Attenuator Peptides That Appears Independent of the Charging Status of Arginyl-tRNAs*. *Journal of Biological Chemistry*, *274*(53), 37565–37574. https://doi.org/10.1074/jbc.274.53.37565

Wang, Z., & Sachs, M. S. (1997). Arginine-specific Regulation Mediated by the Neurospora crassa arg-2 Upstream Open Reading Frame in a Homologous, Cell-free in Vitro Translation System*. *Journal of Biological Chemistry*, *272*(1), 255–261. https://doi.org/10.1074/jbc.272.1.255

Webster, M. W., Chen, Y.-H., Stowell, J. A. W., Alhusaini, N., Sweet, T., Graveley, B. R., Coller, J., & Passmore, L. A. (2018). MRNA Deadenylation Is Coupled to Translation Rates by the Differential Activities of Ccr4-Not Nucleases. *Molecular Cell*, *70*(6), 1089-1100.e8. https://doi.org/10.1016/j.molcel.2018.05.033

Wei, J., Zhang, Y., Ivanov, I. P., & Sachs, M. S. (2013). The Stringency of Start Codon Selection in the Filamentous Fungus Neurospora crassa*. *Journal of Biological Chemistry*, *288*(13), 9549–9562. https://doi.org/10.1074/jbc.M112.447177

Weidberg, H., & Amon, A. (2018). MitoCPR—A surveillance pathway that protects mitochondria in response to protein import stress. *Science*, *360*(6385), eaan4146. https://doi.org/10.1126/science.aan4146

Wilczynska, A., Aigueperse, C., Kress, M., Dautry, F., & Weil, D. (2005). The translational regulator CPEB1 provides a link between dcp1 bodies and stress granules. *Journal of Cell Science*, *118*(5), 981–992. https://doi.org/10.1242/jcs.01692

Williams, C. C., Jan, C. H., & Weissman, J. S. (2014). Targeting and plasticity of mitochondrial proteins revealed by proximity-specific ribosome profiling. *Science*, *346*(6210), 748–751. https://doi.org/10.1126/science.1257522

Wrobel, L., Topf, U., Bragoszewski, P., Wiese, S., Sztolsztener, M. E., Oeljeklaus, S., Varabyova, A., Lirski, M., Chroscicki, P., Mroczek, S., Januszewicz, E., Dziembowski, A., Koblowska, M., Warscheid, B., & Chacinska, A. (2015). Mistargeted mitochondrial proteins activate a proteostatic response in the cytosol. *Nature*, *524*(7566), Article 7566. https://doi.org/10.1038/nature14951

Wu, B., Eliscovich, C., Yoon, Y. J., & Singer, R. H. (2016). Translation dynamics of single mRNAs in live cells and neurons. *Science*, *352*(6292), 1430–1435. https://doi.org/10.1126/science.aaf1084

Wu, C., Amrani, N., Jacobson, A., & Sachs, M. S. (2007). Chapter Ten—The Use of Fungal In Vitro Systems for Studying Translational Regulation. In J. Lorsch (Ed.), *Methods in Enzymology* (Vol. 429, pp. 203–225). Academic Press. https://doi.org/10.1016/S0076-6879(07)29010-X

Xu, B., Liu, L., & Song, G. (2022). Functions and Regulation of Translation Elongation Factors. *Frontiers in Molecular Biosciences*, *8*. https://www.frontiersin.org/articles/10.3389/fmolb.2021.816398

Yamada, M., Suzuki, Y., Nagasaki, S. C., Okuno, H., & Imayoshi, I. (2018). Light Control of the Tet Gene Expression System in Mammalian Cells. *Cell Reports*, *25*(2), 487-500.e6. https://doi.org/10.1016/j.celrep.2018.09.026

Yan, X., Hoek, T. A., Vale, R. D., & Tanenbaum, M. E. (2016). Dynamics of Translation of Single mRNA Molecules In Vivo. *Cell*, *165*(4), 976–989. https://doi.org/10.1016/j.cell.2016.04.034

Young, J. C., Hoogenraad, N. J., & Hartl, F. U. (2003). Molecular Chaperones Hsp90 and Hsp70 Deliver Preproteins to the Mitochondrial Import Receptor Tom70. *Cell*, *112*(1), 41–50. https://doi.org/10.1016/S0092-8674(02)01250-3

Yu, C.-H., Dang, Y., Zhou, Z., Wu, C., Zhao, F., Sachs, M. S., & Liu, Y. (2015). Codon Usage Influences the Local Rate of Translation Elongation to Regulate Co-translational Protein Folding. *Molecular Cell*, *59*(5), 744–754. https://doi.org/10.1016/j.molcel.2015.07.018

Zabezhinsky, D., Slobodin, B., Rapaport, D., & Gerst, J. E. (2016). An Essential Role for COPI in mRNA Localization to Mitochondria and Mitochondrial Function. *Cell Reports*, *15*(3), 540–549. https://doi.org/10.1016/j.celrep.2016.03.053

Zhao, T., Chen, Y.-M., Li, Y., Wang, J., Chen, S., Gao, N., & Qian, W. (2021). Disome-seq reveals widespread ribosome collisions that promote cotranslational protein folding. *Genome Biology*, *22*(1), 16. https://doi.org/10.1186/s13059-020-02256-0

Zhou, C. Y., Stoddard, C. I., Johnston, J. B., Trnka, M. J., Echeverria, I., Palovcak, E., Sali, A., Burlingame, A. L., Cheng, Y., & Narlikar, G. J. (2017). Regulation of Rvb1/Rvb2 by a Domain within the INO80 Chromatin Remodeling Complex Implicates the Yeast Rvbs as Protein Assembly Chaperones. *Cell Reports*, *19*(10), 2033–2044. https://doi.org/10.1016/j.celrep.2017.05.029

Zid, B. M., & O'Shea, E. K. (2014). Promoter sequences direct cytoplasmic localization and translation of mRNAs during starvation in yeast. *Nature*, *514*(7520), Article 7520.

https://doi.org/10.1038/nature13578